2013-04-25

Advances of Interfacial Property Determination Using X-Ray Micro Imaging

Rodriguez Bermudez, Alonso

UNIVERSITY OF CALGARY

Advances of Interfacial Property Determination Using X-Ray Micro Imaging

by

Alonso Rodriguez Bermudez

A THESIS

SUBMITTED TO THE FACULTY OF GRADUATE STUDIES

IN PARTIAL FULFILMENT OF THE REQUIREMENTS FOR THE

DEGREE OF MASTER OF SCIENCE

DEPARTMENT OF CHEMICAL AND PETROLEUM ENGINEERING

CALGARY, ALBERTA

APRIL, 2013

Abstract

The main objectives of this research project are to analyze the challenges X-ray micro imaging has to determine interfacial properties, propose a solution to be able to implement X-rays in the determination of contact angle and interfacial tension and establish the reliability and practicality of microtomography in the determination of interfacial properties.

An extensive set of experiments has been executed using a legacy cell to analyze the challenges previous work faced. A new and improved cell to use in a micro CT-scanner has been designed and constructed which gave us an easier manner to set up the experiments in the micro CT scanner. New experiments were conducted using a proposed solution to these challenges and the results obtained have accuracy and reliability. Finally, the determination of contact angle and interfacial tension was conducted in water-wet, neutral and oil-based substrate systems at standard conditions.

The limitations given by the micro CT-scanner were in a great manner resolved. Even though the procedure is tedious and time consuming it is accurate and reliable. This makes microtomography attractive to be used in the determination of interfacial properties. Further experimentation is recommended in the development of this new method under different conditions, especially reservoir conditions.

Acknowledgements

I appreciate the help, support and encouragement from my supervisor Dr. Apostolos Kantzas. Thanks you Dr. Kantzas for the opportunity you provided for me to pursue my education at master's level. I have learnt not only technical knowledge from you, but also many life lessons that will help me in the future.

Financial support from the sponsoring companies of the Canada Research Chair (CRC) in Energy and Imaging (PetroCanada, Suncor, Nexen, Shell, ConocoPhillips, Laricina, ET-Energy, Schlumberger, Paramount, CMG Foundation, Canadian Natural and Devon Canada), the CRC program and NSERC is gratefully appreciated.

I would like to thank TIPM staff and students for the help they provided me in many aspect of my project. I am very thankful of the administrative staff at the Chemical and Petroleum Engineering Department.

Dedication

To my wife Laura Aurora Pineda Castro.

Table of Contents

List of Tables

List of Figures and Illustrations

List of Symbols, Abbreviations and Nomenclature

Abbreviation	Definition
ADSA	Axisymmetric Drop Shape Analysis
ADSA-P	Axisymmetric Drop Shape Analysis-Profile
ADSA-CD	Axisymmetric Drop Shape Analysis Profile-Contact Diameter
CAT	Computed Axial Tomography
CT	Computed Tomography
IFT	Interfacial Tension
L-G	Liquid-Gas
L-L	Liquid-Liquid
S-G	Solid-Gas
S-L	Solid-Liquid
ST	Surface Tension

Greek Symbol	Definition
α	Mean Linear Coefficient of Thermal Expansion
β	Bond Number
γ	Interfacial Tension Surface Tension
Δ	Difference
θ	Contact Angle
π	Pi Number ≈ 3.14
μ	Viscosity
ρ	Density

Latin Symbol	Definition
A	Area
a	Length Square Root of Capillary Constant
a2	Capillary Constant
b	Length Radius of the Interface at the Apex
c	Length
d	Diameter, Distance Length
E	Objective Function
e	Error
f	Fraction

	Factor
	Function
	Mechanical Force
F	Helmholtz Free Energy
	Force
g	Gravitational Acceleration
G	Gibbs Free Energy
h	Height
H	Contact Angle Hysteresis
	Enthalpy
l	Length
N	Total Number of Items
n	Number of Items
P	Pressure
Q	Heat
R	Radius
r	Radius
s	Arc Length
S	Entropy
σ	Dimensionless Arc Length
T	Temperature
t	Time
u	Experimental Interface Function
U	Internal Energy
v	Calculated Interface Function
V	Volume
w	With
W	Weight, Work
x	Abscissa, Length
	Thickness of material
ξ	Dimensionless x
X	x Coordinate
y	Ordinate, Radius from Axis of Rotation
Z	z Coordinate
z	Axis Perpendicular to xy Plane
	Vertical Height
ζ	Dimensionless z

Subscript	**Definition**
0	Reference Level
A	Curve A
adv	Advancing
allow	Allowable
axial	Axial

B	Curve B
c	Circumferential
C	Compression
cap	Capillary
ef	Effective
i	Item Counter
	Inside
k	Item Counter
l	Longitudinal
m	Minimum
max	Maximum
mean	Mean
min	Inside
	Minimum
n	Item Counter
o	Origin
	Outside
O	Point O
PV	Volume Change
Rec	Receding
Rev	Reversible
Ring	Ring
Slice	Slice
tot	Total
Total	Total
u	Ultimate
w	Water
wire	Wire
y	Yield
θ	Non Zero Contact Angle

Superscript	**Definition**
o	Degree
S	Excess
α	Phase
β	Phase

Chapter One: Introduction

1.1 Background

Knowledge of reservoir fluid properties is essential during the development phase, and the implementation of an optimal reservoir management strategy. Interfacial tensions of reservoir fluids, as well as the contact angle are important parameters for many reservoir engineering studies such as imbibition studies and calculation of fluid saturation in the transition zones.

Interfacial tension and contact angle of the fluids/rock system affect the distribution of fluids within the reservoir rock material. The fluids distribution strongly affects the flow behaviour and hydrocarbon recovery.

A considerable amount of work in the past has been directed towards understanding the mechanisms responsible for oil reservoirs being water-wet, oil-wet or mixed-wet. The factors may affect the reservoir wettability to be altered from one state to another includes oil composition, brine chemistry, rock surface characteristics, capillary pressure, and temperature (Anderson *et al.,* 1986a).

For core analysis to predict the behaviour of a reservoir accurately, the wettability of a core must be the same as the wettability of the undisturbed reservoir rock. A serious problem occurs because many aspects of core handling can drastically affect wettability (Anderson *et al.*, 1986b).

1.2 Research Objective

This research uses every endeavour to analyze the challenges X-ray micro imaging has to determine interfacial properties. More specifically, implements X-rays to capture images of water-wet, neutral and oil-based substrate systems and process them with a state-of-the-art technique of image processing to obtain the contact angle and interfacial tension.

To obtain the desired results, a new cell is designed to make easier the setup of the systems and improve the definition of the images taken using X-rays. The equipment is used to meet the following objectives:

- Evaluate the improvement of the challenges previous research had to capture images using X-ray micro imaging.
- Determine the contact angle and interfacial tension of water-wet, neutral and oil-based substrate systems with known interfacial tension to evaluate the accuracy of new experimental methodology.
- Establish the reliability and practicality of X-ray micro imaging in the determination of interfacial properties.

1.3 Research Methodology

The first part of the experiments on this project were conducted during an extensive amount of time to find the best setup of the micro CT-scanner to obtain images with high contrast. While we were working on the setup of the equipment, we were able to understand what was causing problems with the cell previously designed and a new improved cell was designed and built.

The second part of the experiments allowed us to analyze the influence of the droplet size in the determination of the interfacial properties. The software to enhance digitally the images was chosen and tested. We tested the developed algorithms to obtain the coordinates of the interface as well as the axisymmetric drop shape analysis-profile (ADSA-P) routine.

The last part of the experiments was run to determine the interfacial properties of water-wet, neutral and oil-based substrate systems. The results were analysed. Based on the performance of the equipment, complexity and amount of work, and the accuracy of the results we were able to determine the reliability and practicality of the new experimental methodology to obtain interfacial properties.

Chapter Two: Literature Review

2.1 Surface and Interfacial Tension

2.1.1 Introduction

It is now well-supported that there are four distinctive forces acting in nature. Two of these belong to the domain of nuclear and high-energy physics. These are strong and weak interactions with a short range of action, less than 10^{-5} nm acting between atomic particles. The other two are the electromagnetic and gravitational interactions acting between atoms and molecules in a wide range of distances, from subatomic to infinite distances and are in consequence the forces that govern the behaviour of everyday things (Israelachvili, 1985).

Electromagnetic forces are the source of all intermolecular interactions. They determine the properties of solids, liquids, and gases, the behaviour of particles in solution, chemical reactions and the organization of biological structures. Gravitational forces account for cosmological phenomena. When these two forces act together they determine phenomena such as the height that a liquid will raise in small capillaries (Thompson, 1968).

2.1.2 Definition of Surface and Interface Tension

An interface is defined as the boundary between two phases and it is treated as an ideal mathematical line or an interface with no thickness. This is known as the *Gibbs model*. Gibbs assumed that the contact region of two phases is infinitely thin and it does not have any volume (Butt *et al*., 2006). There are four types of interfaces: liquid-gas (L-G), liquid-liquid (L-L),

solid-gas (S-G) and solid-liquid (S-L). The solid-gas and liquid-gas interfaces are also called surfaces. The liquid-liquid interface appears between two immiscible liquids.

> [There are also] solid-solid interfaces [that] separate two solid phases. They are important for the mechanical behaviour of solid materials. There are no gas-gas interfaces because gases mix (Butt *et al.,* 2006)

Generally, it can be said that

> Where two phases meet is commonly called an *interface*. The term surface is used when one of the phases is gas or vapour (Jaycock *et al.,* 1981).

The term *inter-phase* is also used for the contact region where the properties of two bulk phases change gradually. Therefore, based on the definition, inter-phase has a physical thickness. One of the people who treated the contact area as an inter-phase with a finite volume was Guggenheim (Butt *et al.*, 2006).

The *Gibbs model* is assumed for this work, a mathematical concept that assumes the contact region of two phases is infinitely thin. This assumption makes the understanding of the interface more practical in most applications. Therefore, the terms *surface* and *interface* are used to properly refer to phases in contact with each other.

The existence of surfaces and interfaces has a significant effect on the materials properties because it is on them where the interactions of material happen (Dobrzynski, 1978). Surfaces

and interfaces have an important role in different industries. One of the earliest studies was done in metallurgy including morphology and kinetics of phase changes such as crystals growth, recrystallization, grain growth, twining, and precipitation. The study of chemical reactions and chemical catalysis on surfaces is also well known. Also, numerous surface and interface studies are done on plastic properties, adhesion, friction, wetting, electrochemistry, heterogeneous catalysis, and electronics that include miniaturization of electronic circuits (Dobrzynski, 1978). Some examples of surfaces and interfaces sciences in chemical and petroleum engineering can be the mechanism of detergents and oil recovery surfactant flooding process.

For each different type of interface there is a free energy change associated with its formation which is called *excess interfacial free energy* (or *excess surface free* energy).

> It represents the excess free energy that the molecules possess by virtue of their being in the interface [or surface] (Jaycock *et al.,* 1981).

The conceptual definition of the surface free energy of the material is the work that is done to bring the interior bulk molecules to the surface to create a new surface having a unit area of $1m^2$. Hence, the dimension of the surface free energy is energy per unit area. Also, the interface free energy for two immiscible phases in contact with each other is defined as the work that is done to bring the molecules from inside of each bulk phase to the interface to create a new interface having a unit area of 1 m^2 (Erbil, 2006)

The *surface tension* and *interfacial tension* (γ) are the basic properties used to describe an interface and denote force per unit length or energy per unit area. The term surface tension (ST) is commonly used to describe the tension in the interface of a gas phase with a liquid or a solid phase. In the case of liquid-liquid or solid-liquid interfaces the term interfacial tension (IFT) is used.

> The surface tension of a material is the force that operates inward from the boundaries of its surface perpendicularly, tending to contract and minimize the area of the surface. Its dimension is force per unit length. For a plane surface, the surface tension can be defined as the force acting parallel to the surface and at right angles to a line of unit length anywhere in the surface. This attraction makes the liquid behave as though surrounded by an invisible membrane skin, although there is actually no such skin in real systems.
> When we consider two immiscible phases and an interface between them, we should define the interfacial tension as the force that operates inward from the boundaries of its surface perpendicularly to each phase, tending to contract and minimize the area of the interface. This process decreases the number of molecules in the interface, and this diminishes the interface area. This interface contraction continues until the interior accommodates the maximum possible number of molecules (Erbil, 2006).

The ST and IFT have a significant importance in physicochemical science. They explain the behaviour of liquid-fluid contacts in many applications of science and engineering. The IFT of liquid-liquid contact shows the dispersion magnitude of a liquid on another liquid. The spreading extent of fluids is important in chemical processes and petroleum recovery science. The coating processes and the migration of oil in porous media can be explained by studying the interfacial properties.

> [it] is important in the emulsification of liquids or oils in an immiscible continuous phase, resistance to flow through orifices, and the atomization/dispersion of droplets in a continuous fluid phase (Dingle, 2005).

The dimension of ST and specified excess surface free energy are the same (MT^2). Furthermore, these two concepts are identical for pure liquids in equilibrium with their vapour. This relation is true for IFT and excess interfacial free energy as well and they are identical (Jaycock *et al.*, 1981).

2.2 Young-Laplace Equation

Thermodynamically Surface Tension and Interfacial Tension is the surface free energy per unit area or, in other words, surface force per unit length. The most commonly used units are (*dyne/cm*) or (*mN/m*), indicating force per unit length, or ($ergs/cm^2$) indicating energy per unit area. The physical meaning of these units is:

$$Work = Force * Length = \gamma l dx$$

Or

$$Work = \gamma dA = \gamma l dx$$

To understand better the surface tension, let us consider a spherical soap bubble of radius *r* (Figure 2.2-1) where its total free energy is $4\pi r^2$ (Butt *et al*., 2006).

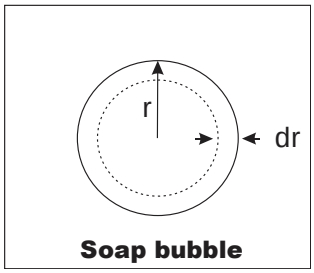

Figure 2.2-1: Soap film for IFT measurements

If the radius is decreased by *dr*, then the changes in surface free energy is $8\pi r\gamma dr$. Since shrinking decreases the surface energy, the tendency to do so must be balanced by a pressure difference through the surface, ΔP, such that the work against this pressure difference is equal to the decrease in surface free energy. In other words:

$$4\pi r^2 dr\, \Delta P = 8\pi r\gamma dr \qquad (2.1)$$

$$\Delta P = \frac{2\gamma}{r} \qquad (2.2)$$

Where ΔP = Inside pressure – Outside pressure

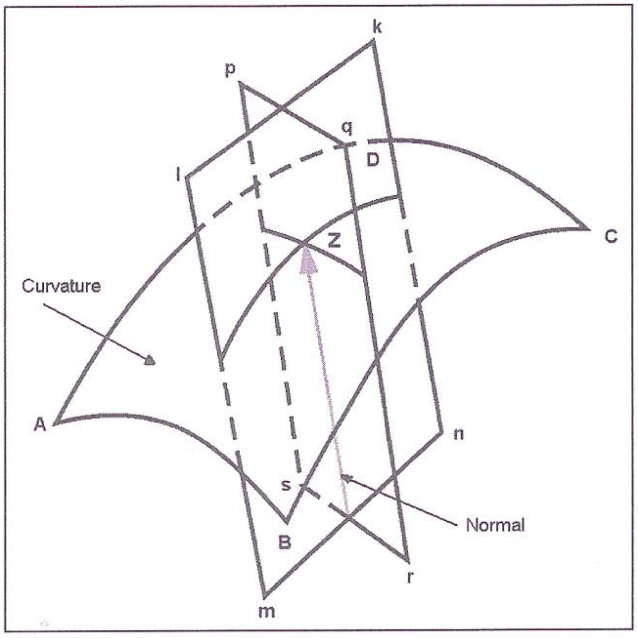

Figure 2.2-2: Description of Young-Laplace equation using plane geometry concept (Ebril, 2006)

Therefore, the smaller the soap bubble, the larger the air pressure inside compared to the outside. Equation (2.2) is the basic equation of capillarity for sphere shape interfaces and was derived by Young and Laplace around 1805 (Peacock *et al*., 1855).

In general, a curved surface is introduced with two independent radii. The two radii of the curvature are determined by cutting the curve surface (ABCD in Figure 2.2-2) with two perpendicular planes intersecting each other on the curve surface. Each plane's intersection with the curved surface generates a two-dimensional curvature containing one of the two independent radii of the curved surface (r_1 and r_2).

If the curved surface becomes a little larger and moves outward by an amount of *dz* (Figure 2.2-3), the new position of the surface will become (A'B'C'C').

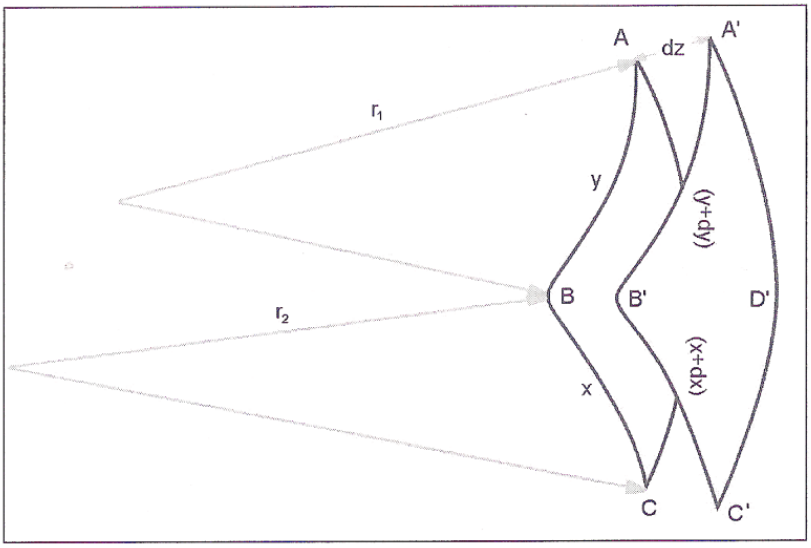

Figure 2.2-3: Description of Young-Laplace equation using plane geometry concept (Erbil, 2006)

Therefore, there will be changes in surface dimension *x* (abscissa), *y* (ordinate), and *z* (normal coordinate to paper plane) to $x + dx$, $y + dy$, and $z + dz$ amounts. Consequently, the changes in area, Gibbs free energy, and work will be:

$$\Delta A = (x+dx)(y+dy) - xy = xdy + ydx + dxdy \approx xdy + ydx \quad (2.3)$$

$$dG = \gamma(xdy + ydx) \quad (2.4)$$

$$W = \Delta PdV = \Delta Pxydz = \gamma(xdy + ydx) \quad (2.5)$$

From Figure (2.2-3) r_1 and r_2 are changing when *x, y,* and *z* change. Applying the triangle rule of geometry:

$$\frac{x+dx}{r_1+dz} = \frac{x}{r_1} \tag{2.6}$$

Which simplifies to:

$$\frac{dx}{xdz} = \frac{1}{r_1} \tag{2.7}$$

And

$$\frac{y+dy}{r_2+dz} = \frac{y}{r_2} \tag{2.8}$$

Which simplifies to:

$$\frac{dy}{ydz} = \frac{1}{r_2} \tag{2.9}$$

Substituting equations (2.9) and (2.7) into equation (2.5) generates equation (2.10) which is the Young-Laplace equation of capillarity.

$$\Delta P = \gamma\left(\frac{1}{r_1} + \frac{1}{r_2}\right) \quad (2.10)$$

2.3 Wettability and Contact Angle

2.3.1 Definition of wettability

Wetting is the direct consequent of the interactions between three phases in the contact area. Two of the three phases are fluids, either gas or liquid. Wettability and the methods used to measure wettability are completely reviewed by Anderson (Anderson, 1986a; Anderson, 1986b). He defines *wettability* as

> The tendency of one fluid to spread on or adhere to a solid surface in the presence of the other immiscible fluids (Anderson, 1986a).

Wettability has a major role in controlling the flow and distribution of reservoir fluids. For a rock-brine-oil system wettability is defined as

> A measure of the preference that the rock has for either the oil or water. When the rock is water-wet, there is a tendency for water to occupy the small pores and to contact the majority of the rock surfaces. Similarly, the rock is preferentially in contact with the oil; the location of the two fluids is reversed from the water-wet case, and oil will occupy the small pores and contact the majority of the rock surface (Anderson, 1986a).
>
> Depending of the specific interactions of rock, oil, and brine, the wettability of a system can range from strongly *water-wet* to strongly *oil-wet*. When the rock has not strong preference for either oil or water, the system is said to be of *neutral* (or intermediate) wettability. Besides strong and neutral

> wettability, a third type is *fractional wettability*, where different areas of the core have different wetting preferences (Anderson, 1986a).

Almost all clean sedimentary rocks are strongly water-wet. Specially sandstones, which were deposited in an aqueous environment and stayed there for a long time before the oil migrated and drained the water. Therefore, it is believed that most petroleum reservoirs are water-wet. However, further researchers showed that not only that most carbonate reservoirs are oil-wet, but also some quartz surfaces (sandstone) are strongly oil-wet (Anderson, 1986a). The fact is that reservoir rock preference can alter from strongly water-wet by adsorption of polar compounds or even the deposition of organic materials present in the crude oil. Some of these materials are also soluble in water so they can migrate through water and place themselves on the rock surface. Therefore, the wettability of reservoir rocks can change in time.

Fractional or heterogeneous wettability of reservoir rock can be the consequence of altered wettability in some parts of oil reservoirs. In general, the rock surface inside a reservoir can attract some components of the crude oil. In the spots coated with more oil components, more oil-wet tendency of rock is observed.

2.3.2 Methods of Wettability Measurement

Wettability measurement in the oil recovery industry is quite popular and several different methods have been used to characterize the wettability of different reservoirs. The methods are reviewed in detail by Anderson (Anderson, 1986b). They are generally categorized in two major groups; qualitative and quantitative methods.

Some of the most common qualitative methods are imbibition rates, microscope examination, floatation, glass slide method, relative permeability curves, permeability-saturation relationships, capillary pressure curves, capillarimetric method, displacement capillary pressure, reservoir logs, nuclear magnetic resonance (NMR) and dye adsorption. Quantitative methods include *contact angle,* spontaneous imbibition and forced displacement (Amott), and USBM wettability method (Anderson, 1986b; Dandekar, 2006).

Among all the methods, the quantitative methods are commonly used to measure the wettability of different systems. Nevertheless, there is no single universally accepted method. According to Anderson (Anderson, 1986b) the contact angle method is used to measure the wettability of a certain surface, but the Amott and USBM methods are used for core wettability measurements.

2.3.3 Definition of Contact Angle

When a liquid is located on a solid, it sometimes wets the surface thoroughly and spreads over the solid. However in most of the situations, the liquid does not wet the surface completely and remains as a drop having a finite contact angle between the solid surface and the liquid phase (Figure 2.3-1). In general term, *contact angle (θ)* is the angle at which a fluid-fluid interface meets the solid surface. The contact angle method is a common and useful means of measuring wettability. Measuring the contact angle of a S-L-F system will give information about surface energy, roughness, heterogeneity, and contamination (Majitevic, 1969b). Contact angle is always measured relative to the denser phase; it is very useful for wettability measurement when working with clean surfaces and pure fluids.

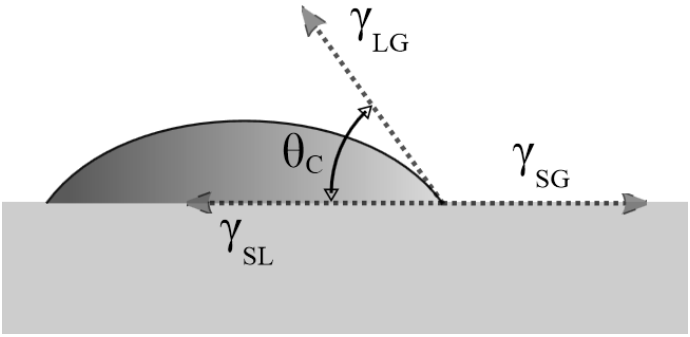

Figure 2.3-1: The angle of contact at the liquid-solid interface

Contact angle is dependant to ST or IFT by Young's Equation:

$$\gamma_{lg}\text{Cos}\theta_c = \gamma_{sg} + \gamma_{sl} \qquad (2.11)$$

For contact angle measurement two immiscible fluids are placed on a solid surface; fluid 1 is the denser fluid and fluid 2 is the lighter phase. The contact angle that two fluids make in the intersection area with the solid, can vary between 0^o and 180^o. When contact angle is less than 75^o, fluid 1 is the wetting phase and if contact angle is more than 105^o fluid 2 is the wetting phase. The contact angle between 75^o and 105^o defines what is known as neutral wettability and indicate that the surface does not have any preference to contact more with any of the fluids.

2.3.3.1 Contact Angle Hysteresis

The Young's equation implies the surface has to be completely homogeneous, flat in microscopic scale, rigid, and not perturbed by fluid adsorption or chemical interactions. The

contact angle measure on an ideal solid surface would be unique (Erbil, 2006), but on real surfaces there will be contact angle hysteresis. If the denser fluid phase is displacing the other fluid, the contact angle measured is call *advancing contact angle* (θ_{adv}) and if the denser fluid is displaced by the lighter one, the measured contact angle is name *receding contact angle* (θ_{rec}) (Butt *et al*., 2006) while this two contact angles are identical for an ideal solid surface, they usually have a significant difference in real systems. The contact angle hysteresis is the difference between these two angles:

$$H = \theta_{adv} - \theta_{rec} \qquad (2.12)$$

H is typically between 5^o to 20^o degrees but it can be even more (Butt *et al*., 2006). The dominant phenomena that can cause hysteresis in contact angle are surface roughness, heterogeneity and contamination. Other possible factors can be molecular orientation and deformation on the solid surface, drop size, liquid adsorption (Erbil, 2006), swelling, and effect of solvents on the solid surface (Adamson *et al.*, 1997).

2.3.4 Methods of Interfacial Tension and Contact Angle Measurement

There are several different ways to measure the IFT and contact angle. The most commonly used methods are categorized into shape methods and force methods for IFT and into static and dynamic for the contact angle. Some of the shape methods to measure IFT are classified as static methods when they are used to measure contact angle. The advantage of having the same method to measure both interfacial properties and at the same time overcoming the limitations of the Micro CT-Scanner made us chose the drop shape method.

2.3.4.1 The Drop or Bubble Shape Method

The method uses a solid surface where a drop or bubble is placed. The shape of the drop or bubble is defined by interfacial forces along with gravitational forces. These drops or bubbles are categorized as pendant and sessile (Figure 2.3-2).

Sessile and pendant methods require the solution of the Young-Laplace equation of capillarity. The equation is the mechanical equilibrium condition for two homogeneous fluids separated by a curve interface (Bashforth *et al*., 1883). It relates the pressure difference across a curved interface to the surface tension and the curvature of the interface:

$$\gamma \left[\frac{1}{R_1} + \frac{1}{R_2}\right] = \Delta P \qquad (2.13)$$

Where:

γ Interfacial Tension

R_1 And R_2 Two principal radii of curvature

ΔP Pressure difference across the interface

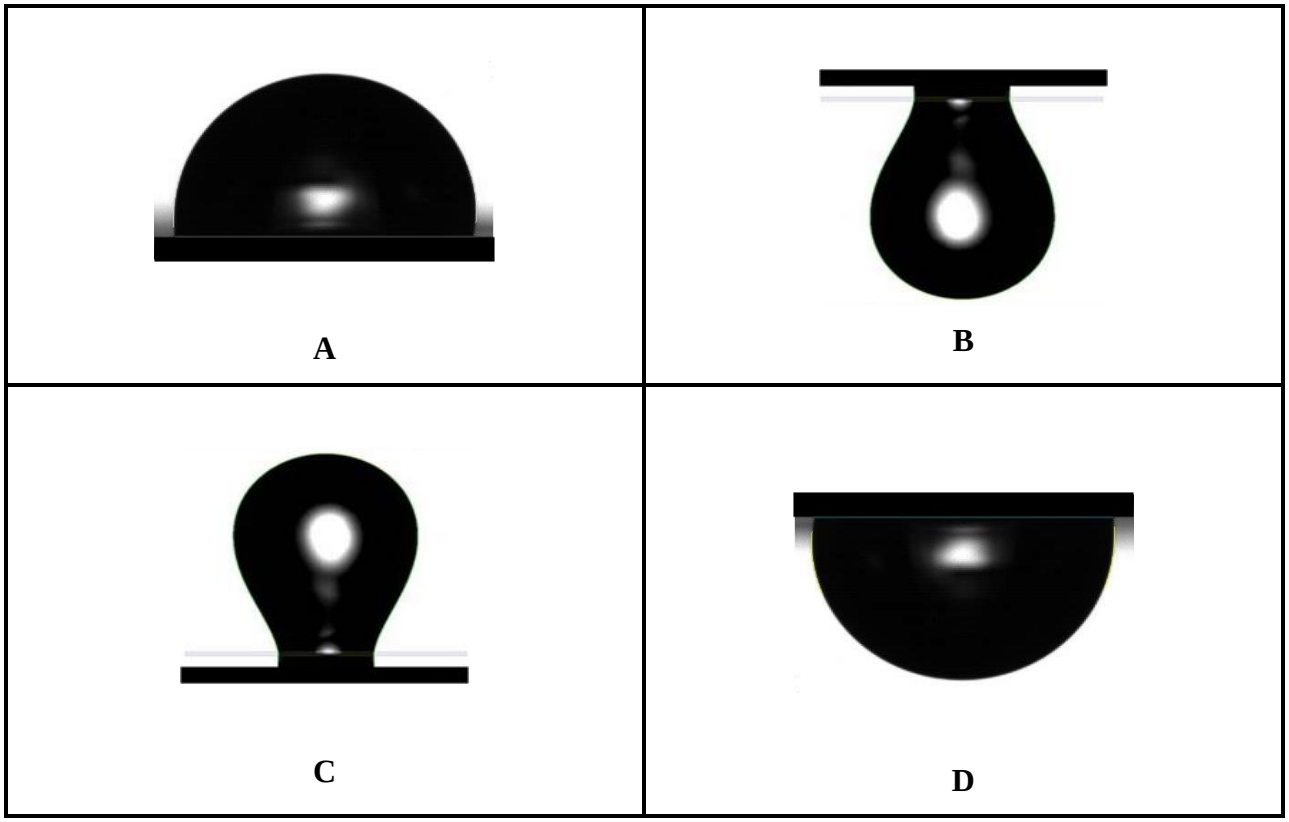

Figure 2.3-2: A Sessile Drop, B Pendant Drop, C Pendant Bubble, D Sessile Bubble

The advantage of using the sessile drop methods are: first, only small quantities of liquids are required. Second, it can be used to study liquid-vapour and liquid-liquid interfacial tensions. The method has been applied to materials ranging from organic to molten metals and from pure solvent to concentrated solutions. It has been also applied at low or high temperatures and pressures and under vacuum conditions. Another application to this method is in aging systems where the properties are changing with time because the profile of the drops can be easily recorded.

The advantages of the sessile drop method to measure contact angle and interfacial tension fit well in the use of the micro CT-scanner which has a small chamber to place the system to be analyzed. The micro CT-scanner offers a unique advantage to take images since it can be taken from different angles which allow us to observe the truly shape of the drop.

The drop shape analysis started with Bashforth and Adams (Bashford *et al*., 1883) who generated numerous series of tables containing the shape parameters from known values of the interfacial tension and contact angle for sessile drops and by Fordham (Fordham, 1948) for pendant drops. To calculate the interfacial properties the experimental information has to be interpreted using the values of this tables which were suitable for a certain range of size and shape of drops. More tables were generated by Padday (Padday, 1969). Hartland and Hartley found numerous solutions to determine the interfacial tension of axisymmetric liquid-liquid interfaces of different shapes and sizes and presented their work tabulated (Hartland *et al.*, 1976). In their book, they also presented a modified form of existing tables to determine the interfacial tension and contact angles from sessile and pendant drops and extended these tables to cover a wide range of configurations.

The experimental data was reduced to the measurements of a few preselected data points which are compatible to the values of these tables. The points correspond to special features, such as inflection points on the interface, and they must be determined with high precision. In addition, to obtain the value of the contact angle, the location of the contact point has to be determined. Since these measurements were not easy to obtain, a serious and possibly major source of error in these methods is connected with data acquisition.

These problems leaded others to try new analytical approaches. Malcolm and Painter (Malcolm *et al*, 1981) proposed another analytical method to determine contact angle and surface tension from sessile drop measurements. The method was limited to not-wetting sessile drops ($\theta>90^{\circ}$) and similarly to some of the previous approaches the data points are specific geometric points of the drop interface.

Maze and Burnet (Maze *et al*., 1969; Maze *et al*., 1971) developed a more satisfactory scheme to determine the interfacial tension from sessile drops. They generated a numerical algorithm consisting of a non-linear regression procedure. The algorithm calculates a drop shape to fit a number of arbitrary selected and measured points on the drop profile. The best fit is obtained varying two parameters. In order to start the calculation, reasonable estimates of the drop shape and size parameters are required. They used values from the tables of Bashford and Adams to obtain the initial estimates.

The strategy was great but there are several deficiencies in their algorithm. The error function was the summation of the squares of the horizontal distances between the measured points and the calculated curve. This approach is not adequate when using sessile drops of large size at low surface tension. The gravity will flatten the drop near the apex which may cause a large error. Furthermore, the location of the apex will be hard to obtain.

Rotenberg (Rotenberg *et al*,. 1983; Rotenberg *et al*., 1982) proposed a new two techniques that relied on a numerical integration of the Young-Laplace equation of capillarity in presence of gravity forces (Equation 2.44). The new techniques were named *Axisymmetric Drop Shape*

Analysis – Profile (ADSA-P) and *Axisymmetric Drop Shape Analysis – Contact Diameter* (ADSA-CD). These techniques were a great achievement in surface science; for the first time there was no need to use any previously generated tables.

ADSA-P differs from the method developed by Maze and Burnet in the way the error function is calculated. The error function is a measure of the discrepancy between the calculated Laplacian curve and the measured curve point obtained from the image of the interface. The function is the summation of the normal distances between the measured points and the calculated curve. During the calculation any parameter is generated and a final value is found at the end of the optimization. The minimization of the error function requires solving numerically a system of non-linear algebraic equations. The minimum value of the error function will give the best fit of the calculated curve with respect to the experimental curve. The function and the derivatives, first and second, are calculated by a numerical integration scheme. The integrands are all determined analytically, and therefore the derivatives do not suffer a loss of accuracy.

This method unifies the method of the sessile drop and the method of the pendant drop. There is no need for any table nor is there any restriction on the applicability of the method. The method also determines contact angle, surface area, the contact radius and the volume of the drop.

ADSA is suitable for liquid-liquid and liquid-gas systems in all range of fluids. It is applicable to low and high temperatures and pressures. It is suitable for aging and dynamic systems. Small amount of liquid is needed to produce the drop and a very small piece of solid substrate is

required to place the drop on it (Skinner *et al*., 1989; Cheng *et al*., 1990; Li *et al*., 1992; Rio *et al*., 1997; Holgado-Terriza *et al*., 1999).

The ADSA method initially was lacking high accuracy. The experimental points of the interface were generated using manual digitalizing tablets or a telescope equipped with a goniometer eye piece. The precision of the methods is approximately ±2˚ (Li *et al*., 1992). Other source of error was optical distortion that negatively affects the sharpness of the taken image (Cheng *et al*., 1990). The appearance of a digital image processor give the method an improvement in accuracy and day a day the development of new software to process images gives to the method more acceptance.

2.3.4.2 Axisymmetric Drop Shape Analysis Profile (ADSA-P)

Rotenberg and his colleagues Boruvka and Neumann (Rotenberg *et al*., 1982) introduced these techniques to determine liquid-fluid interfacial tension and contact angle from the shapes of axisymmetric menisci. The method is used with some modifications in this present work and the derivation of this is as follows.

The Young-Laplace equation of capillarity can be applied to a sessile or pendant drop if the radii of curvature are sufficiently larger than the thickness of the interface separating two bulk phases. The pressure difference across a curved interface is described by Equation (2.13). In the presence of gravity as the only external force, ΔP is a linear function of the elevation as shown in the following equation.

$$\Delta P = \Delta P_o + (\Delta\rho)gz \quad (2.14)$$

Where:

ΔP_o Pressure difference at the datum level plane.

$\Delta\rho$ difference in the densities of the two bulk phases.

z vertical height measure from the reference plane.

g gravitational acceleration.

We could see from the Figure (2.3-3), the x axis is tangent to the curved interface and normal to the axis of symmetry and the origin is placed at the apex. R_1 Turns in the plane of the paper and R_2 rotates in a plane perpendicular to the plane of the paper and about the axis of symmetry. Consequently, R_2 equals to:

$$R_2 = \frac{x}{Sin\ \phi} \quad (2.15)$$

Where ϕ is the turning angle measured between the tangent to the interface at the point (x,z) and the datum plane.

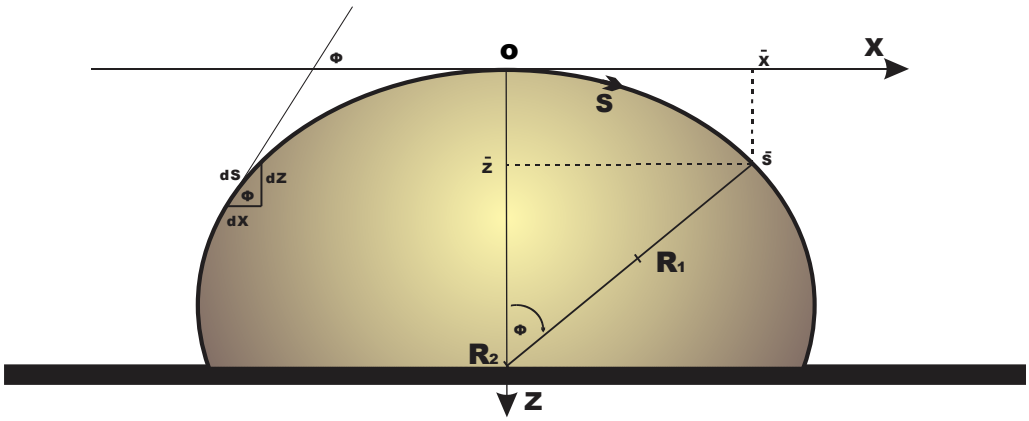

Figure 2.3-3: Schematic of an axisymmetric drop

Combining the equations (2.13), (2.14) and (2.15) we obtained:

$$\gamma\left(\frac{1}{R_1}+\frac{\sin\phi}{x}\right)=\frac{2\gamma}{R_o}+(\Delta\rho)gz \qquad (2.16)$$

Where R_o is the radius of curvature at the origin of the *x*-*z* coordinate system. Both radii of curvature (R_1 and R_2) are equal to R_o at the apex or origin of the *x*-*z* coordinate system.

Mathematically the interface is described as $u = u(x, y, z)$. A description of the meridian section alone shown in Figure (2.3-3) in a parametric form due to the symmetry in the system will be reduced to:

$$x = x(s) \text{ and } z = z(s) \qquad (2.17)$$

Where *s* is the arc length measured from the origin *0*. In this representation *x* and *z* are only function of *s*. In the differential form:

$$\frac{dx}{ds} = Cos\ \phi, \tag{2.18}$$

And

$$\frac{dz}{ds} = Sin\ \phi \tag{2.19}$$

By definition

$$\frac{1}{R_1} = \frac{d\phi}{ds} \tag{2.20}$$

Is the rate of change of the turning angle ϕ with respect to the arc-length parameter *s*. Hence, combining the equations and rearranging is generated:

$$\frac{d\phi}{ds} = \frac{2}{R_o} + \frac{(\Delta\rho)g}{\gamma} z - \frac{sin\ \phi}{x} \tag{2.21}$$

The boundary conditions are:

$$x(0) = z(0) = \phi(0) = 0 \tag{2.22}$$

This is a set of first-order differential equations for *x*, *z* and ϕ as functions of the argument *s*. For given R_0 and $(\Delta\rho)g/\gamma$ the complete shape of the curve *v* is obtained by integrating simultaneously the equations (2.18), (2.19), and (2.21) and the boundary conditions in Equation (2.22).

2.3.4.2.1 The Objective Function

In order to obtain the values of the interfacial tension and the contact angle, the calculated Laplacian curve *v* should fit the experimental curve *u*. For this purpose, an objective function is introduced as Equation (2.23)

$$E = \frac{1}{2}\sum_{n=1}^{N}[d(u_n, v)]^2 \qquad (2.23)$$

Where u_n, *n= 1, 2, ..., N*, are a set of experimental points which describe the meridian section of an interface and *v* = *v*(s) is the calculated Laplacian curve. $d(u_n, v)$ is the normal distance between *u*, and the curve *v*, shown in the Figure (2.3-4).

The value of the objective function depends on the shape of the curve *v*, and on its position relative to the measure curve *u*. The position of the curve *v*, relative to the measured curve *u*, is fixed by the location of the origin (X_o, Z_0). The minimum value of the objective function will have the least deviation between the calculated curve and the experimental. It is then when we can obtain the value of the interfacial tension and contact angle.

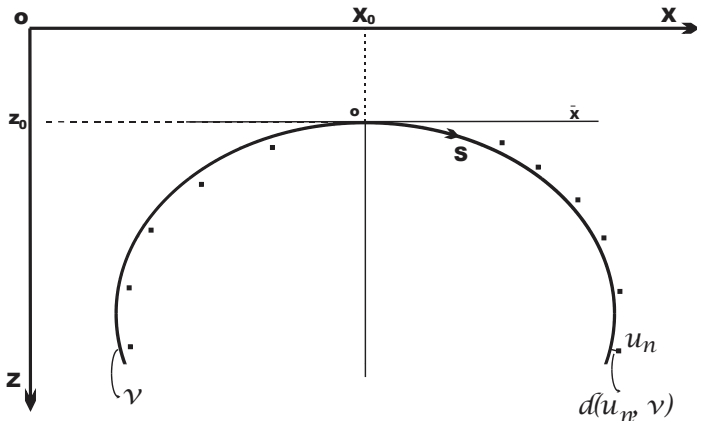

Figure 2.3-4: Experimental curve (*u*), calculated Laplacian curve (*v*) and normal distances between points u_n and curve *v*(*d*(u_n, *v*)) (Rotenberg *et al.*, 1982)

The mathematical formulation of the objective function has to be done by transforming the coordinates *x*, *z* and *s* into dimensionless coordinates. This transformation will transform the system of equations into a one-parameter family of curves.

The dimensionless parameters are defined:

$$s = \frac{s}{R_o} \tag{2.24}$$

$$x = \frac{x}{R_o} \tag{2.25}$$

$$z = \frac{z}{R_o} \tag{2.26}$$

Therefore, the system of first-order differential equation becomes

$$\dot{X} = \frac{dX}{dS} = Cos\ \phi \tag{2.27}$$

$$\dot{Z} = \frac{dZ}{dS} = Sin\ \phi \tag{2.28}$$

$$\dot{\phi} = \frac{d\phi}{dS} = 2 + \frac{(\Delta\rho)gR_o^2}{\gamma} z - \frac{\sin\phi}{X} \tag{2.29}$$

The four parameters which will be regarded as the variables of the objective function *E* are define as:

$q_1 = X_o$ (2.30)

$q_2 = Z_o$ (2.31)

$q_3 = R_o$ (2.32)

$q_4 = \frac{(\Delta\rho)gR_0^2}{\gamma} = \beta$, is the shape parameter of the capillary system (2.33)

The objective function is redefined as:

$E(q_1, q_2, q_3, q_4) = \sum_{n=1}^{N} e_n\,(q_1, q_2, q_3, q_4)$ (2.34)

Where

$e_n = 1/2[d(u_n, v)]^2$ (2.35)

Since all the curves under consideration possess symmetry with respect to the x axis, it is only required to consider one-half of the meridian section. Any datum point which falls on the other portion of the curve can be simply reflected and accounted for by remembering that this point is on the negative side. This is accomplished by using the positive sign in the following equation for $X_n \geq q_1$ and using the negative sign for $X_n < q_1$.

The objective function is the summed squares of the normal distances between the calculated curve and the data points. Therefore, it is sufficient to develop the analysis of one single data point and simplify the notation by eliminating the subscript *n*. For the *n*th data point the error is written as:

$$e = ½[(q_3 * x(s_m, q_4) \pm (q_1 - X))^2 + (q_3 * z(s_m, q_4) + (q_2 - X))^2] \quad (2.36)$$

Where

$$q_3 * x(s_m, q_4) = x \quad (2.37)$$

$$(q_3 * z(s_m, q_4) = z \quad (2.38)$$

Equations (2.37) and (2.38) are the coordinates of a point on the curve v that is closest to the experimental point (X, Z) and s_m is the corresponding value of the arc length s at that point.

The value of s_m at which e is evaluated is determined as the distance between every point on the calculated curve for which the values of q_1, q_2, q_3, q_4 are fixed and a datum point. It is regarded as a function of the argument s. f*(s)* has a minimum value where the distance between a datum point and the curve *v*, is normal to *v*. The corresponding value of s = s_m at that minimum is used in the above equation. Therefore, at a constant q_1, q_2, q_3, q_4:

$$\frac{\partial f}{\partial s} \approx 0 \approx \frac{\partial e}{\partial s_m} \quad (2.39)$$

It is clear that the value of s_m vary for different values of q_1, q_2, q_3, q_4. The equation (2.36) can be written as:

$$e = e(s_m(q_1, q_2, q_3, q_4), q_1, q_2, q_3, q_4) \quad (2.40)$$

When the error function reaches its minimum value Equation (2.34) is rewritten as:

$$\frac{\partial E}{\partial q_k} = \sum_{n=1}^{N} \frac{\partial e_n}{\partial q_k} = 0, \quad k = 1,2,3,4 \tag{2.41}$$

For a single datum point

$$\frac{\partial e}{\partial q_k} = \left(\frac{\partial e}{\partial s_m}\right)\frac{\partial s_m}{\partial q_k} + \left(\frac{\partial e}{\partial q_k}\right) \tag{2.42}$$

The brackets in the equation (2.42) indicate partial differentiation. ($\frac{\partial e}{\partial s_m}$) is the derivative of e with respect to s_m at constant values of q_1, q_2, q_3, q_4. $\left(\frac{\partial e}{\partial q_k}\right)$ the derivative of e with respect to q_k at fixed s_m. The first term according to Equation (2.39) is equal to zero. At the minimum values of the error function, the objective function can be express as:

$$\frac{\partial E}{\partial q_k} = \sum_{n=1}^{N}\left(\frac{\partial e_n}{\partial q_k}\right) = 0 \tag{2.43}$$

The system constitutes a set of non-linear algebraic equations in the parameters q_1, q_2, q_3, q_4. To solve for these parameters Rotenberg (Rotenberg *et al*., 1983) employed the Newton-Raphson method and the incremental loading method to calculate and minimize the objective function. The loading started with $q_1 = Xo$, $q_2 = Zo$, $q_3 = R$ and $q_4 = 0$. The latter statement means we will start from a circular shape Laplacian curve with the apex located at the apex of the experimental curve. The incremental loading finishes when the objective function value or the values of the derivatives fall below a threshold value of 10^{-9}. At this point the best fit of the Laplacian curve to the experimental curve is reached and the interfacial properties are calculated.

The present work uses the Runge-Kutta four order numerical method to solve the differential equation system and the minimization of the objective function uses Microsoft Excel solver. The Runge-Kutta numerical method algorithm was written in Visual Basic which is convenient to load the experimental points in a spread sheet of Excel, enable the use of Visual Basic macros to find the solution of the ASDA-P method.

Chapter Three: Analysis Methodology

Different analysis have been done using X-ray micro imaging and particularly to interfacial properties determination there has been one project where the results suggest the necessity of a more thorough review of the equipment used along with the methodology employed to set up the system to be analyzed.

The present project starts using previous designed equipment and experimental methodology. With data from preliminary testing, we designed new equipment to be used and applied changes in the methodology to obtain experimental data.

3.1 Determine the method used to measure the contact angle and interfacial tension.

Among all the techniques used to measure the contact angle the direct measurement of the contact angle from sessile drops or photographs of sessile drops is the most widely used. In this technique, the angle is measure by aligning a tangent with the drop profile at the point of contact with the solid surface. The measurement can be performed either using a telescope equipped with a goniometer eyepiece or a protractor. A precision of $\pm 2^{\circ}$ is usually claimed.

Compare to these specialized techniques, analysis of the shape of a drop offers distinct advantages. In essence, the shape of the drop is determined by the combination of surface tension and gravity effects. Small drops or bubbles will tend to be spherical because surface forces depend on the area, which changes with the square of a linear dimension, whereas distortions due to gravitational effects depend on the volume, which changes with the cube of a

linear dimension. However, when the gravitational and surface tensional effects are comparable, then one can, in principle, determine the surface tension from the measurements of the shape of the drop or bubble.

The suggested use of X-ray micro imaging which implies analysis of images left us with the only choice of analysis of a drop shape to determine the contact angle and interfacial tension. The micro CT-scanner has another hurdle to the analysis method. It has a very small chamber where we have to place the sample to be analyzed and during the analysis it has to be isolated.

One of the most common drop shape method to determine the contact angles is the sessile drop method. However, the most common method to determine the interfacial tension is the pendant drop method which suggests the use of two different procedures to calculate the interfacial properties. The latter was very soon not an option since the chamber mention before is small and has to be isolated when we take the images.

The sessile drop method is the only one which suits the limitations given by the micro CT-scanner. However, by itself it does not do a good work determining the interfacial tension. To address this problem, we used it along with the ADSA-P which applies the Laplace equation of capillarity to create a theoretical curve of the interface and fits this curve to the experimental curve obtained from an image of the sessile drop. The result of this minimization is the calculation of the contact angle and interfacial tension of the system.

In the literature review we covered the theory of the Drop or Bubble shape method and the Axisymmetric Drop Shape Analysis Profile (ADSA-P) technique. The success of the ADSA-P relies on image processing and edge detection.

3.2 Image Processing and Edge Detection

Digital Image Processing uses a specialize software to analyze digital images. It has many advantages over analog image processing; it allows a wider range of algorithms to be applied to the input data, it is noise resistance and can avoid signal distortion during the process.

3.2.1 Edge Detection

In image processing, it refers to algorithms developed to identify points in a digital image. The points identified are where the image brightness changes sharply or there are discontinuities in the digital image.

There are many specialized methods for edge detection and most of them are grouped in two categories, search-based and zero-crossing based. The search-based methods detect edges by first computing a measure of edge strength, usually a first-order derivative expression such as the gradient magnitude, and then searching for local directional maxima of the gradient magnitude using a computed estimate of the local orientation of the edge, usually the gradient direction.

The zero-crossing methods search for zero crossings in a second-order derivative expression computed from the image in order to find edges, usually the zero-crossings of the Laplacian or the zero-crossings of a non-linear differential expression. As a pre-processing step to edge

detection, a smoothing stage, typical Gaussian smoothing, is almost always applied. Smoothing results in noise reduction.

There are many edge detection methods and among all of them Canny Edge detector is the strongest and the most popular one. It is considered the optimal edge detector which means it marks as many real edges as possible in the image; the marked edges are as close as possible to the edge in the real image and a given edge in the real image is only marked once. The optimal edge detector should where possible not to create false edges from image noise.

3.2.2 Canny Edge detector

Canny in 1986 considered the mathematical problem of deriving an optical smoothing filter given the criteria of detection, localization a minimization of the number of responses to a single edge. His results were the optimal filter which for these assumptions is a sum of four exponential terms. His filter can be well approximated by first-order derivatives of Gaussians.
Given estimates of the image gradients, a search is carried out to determine if the gradient magnitude assumes a local maximum in the gradient direction. As an example, if the rounded angle is zero degrees the point will be consider to be on the edge if its intensity is greater than the intensities in the north and south directions, if the rounded angle is 90 degrees the point will be consider to be on the edge if its intensity is greater than the intensities in the west and east directions, if the rounded angle is 135 degrees the point will be consider to be on the edge if its intensity is greater than the intensities in the north east and south west directions, and finally if the rounded angle is 45 degrees the point will be consider to be on the edge if its intensity is

greater than the intensities in the north west and south east directions. This is work out by passing a 3x3 grid over the intensity map.

We tried to obtain the interface using different edge detectors and it was always the Canny Edge Detector which gave us the best results. It is consider an estate-of-the-art edge detector despite it was developed in the early days of computer vision.

3.2.3 Threshold

In order to determine the edges in a digital image, a threshold is applied to decide if the edges detected are the ones we are interested in. The lower the threshold, the more edges will be detected and the result will be increasingly susceptible to noise. In the other hand, a high threshold may miss subtle edges, or result in fragmented edges.

Appropriate thresholds are found by using thresholding with hysteresis. It begins by using the upper threshold to find the start of an edge. Once the start point is obtained, then the path of the edge through the image is traceable and the lower threshold is determined.

The pre-processing of the image in this work enhanced the brightness and contrast of the images to be analyzed which help in the detection of the interface. The threshold was adjusted to each image to get the least extra edges and get the best drop profile.

3.2.4 Edge Detection Routine

Once the images taken were enhanced two algorithms were developed to obtain the coordinates of the interface. Initially the cropped images were processed with a simple Matlab algorithm that used the canny edge detector and a given threshold. An example of the analysis is shown in Figure (3.2-1). This image is taken from the visual experiments. As we could see, the image on the right shows the drop profile, the substrate and part of the wall of the core holder as the detected edges.

To delete the extra edges obtained before we can get the coordinates of the interface, we had to use photo editors, and the whole procedure is analyzed in the next chapter. Once the only edge left on the image was the drop profile another Matlab algorithm gave us the coordinates of the drop profile and the apex of the drop.

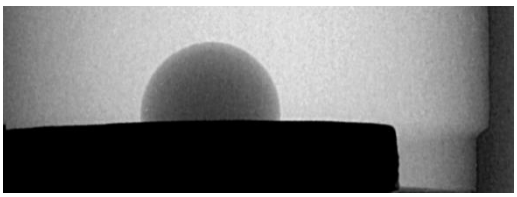

Cropped enhanced digital image

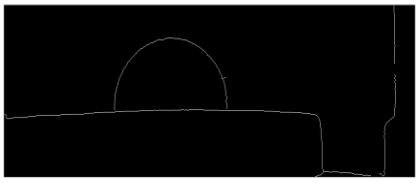

Edge detected by Canny Edge Detector

Figure 3.2-1: A Digital Image and its Edge detected by Canny Edge Detector

3.3 Design the appropriate cell that fits the necessities of the method chosen.

Several images were taking initially with the aluminum cell left from a previous research (Rajayi, 2010). The images helped to determine a better setup of the micro CT-Scanner to get better definition of the images and at the same time to start the analysis of the interfacial properties.

After several attempts to improve the definition of the image the best outcome obtain using the aluminum cell was not fulfilling our expectations which led us to see other possible materials to be used. The material used to make the core holder has to be transparent to X-rays so the system can be captured in an X-ray image. Plastics are transparent to X-rays and out of many different plastics, Plexiglas is cheap and transparent to our bare eye when the thickness is small which is helpful when we are placing the droplet on the substrate. Those advantages convinced us to make the core holder out of Plexiglas.

Figure (3.3-1) shows the Plexiglas cell place in the chamber of the micro CT-scanner. In essence, it is a cylinder of Plexiglas with a chamber at the top where the system is place. It has a base that fits precisely in the shaft coupling not allowing lateral movement. The chamber at the top of the cell has a cap made out of a closed fitting and can be tighten to isolate the system. The cell's body is high enough to avoid being lifted when we capture the images. The high was designed according to the magnification of the images we used.

We can also notice from Figure (3.3-1) the transparency of the cell. The new cell is easier to level and does not need to be moved to capture images. Once the design was made we took

more images to calibrate the micro CT-Scanner to the optimal condition and were able to obtained good quality images. We can see the cross section and top view of the micro CT cell on Figure (3.3-2).

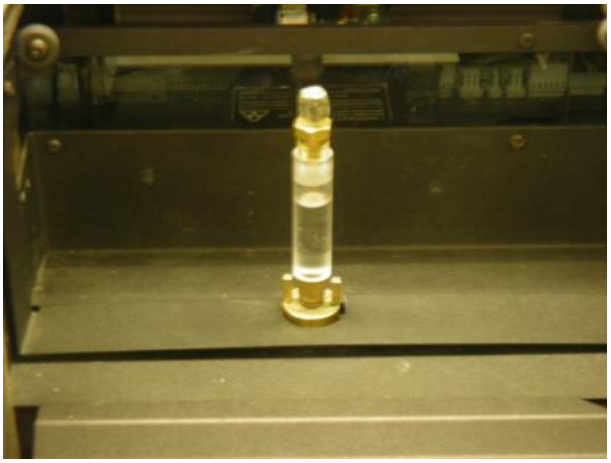

Figure 3.3-1: Plexiglas cell

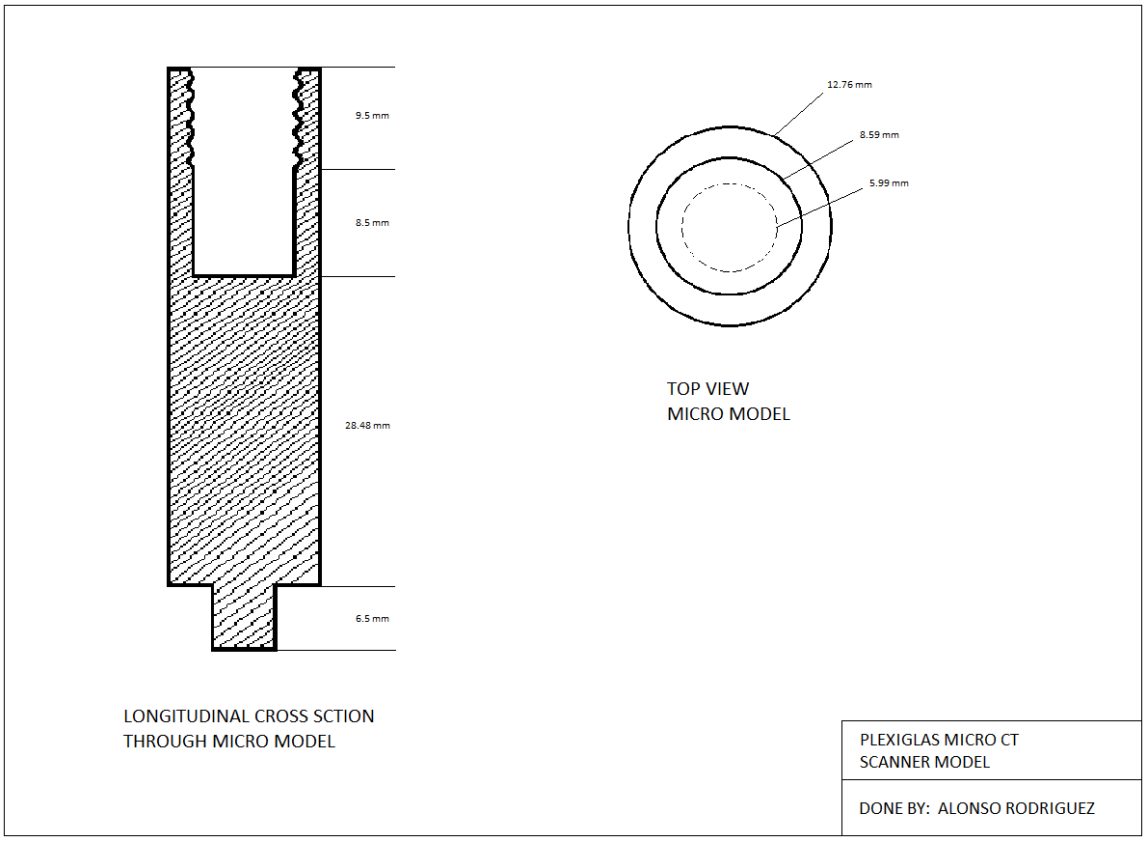

Figure 3.3-2: Plexiglas cell detail drawing

3.4 Finding the proper setup to maximize the image definition of the micro CT-Scanner

3.4.1 Micro CT Imaging

Computed Tomography (CT) Scanning or Computed Axial Tomography (CAT) Scanning is a radiological imaging technique initially developed and used by Hounsfield in 1972. The first application was in medicine and more recently CT-scanning has become routine procedure in geosciences, physics, petrophysics, reservoir engineering (Wellington *et al.*, 1987), and life sciences.

Micro CT-scanning was created to be able to analyzed smaller samples with high resolution. The technique is the same as the CT-scanning. The advantages of the CT-scanning technique to other imaging techniques are its rapidness, non-destructive visualization and accuracy in analysis of internal structure of materials. CT technology is very versatile and it is not restricted by the shape or the composition of the object being inspected.

In a micro CT-scanner, as well as a regular CT-scanner, by passing an X-ray beam, cross sections of a real three dimensional object are created that later can be used to recreate a virtual model of the internal structure without destroying the original model. In the micro CT-scanner model the best spatial resolution that can be reached is 5μm corresponding to near $1x10^{-7}$ mm^3 voxel size. An image of the micro CT-scanner device is presented in Figure (3.4-1) and its chamber in Figure (3.4-2).

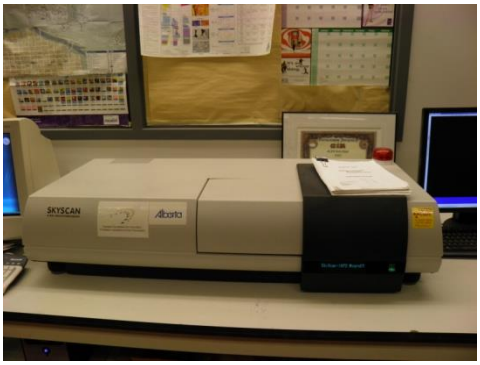

Figure 3.4-1: Micro CT-Scanner

Figure 3.4-2: Micro CT-Scanner's Chamber

There are two types of scanner setups. The micro CT-scanner setup of the one used in this project has stationary the X-ray source and detector during the scan while the object rotates. The scanner has four main variables that allow us to improve the image definition. These are the

voltage, electrical current, magnification of the image and exposure time to the X-rays. Several images were taking trying different combinations and the best set up was the maximum electrical current and voltage.

The magnification will depend on the system size and the exposure time on the type of system and type of material used to make the cell. In this work we used the same magnification for every experiment to avoid having to make different cell sizes. To get the best contrast between phases we decided to use air with water and air with decane. By using these components we could give the biggest differential in densities which help us to get a better contrast for the interface.

3.5 Finding the equilibrium time of the system

Preliminary experiments suggested the possibility of a time needed to reach the equilibrium in the system when placing a sessile drop on the substrate. The drop was made with a needle of small diameter and then carefully placed on the substrate. Despite the closeness of the drop to the substrate, moving it towards the substrate will cause some agitation on the drop. When we used bigger drop this effect was greater which made us believe we needed to establish the equilibrium time of the system.

The initial systems were air-water-quartz. We tried with several different volumes of water and the closed fitting was as tight as we could to try to isolate the system to avoid vaporization of the drop from the heat from the micro CT-scanner. Then, we decided to cut smaller the substrate so we could add some water on the surroundings of the substrate to help to saturate the air inside the

chamber of the cell and after trying with different drop sizes the water of the surroundings along with the drop were gradually evaporated.

We needed to try a system with a possible less vaporization or a possible easier way to control the vaporization. The best idea to this point was to use a liquid-liquid interface so we could control the vaporization of the external phase. We used decane-water-quartz; the drop was made of water and the external phase was decane which we poured up to the top of the chamber of the cell and the closed fitting was tightened. The result of this was a minimum vaporization of the decane which gave us enough time to analyze the possible changes the system could have with time. The results are shown in chapter five.

3.6 Keeping the cleanness of the substrate

Interfacial properties define the way substances behave in their interfaces. For our particular system we use liquid-liquid or gas-liquid on a solid substrate to create the interface necessary to determine the interfacial properties. The substrates have their own surface tension and when it is considerably high dirt or particles on the air can quickly be captured on their surface. The interaction of these particles with the liquid or gas phases can affect considerably the calculated values.

Interfacial tension can be determined using low surface tension substrates which are easier to keep clean; however, contact angles are the result of the interaction of the three phases present which in some cases where the substrate has high surface tension can be difficult to keep clean. The two substrates used in this work were quartz and quartz coated with teflon. To keep them as

clean as possible they were left in water for several days, rinsed every other day and dried with nitrogen every time we used them.

Chapter Four: Experimental Methodology

We considered the possible experimental methodology used in the previous work to start our preliminary set of experiments. There was no clear methodology and most of what we collected was the word of mouth from laboratory technicians who helped the student with the work.

4.1 Preliminary Experiments

Preliminary experiments were conducted using an aluminum cell designed for a previous research project (Rajayi, 2010). These experiments were of great importance to find the best setup of the micro CT-scanner to obtain high quality images and analyze the deficiencies of the equipment used.

Initially the focus was to obtain the best possible contrast in the images capture. To find the best setup for the micro CT-scanner we have to capture a great amount of images. The micro CT-scanner has many variables to improve the quality of the images taken, to consider each one of them could alter its system. The laboratory technician recommended playing with the four more influential variables.

Getting the best setup of the micro CT-scanner to capture images using an aluminum cell helped us to become more acquainted with the equipment which make easier to find faster the setup using cells of different materials. While the images were improving, it was apparent the changes in the shape of the droplets with time.

The system we have is not as stable as it is a solid piece of rock or any other material commonly analyzed with the micro CT-scanner. It is important to keep the aluminum cell levelled and the shape of it gave us a constant problem. The cell has a long base and a body that gets bigger at the top; this makes it very difficult to level. Besides, it is not as high as we need to be able to capture the system with the magnification we want to use, so we have to lift it. This analysis from the preliminary tests gives us the idea to design a new cell more stable and transparent to X-rays.

4.2 Procedure of the equilibrium time experiments

Preliminary experiments suggested there was an equilibrium time for the system since the images taken were showing a change in the contact angle. A main reason for this to happen was the constant movement the cell was exposed during the time it was in the micro CT-scanner's chamber. To avoid this, once the system was levelled the micro CT-scanner was left on.

In order to determine the equilibrium time of the system we run experiments for many days taking images every two hours to establish the time where the contact angle will not change. As a system we use decane-water on quartz. To keep the quartz as clean as possible the pieces were left in distilled water for over a month and every other day they were rinsed and put back in water. Before the piece was placed in the cell, it was dried with nitrogen. Once the substrate was in the cell a drop of water was carefully placed on it and immediately after the cell was filled with decane to avoid as much as possible the precipitation of dirt on the substrate. The cell was closed and the whole system was levelled in the micro CT-scanner's chamber. The equipment

allows moving the sample in any direction to take images of it but unfortunately this is only useful with solid systems.

Images were taken at the start of each experiment and after every two hours for the first experiment and every hour and a half for the remaining two. For each experiment 6 images were taking and an extra image from 90 degrees was taking to check on the level of the drop. The images were right away processed to keep track on the possible changes of the contact angle. The results from these experiments are shown in chapter five.

Each experiment was conducted using different volumes, and the volume injected was not controlled. To this point, we wanted to see the evolution of the system with time, determining the contact angle. These experiments gave us a hint about the possible influence of the drop size in the determination of contact angle and interfacial tension when we use the sessile drop shape method.

4.3 Calibration of the micro CT-scanner and software

The initial calibration of the micro CT-scanner was performed on the setup to obtain the best quality of images as we have mentioned at the beginning of this chapter. Once we were satisfied with the quality of the images a second calibration was performed in the equipment.

The second calibration was performed to check on the dimensions of the image we were taking. A sphere of known diameter was used to determine if the image taken represent the dimensions of the object. Initially the diameter of the sphere was determines using a caliper measurement

tool. The micro CT-scanner software allows us to see the last image taken and has an option that let us measure any distance inside the image. Using this option we could determine the diameter of the sphere from the image. The results are shown in Table (4.3-1). The diameter measured with the CT-scanner software and the diameter of the sphere measured with a caliper is very much the same. This result proved us that the images taken with the CT-scanner represent the analyzed system.

Table 4.3-1 Calibration measurements

Diameter of sphere with caliper measurement tool (mm)		**Diameter of the sphere from Image (mm)**	
Measurement	**Average**	**Measurement**	**Average**
5.93 5.96 5.95	5.95	5.93 5.97 5.96	5.95
		5.94 5.97 5.98	5.96
		5.95 5.92 5.97	5.94

Once the CT-scanner was calibrated the next step was to calibrate the software used to process the images. The images taken from a sphere of known dimension were processed to determine the interface or in this case to determine the sphere's profile. Using the profile detected we superimposed the processed image on the initial image. The profile detected fits perfectly on the original image.

The next stage in the calibration of the software was to determine if the contact angle calculated represent the contact angle the profile of the droplet creates with the substrate. This calibration was performed initially using the profile of the droplet capture by the edge detector from the equilibrium time experiments. Initially we compare the results obtained from the software with the contact angle from the image of the profile of the droplet obtained with the edge detector. By doing this we verify the contact angle calculated with the software represents the contact angle we can see from the image. The results were within a degree of difference. To keep on checking the results we decided to do this with every first image taken from every droplet.

4.4 General procedure of the experiments using the micro CT-scanner

From the experiments to establish the equilibrium time, we decided to design and build a new improved cell. Once we determined there were no substantial changes in the contact angle with time we decided to implement the new experimental procedure along with the analysis procedure to calculate the interfacial properties on water-wet, neutral, and oil-based substrate systems. An important observation form the determination of the equilibrium time was taken into account. The results from the equilibrium time set of experiments showed a difference in the value of the contact angle for Experiment 2 of about 7 degrees when we compare with the results from Experiment 1 and 3. This difference could have been the result of a cell not properly leveled and absence of symmetry of the droplet. A better control of the leveling process along with a more consistent review of the symmetry of the droplet was implemented in the next set of experiments to analyze the possible influence of the volume of the droplet in the determination of interfacial properties using the interface of a sessile droplet with the ADSA-P technique. Thus, we decided to create many droplets with volumes controlled by a syringe pump. The volumes chosen were

in the range a droplet could fit the size of the substrate. As last resource to improve the contrast of the images, we decided to use air as the surrounding phase.

Several attempts were made to create an axisymmetric droplet and, to keep it this way after the cell was levelled. To place the droplet on the substrate and keep it as spherical cap was not an easy task. Factors for this behavior are analyzed and discussed in chapter five. Once the droplet was in place the movement to level the cell in many occasions caused the deformation of the droplet.

Experiments were conducted using volumes of water from 3.5µL to 9µL increasing the volume by 0.5µL. For the system air-water-teflon 10 drops were analyzed for each volume, and seven images were taken from each drop; an extra image at 90 degrees was taken to analyze the shape and level of the drop. For the remaining systems 5 drops were analyzed for each volume, and seven images were taken from each drop; an extra image at 90 degrees was taken to analyze the shape and level of the drop. From the three systems a total of 1,680 images were analyzed.

4.4.1 Preparation of the experiments

Each experiment was conducted under the same setup of the micro CT-scanner. In the preliminary testing we determined the best setup to get the best quality of images as we discuss in the chapter three. However, the setup of the equipment had to be done again since the material of the new cell is Plexiglas. The cell was initially placed in the micro CT-scanner's chamber and levelled. The substrate was dried with nitrogen before it was placed in the cell and immediately the drop was placed on it. Once the system was in place the cell was closed to

avoid the precipitation of dirt on it. The micro CT-scanner's chamber was closed and the first images taken were to analyze the level of the system. Two images were taken, one at 0 degrees and other at 90 degrees. With these two images we were able to decide what to do to level the system. This could take between 4 minutes to 8 minutes where the micro CT-scanner's chamber was opened and closed as many time as necessary to get the cell levelled. Even though it may appears to be a considerable amount of time to level the system, the new design of the cell allowed as to make it faster.

The syringe pump was set to the same injection rate for every experiment. Initially the volume set to be dispensed was 3.5μL, and after the 10 experiments or drops for this volume were analyzed then a new volume was set until all the volumes were analyzed. This preparation took between 5 to 10 minutes and it was done for every drop.

4.4.2 Taking the images

The images taken at 0 and 90 degrees not only allow us to level the holder but also to see if the drop was axisymmetric in shape. If it was not then the drop was disposed and a new system was prepared.

Once the system was levelled, seven images were taken sequentially for each drop analyzed. The images were taken under the same conditions of voltage, electrical current, magnification of the image and exposure time to the X-rays. In the set of images on Figure (4.4-1) we could see the typical images captured from an experiment.

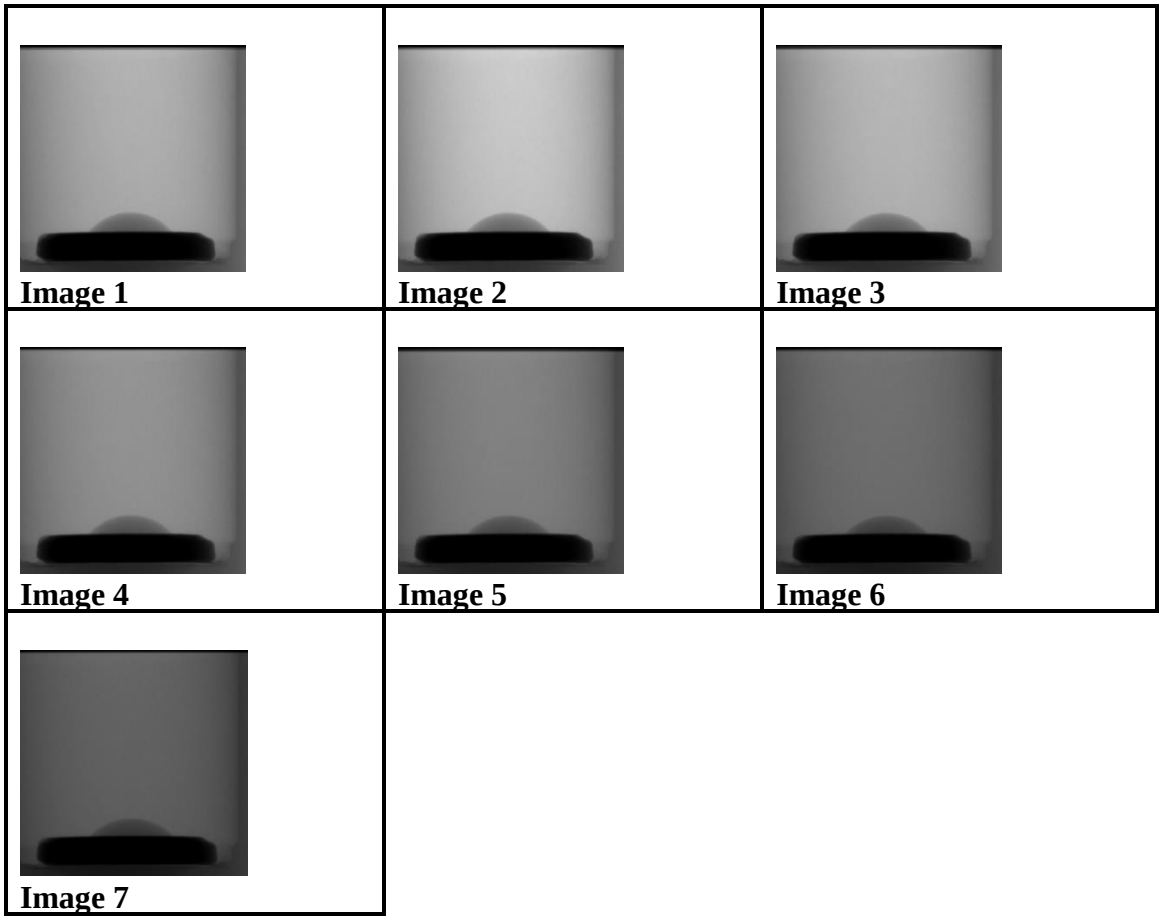

Figure 4.4-1: Initial Images "Air-Water-Quartz" Volume 4.5µl Drop 1

4.4.3 Image processing

The sequence of images from image 1 to image 7 shows differences in contrast and brightness which got worse with the sequence. This behaviour from the micro CT-scanner was experienced from preliminary experiments and even though we try to change the contrast and brightness in the equipment to obtain a better image, when we used the edge detector, the last images of the sequence gave us the worse results. The expected definition of the images is to be the same since the setup of the equipment was not changed during the time the images were taking. It took approximately 10 minutes to take the 7 images.

The images taken were analyzed to enhanced definition in different manners trying to improve the outcome from preliminary analysis. The best results were obtained using PhotoScape v3.5 photo editing software that enables to fix and enhance images. The time expended in each image was variable depending of the quality of it. It could be between 3 minutes and 10 minutes per image which give us a total of 21 to 70 minutes for each experiment. A typical result from the editor is the images shown in Figure (4.4-2).

The first analyzed system was Air-Water-Teflon. Initially, we decided to obtain the interface from images enhanced only with the photo editor using an edge detector. This could speed up the processing of the images. Currently, Matlab has the best edge detectors. Out of them the best one is the Canny edge detector.

The Canny edge detector is an edge detection operator that uses a multi-stage algorithm to detect a wide range of edges in images. In chapter three we covered the principles of this detector. The number of edges from an image capable of detect depends of a threshold given by the user.

To minimize the number of edges detected by the Canny edge detector we cropped the original image to a small image where only part of the substrate and the drop are seen and then we processed the images using a small algorithm developed for Matlab. The time expended to do this was approximately 10 minutes per experiment and the typical results were as show in Figure (4.4-3).

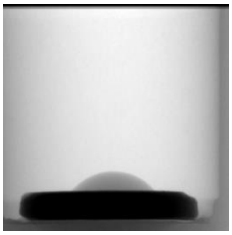

Image 1

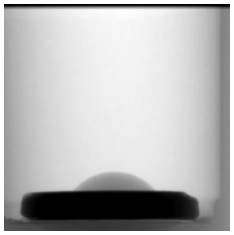

Image 2

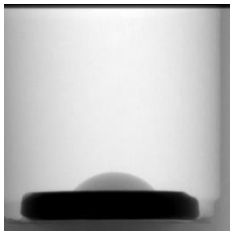

Image 3

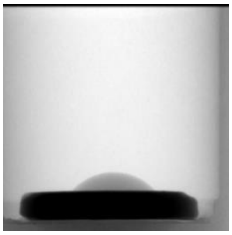

Image 4

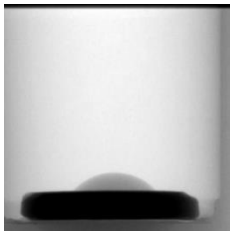

Image 5

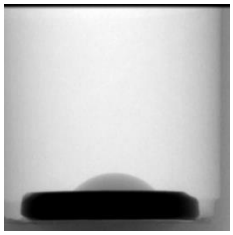

Image 6

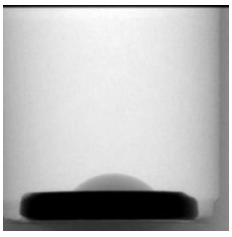

Image 7

Figure 4.4-2: Enhanced images "Air-Water-Quartz" Volume 4.5µl Drop 1

Image 1

Image 2

Image 3

Image 4

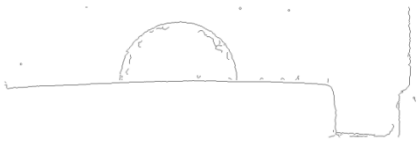

Image 5

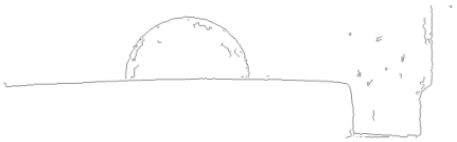

Image 6

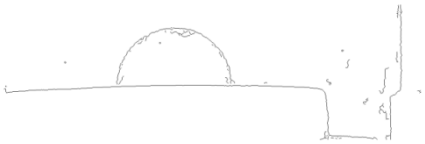

Image 7

Figure 4.4-3: Canny edge detector results: "Air-Water-Teflon" Volume 4.5µl Drop 2

In the sequence of images on Figure (4.4-3) we can notice the main edges of the image which are the drop profile, the substrate and the wall of the cell. In the sequence we can also notice the

appearance of noise as edges as well as the deterioration of the drop profile. This could be the result of the lower quality in the initial images taken considering that all of the images were taken under the same conditions we could think about a malfunction of the equipment.

With PhotoScape, we were able to generate digitally a better definition of the images however this does not completely help when we use an edge detector. To continue the processing of the images we had to erase all the edges that are not part of the interface; this was done using Paint which is a simple photo editor. To eliminate all the unnecessary edges the time varies from 4 minutes to 10 minutes depending of the complexity of the work as we can see in the above images.

The Canny edge detector was used directly after the images were enhanced with PhotoScape for the system “air-water-teflon”; to try to get better interfaces we decided to manually enhanced the interface to take the most of the enhancing work done by the PhotoScape. This was done for the systems “air-water-quartz” and “air-decane-teflon”. The typical results of this analysis are shown in the Figure (4.4-4).

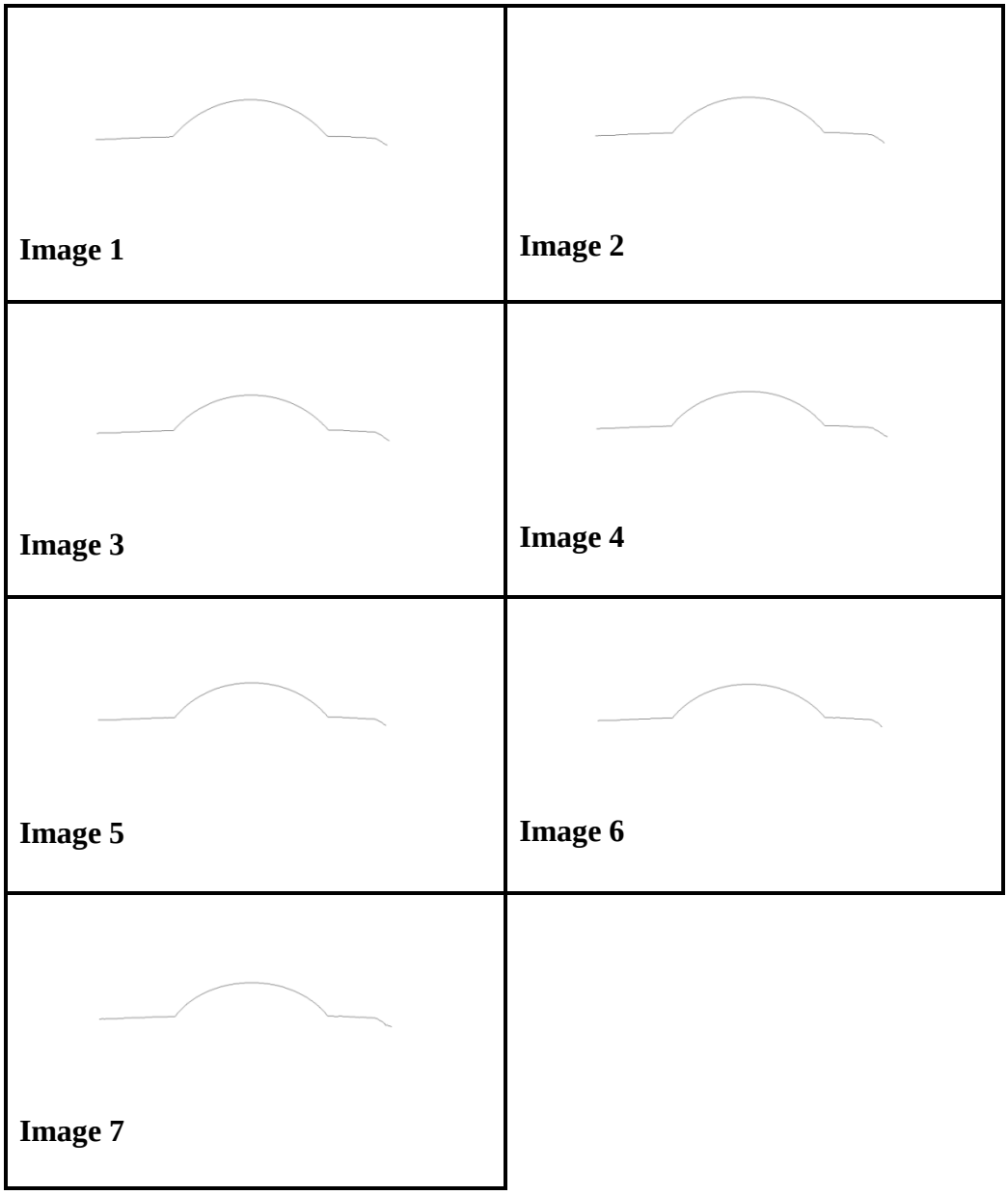

Figure 4.4-4: Visually Marked Interface "Air-Water-Quartz" Volume 4.5µl Drop 1

From these results we can see a much better interface and less noise in the image. The noise was reduced by having a more defined interface which allows us to use a higher threshold. With this we gained definition in the interface but we added considerable time to the image processing. To each experiment we expended about 10 more minutes.

Once the interface was determined we used another Matlab algorithm to obtain the coordinates of the interface and the apex of the drop so we can apply the ADSA-P technique to determine the interfacial tension and contact angle of each experiment. The ADSA-P technique was programmed in Visual Basic as a macro to an excel spreadsheet. To each experiment it took approximately 20 minutes to get the values of the interfacial tension and contact angle of the 7 images.

Once the images were processed and the data computed we try to analyze the possible dependence of the interfacial tension and contact angle from the volume used when we calculate these properties using the Sessile Drop Method. This method is commonly used to calculate contact angles but there is not much information on being used to calculate interfacial tension. Most of the work done to calculate interfacial tension with drop shape methods has been done with the Pendant Drop Method which is considered very reliable. In our case, the equipment does not allow us to prepare experiments using this method due to lack of space, and the system has to be completely isolated to take images.

The initial results for interfacial tension were spread out when we plotted Interfacial Tension *vs* Volume. Thus, we decided to compare the profiles of the drops made with the same volume. To do this we used Adobe Photoshop 7 which is graphics software that enable user to manipulate visual images. Initially we superimposed the first image taken of a drop with the other first images taken from the other drops from the same volume. After we did that we found different sizes of droplets even though we calibrated the syringe pump to dispense the same amount of volume. The real volumes of the droplets have to be calculated based on the profile of the

droplet. To calculate the real volume we assumed the droplet shape is a spherical cap which is what we have as the axisymmetric sessile drop. Once we corrected to the experimental volume, new plots were generated and the results are discussed in the next chapter.

4.5 Description of developed routines

Once the images were enhanced, a file was created for each image. A routine in Matlab was developed to use the Canny Edge detector. This routine loads the files containing the images one at the time. The loading is done manually changing the name of the file in the code. The routine is run and an image of the profile of the droplet is obtained. Depending of the number of edges detected we can manually change the threshold in the code to minimize the detected edges and run the routine once again. Once we obtain the best interface, a new file is recorded with the interface. The images recorded would look like the images show in Figures (4.4-3) and Figure (4.4-4).

The best detection will show the interface and the substrate as the only edges. To make sure the only edge on the image is the interface, we manually deleted the substrate and the rest of the edges detected using Paint photo editor.

The improved interface files are now brought to another Matlab routine which was developed to obtain the coordinates of the interface and the apex of the interface. Once again this procedure is done loading the files one at the time. The loading is done manually changing the name of the file in the code.

While we are obtaining the coordinates and apex of the interface we have an excel spreadsheet with the macros to calculate the contact angle and interfacial tension. The matrix containing the coordinates of the interface and the variables containing coordinates of the apex are copied to the spreadsheet. This is done for each image.

The coordinates of the interface are organized from left to right. The list of points starts with the coordinate of the contact point at the left of the interface and finishes with the contact point at the right of the interface.

Once the coordinates are copied to the excel spreadsheet it is necessary to load the starting values of the parameters q_1, q_2, q_3, and q_4. As it was explained in chapter two, the starting values are q_1 the x coordinated of the apex, q_2 the z coordinate of the apex, q_3 the radius which is calculated according to the profile of the drop. In our case we calculated the starting value as the radius at the contact point. q_4 is 0. The latter statement means we will start from a circular shape Laplacian curve with the apex located at the apex of the experimental curve.

To run the macros the active cell has to be the first value of the x coordinates which is the x coordinate value of the contact point. In the spreadsheet there are two values for the four parameters; one is for the starting values and the other for the optimized values. Before start the calculations these values are the starting values. Microsoft Excel Solver will change these values while is finding the optimal Laplacian curve.

There are some others variables that are self-explanatory such as the difference in density between the phases, the gravity, and the length of a pixel in mm which depends on the magnification used when we took the X-ray images. This can be found on the screen associated with the micro CT-scanner during the time we take the images. The code for these algorithms and macros is reported as Appendix A.

Chapter Five: Results, Discussion and Error Analysis

5.1 Equilibrium Time

Three different experiments were run to determine the time needed to reach the equilibrium of the system. Each experiment was conducted with quartz plates and for each experiment we used a different plate. The volume used in each experiment was dispensed with a regular syringe; the volume was calculated using the mathematical equation for a spherical cap, which is the shape of an axisymmetric sessile drop.

The first experiment was run for 48 hours, and images were taken every 2 hours. A set of 6 images were taken from the position 0^o every time and one extra image was taken from 90^o to analyze visually the shape of the drop. The results of this experiment are shown in Figure (5.1-1).

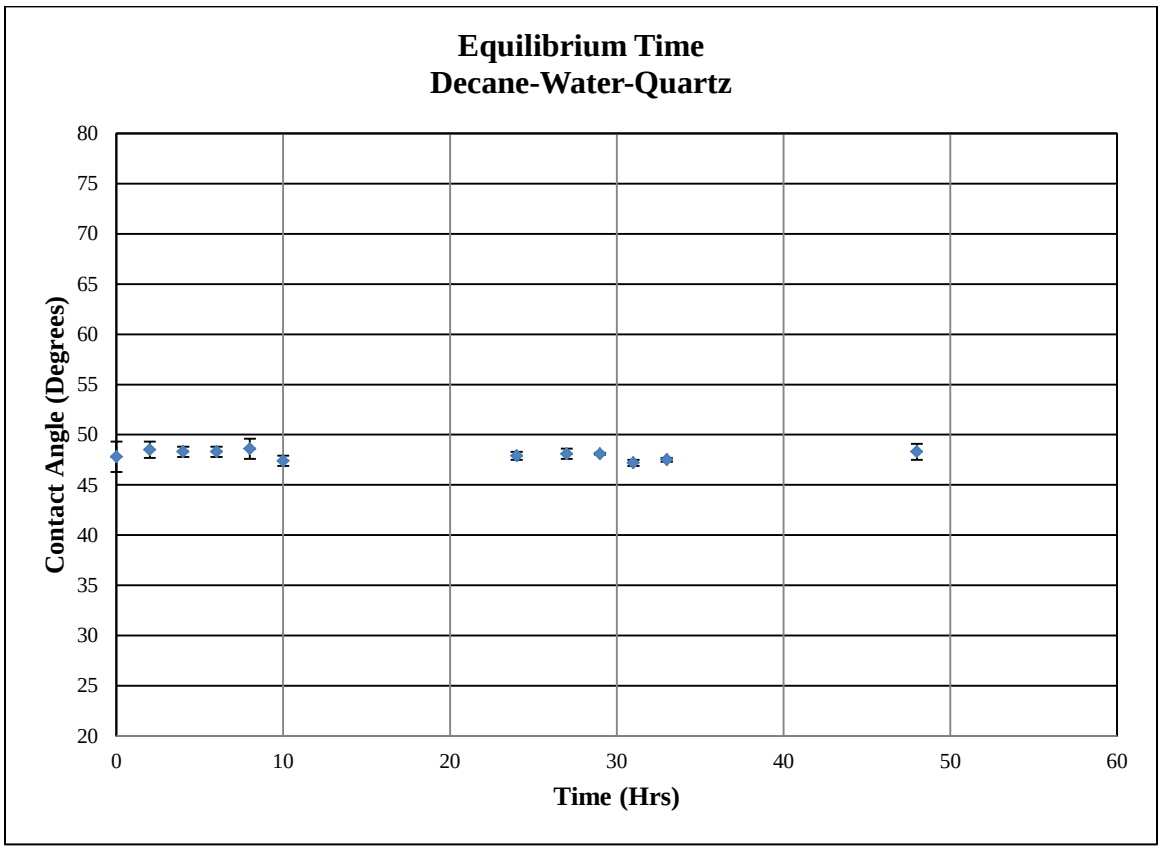

Figure 5.1-1: Decane-Water-Quartz Contact Angle Equilibrium Time – Exp. 1

5.1.1 Analysis of the results Experiment 1

Each point in the Figure represents a set of images taken and its standard deviation. The results show a variation between the first images taken and the last images taken of less than 3 degrees. The contact angle has a minimum variation during the time the experiment was run.

Most of the deviation from each set of images comes from the images taken last. In Table (5.1.6-2) we have the calculated values after the images were digitally processed. Each image was taken with the exact same setup of the micro CT-scanner and their definition was getting worse with the sequence. These could have account for the variation of the calculated values.

The processing of these images had to be manually enhanced. Images with lower definition were not possible to get a good drop profile using only the edge detector. These images contained more noise and a possible misplacing of the drop profile. They were hard to manually enhance the interface which could account for more error.

Since the change in the contact angle with time was not significant, we decided to run a second experiment during a shorter period of time. For the second experiment we used different piece of substrate.

5.1.2 Normality test analysis experiment 1

The normality test was performed using the normal probability plot method and the Anderson-Darling method. The Anderson-Darling method uses the values of A-squared, *p*-value and critical values at 95% and 99%. The results are shown in Table (1.1.6-1) for the three experiments and the normal probability plot method for the experiment 1 is shown in Figure (5.1-2).

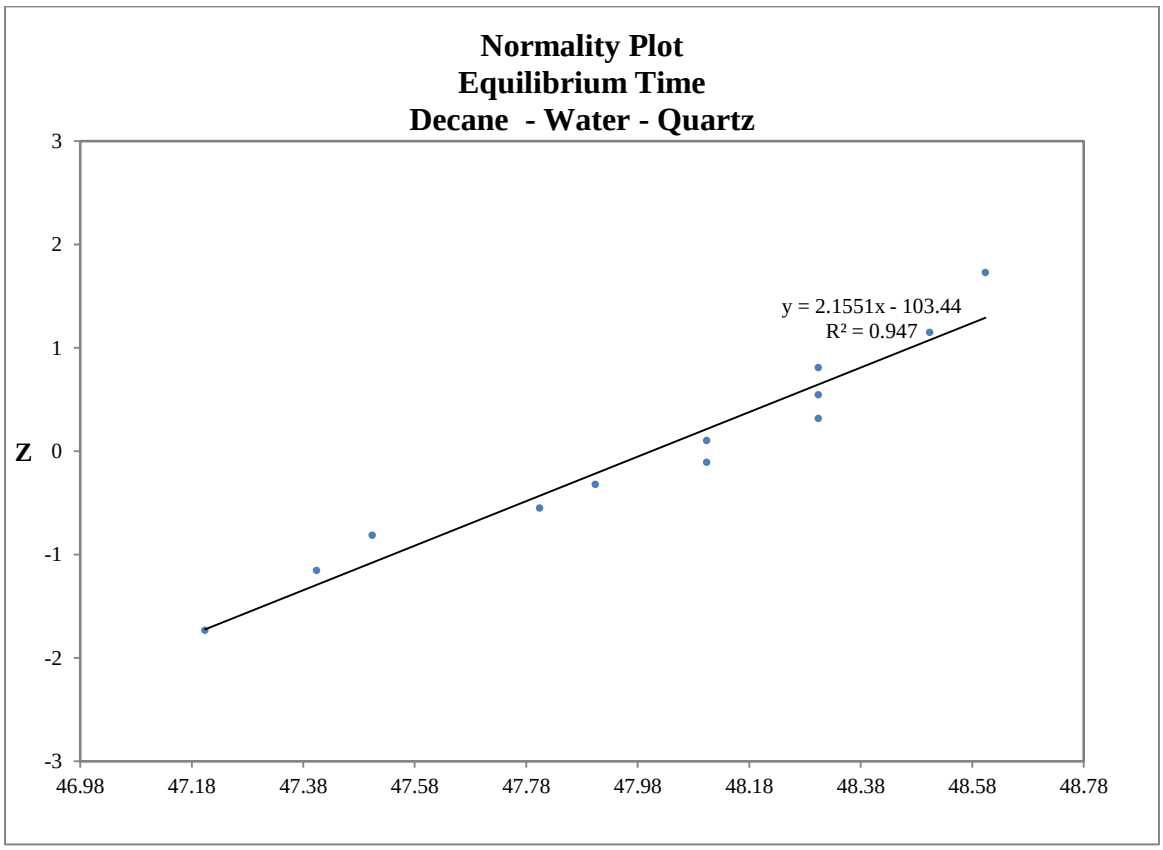

Figure 5.1-2: Decane-Water-Quartz Z normality test – Exp. 1

The Anderson-Darling method uses the null hypothesis for the data being normal. It states that the data is normal if p >= alpha (level of significance) or if the A-squared value is smaller than the critical values. The results from Table (1.1.6-1) for experiment 1 show a *p*-value of 0.427 which is bigger than 0.05 and an A-squared value of 0.343 which is smaller than the critical value at 95% which is 0.787 and at 99% which is 1.092. These mean we can be at least 99% confident that the data is normally distributed.

From Figure (5.1-2) we can observe the data is fairly normal distributed around the straight line which confirms what was calculated using the Anderson-Darling method.

The second experiment was run during 24.5 hours, and images were taken every 1 and a half hours. A set of 6 images were taken from the position 0^o every time and one extra image was taken from 90^o to analyze visually the shape of the drop. The results of this experiment are shown in Figure (5.1-3).

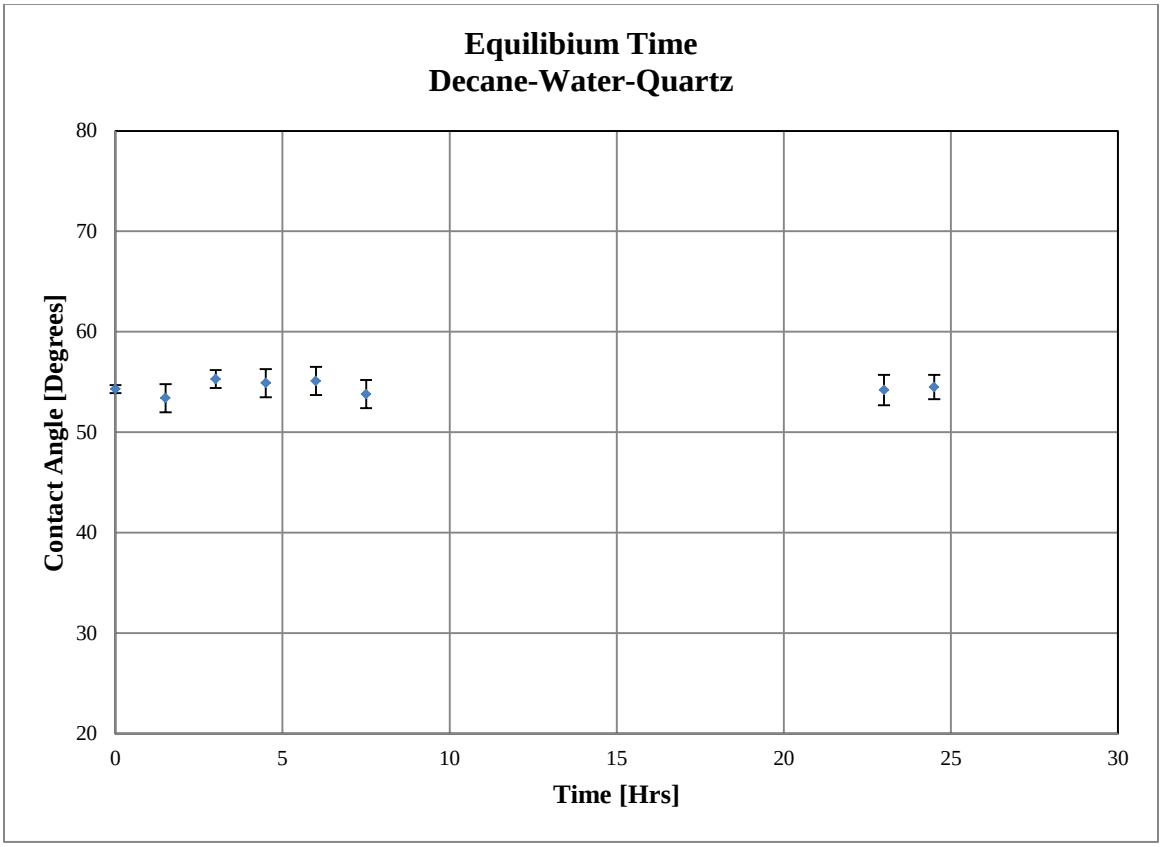

Figure 5.1-3: Decane-Water-Quartz Contact Angle Equilibrium Time – Exp. 2

5.1.3 Analysis of the results Experiment 2

Each point in the Figure represents a set of images taken and its standard deviation. The results show a variation between the first images taken and the last images taken of less than 3 degrees. The contact angle has a minimum variation during the time the experiment was run.

During this experiment we observed a minimum change in the contact angle value. However, the value of the angle was around 7 degrees bigger than the one calculated from the experiment 1. This could have been because to this point we were not meticulously controlling the symmetry of the droplets. We were more interested in the changes of the contact angle with time. This observation helped us to improve setup in the following experiment for the equilibrium time and for the three systems later analyzed. The volume used in this experiment was bigger than in Experiment 1. Overall, the distribution from each set of images was worse than the one obtained for Experiment 1. This could be the result of getting lower definition of images from the micro CT-scanner. The calculated values are shown in Table (5.1.6-2).

The contact angle is defined as function of the interfacial tensions of the phases present; Equation (2.11). This means, the value should be only one for each system. Another possible explanation for the difference in the value of the contact angle calculated in experiment 2 comparing with experiment 1 could have been a minimum inclination of the quartz plate. Since we were only interested in the equilibrium time we did not expend too much time leveling the system. This observation helped us to improve our setup in the following experiment for the equilibrium time and for the three systems later analyzed. Another possible explanation to these results was the presence of dirt and possible hydrophilic patches on the substrate.

The equilibrium was again reached very rapidly. A new experiment was run with a volume similar to the one used in experiment 1. For the third experiment we used different piece of substrate.

5.1.4 Normality test results analysis experiment 2

The normality test was performed using the normal probability plot method and the Anderson-Darling method. The results are shown in Table (1.1.6-1) for the three experiments and the normal probability plot method for the experiment 2 is shown in Figure (5.1-4).

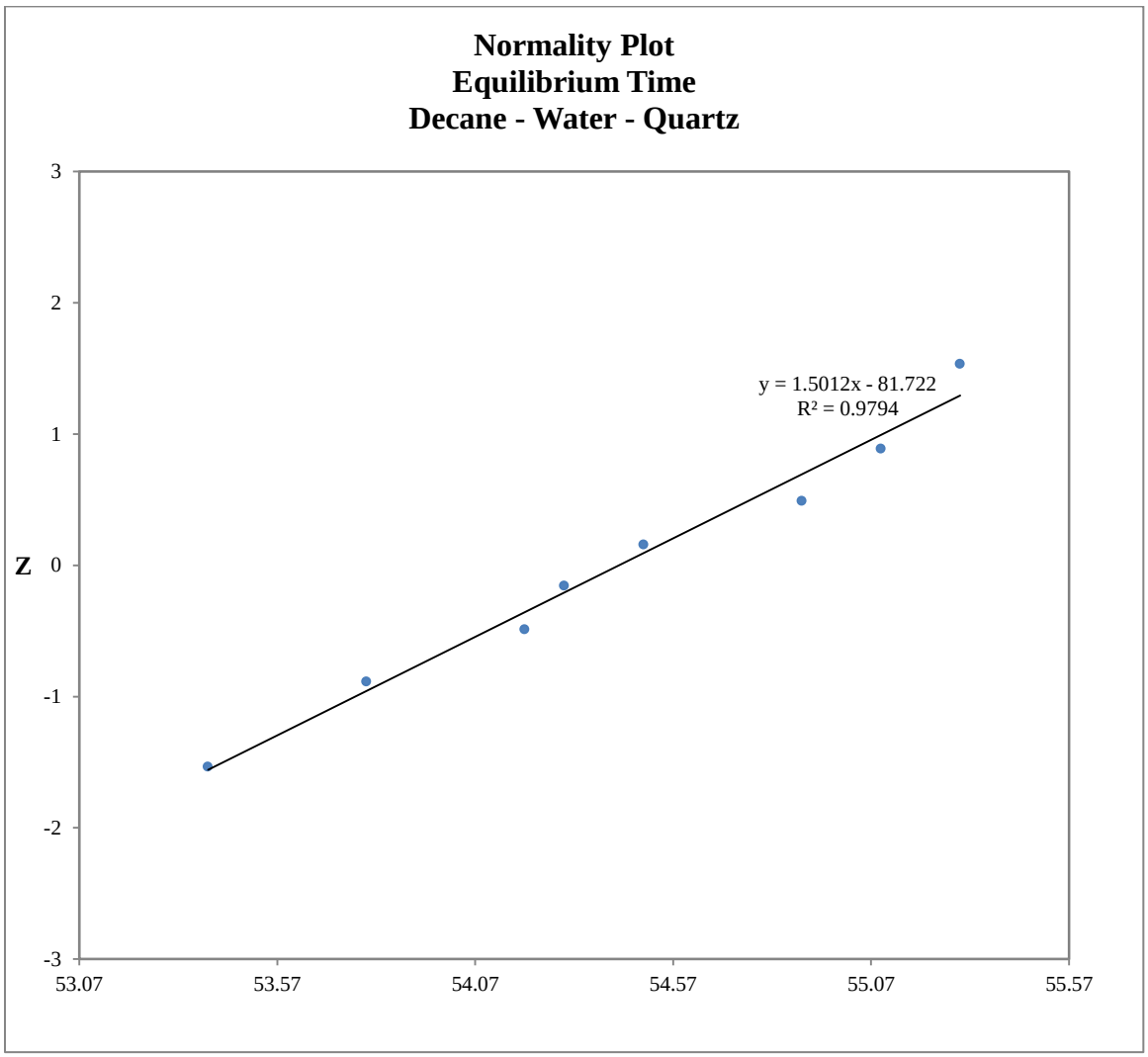

Figure 5.1-4: Decane-Water-Quartz Z normality test – Exp. 2

The results from Table (1.1.6-1) for experiment 2 show a *p*-value of 0.920 which is bigger than 0.05 and an A-squared value of 0.158 which is smaller than the critical value at 95% which is 0.787 and at 99% which is 1.092. These mean we can be at least 99% confident that the data is normally distributed.

From Figure (5.1-4) we can see the data is fairly normal distribute around the straight line which confirms what was calculated using the Anderson-Darling method.

The third experiment was run during 9 hours, and images were taken every 1 and a half hours. A set of 6 images were taken from the position 0^o every time and one extra image was taken from 90^o to analyze visually the shape of the drop. The results of this experiment are shown in the Figure (5.1-5).

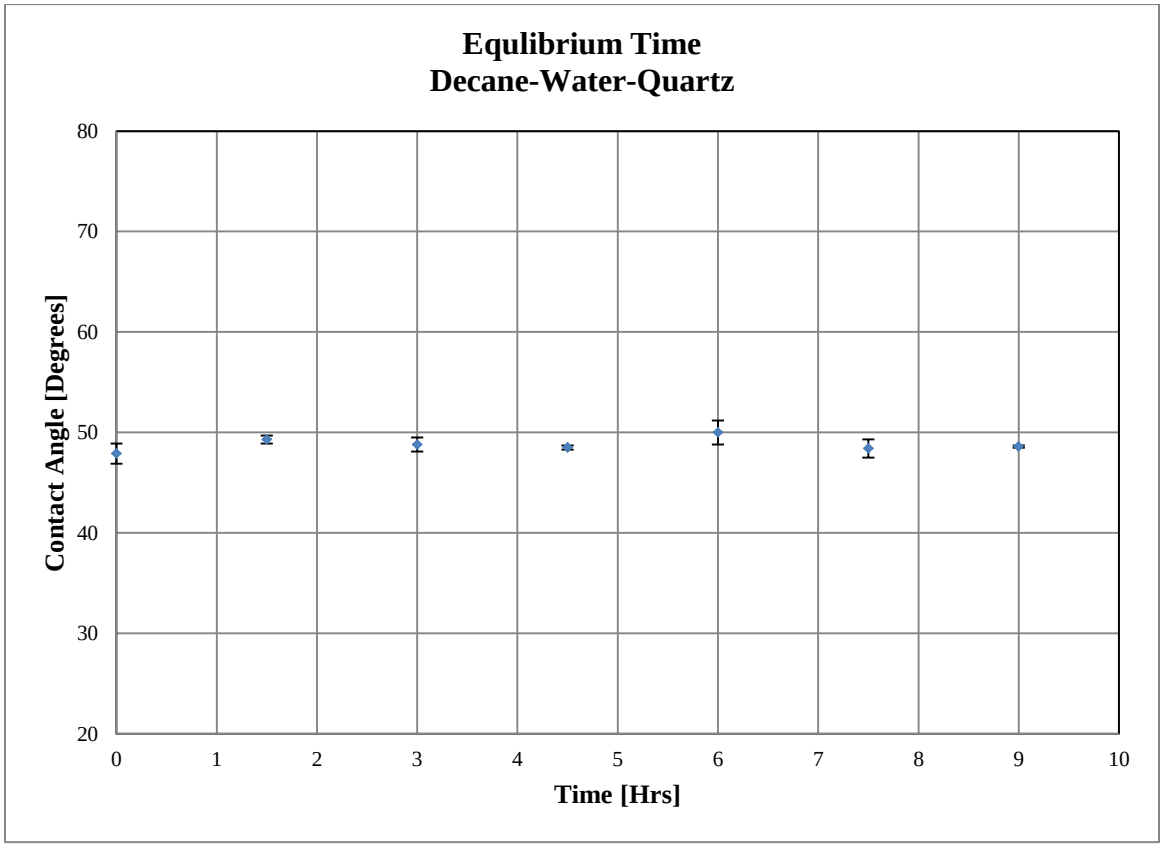

Figure 5.1-5: Decane-Water-Quartz Contact Angle Equilibrium Time – Exp. 3

5.1.5 Analysis of the results Experiment 3

Each point in the Figure represents a set of images taken and its standard deviation. The results show a variation between the first images taken and the last images taken of less than 3 degrees. The contact angle has a minimum variation during the time the experiment was run.

During this experiment we observed a minimum change in the contact angle value. The value of the angle was close to the value calculated on experiment 1. The calculated values are shown in Table (5.1.6-2).

From the three experiments the equilibrium time have been reached immediately after the system has been placed. The contact angle values for experiment 1 and 3 are fairly similar and experiment 2 shows a value of around 7 degrees higher. We can conclude from the equilibrium time experiments that it is very important to keep the system as level as we can to minimize the changes in the contact angle value. Another important conclusion from the equilibrium time experiments is the necessity of a better control during the formation of the droplet. It is very important the droplet is axisymmetric otherwise the contact angle calculated depends on the angle the X-ray image is taken. The influence of the volume in the contact angle observed when comparing experiment 1 and 3 with experiment 2 makes us consider to take into account these observations and set up for the next set of experiments a better control of the volume injected to analyze the possible influence on the contact angle.

5.1.6 Normality test results analysis experiment 3

The normality test was performed using the normal probability plot method and the Anderson-Darling method. The results are shown in Table (1.1.6-1) for the three experiments and the normal probability plot method for the experiment 3 is shown in Figure (5.1-6).

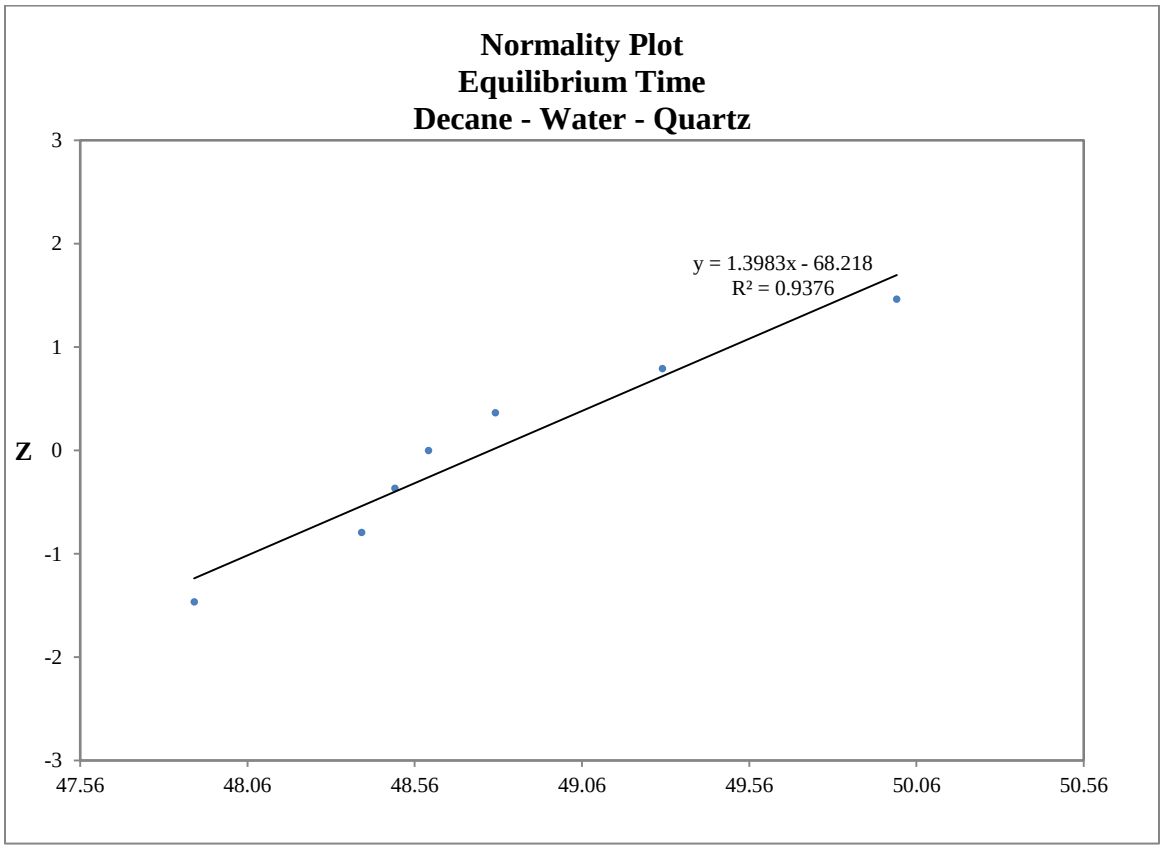

Figure 5.1-6: Decane-Water-Quartz Z normality test – Exp. 3

The results from Table (1.1.6-1) for experiment 2 show a p-value of 0.518 which is bigger than 0.05 and an A-squared value of 0.284 which is smaller than the critical value at 95% which is

0.787 and at 99% which is 1.092. These mean we can be at least 99% confident that the data is normally distributed.

From Figure (5.1-6) we can see the data is fairly normal distribute around the straight line which confirms what was calculated using the Anderson-Darling method.

Table 5.1-1: Air-Water-Quartz normality test results equilibrium time

Experiment	**A-Squared**	***p***	**95% Critical Value**	**99% Critical Value**
Experiment 1	0.343	0.427	0.787	1.092
Experiment 2	0.158	0.920	0.787	1.092
Experiment 3	0.284	0.518	0.787	1.092

Table 5.1-2: Air-Water-Quartz Contact Angle equilibrium time

Experiment	Time (Hrs)	Contact Angle (Degrees)	Standard Deviation (Degrees)
Experiment 1	0	47.8	1.5
	2	48.5	0.8
	4	48.3	0.5
	6	48.3	0.5
	8	48.6	1
	10	47.4	0.5
	24	47.9	0.4
	27	48.1	0.5
	29	48.1	0.1
	31	47.2	0.3
	33	47.5	0.2
	48	48.3	0.8
Experiment 2	0	54.3	0.4
	1.5	53.4	1.4
	3	55.3	0.9
	4.5	54.9	1.4
	6	55.1	1.4
	7.5	53.8	1.4
	23	54.2	1.5
	24.5	54.5	1.2
Experiment 3	0	47.9	1
	1.5	49.3	0.4
	3	48.8	0.7
	4.5	48.5	0.2
	6	50	1.2
	7.5	48.4	0.9
	9	48.6	0.1

5.2 Analysis of the results for water-wet, neutral and oil-based substrate systems using all the data collected

To establish the use of X-ray micro imaging in determining interfacial properties; three systems were analyzed; a water-wet system air-water-quartz, a neutral system air-water-teflon and an oil-

based substrate system air-decane-teflon. The three systems were processed using two procedures. The first procedure uses the edge detector directly from the enhanced images and the second procedure we redefined the interface after the initial image was enhanced and then the edge detector was used. The latter procedure adds time to the analysis but gives a better interface.

5.2.1 Neutral system

As a neutral system we used air-water-teflon. Air and water have a high density difference which helps us to obtain a better differentiated interface on the X-ray images. Furthermore, the images will have less noise making them easier to process. The Teflon surface is a piece of quartz coated with a 2 mm film of teflon. The coating was done by Topgun a specialized coating company. Teflon is a chemical compound with a very low surface tension which makes it more suitable to measure the interfacial tension of water. The teflon substrates were kept in water for some weeks. The substrate piece chosen was analyzed carefully with a magnifying lens.

The experiments were conducted using volumes from 3.5µL to 9µL to create the water droplet. The volume was increased by 0.5µL to work with a total of 12 volumes. To control the injected volume we used a syringe pump. The rate of injection was kept constant for all volumes. For each volume we worked with, 10 droplets of water were analyzed. A total of 120 droplets of water were analyzed. The setup of each droplet of water was the same. The substrate was carefully dry with nitrogen and placed in the cell, the syringe pump dispensed the volume and the droplet created at the tip of the needle was slowly placed on the substrate. Then the cell was closed. Before a droplet was placed, the cell was levelled. This procedure was done every day

when we had to re-start the micro CT-scanner. Sometimes it was done more than once a day because after some hours of operation the micro CT-scanner gave bad quality images. To solve this we had to turn off the equipment for two hours or in some cases start fresh the next day.

For each droplet of water 8 images were taken; 7 from 0^o angle and 1 from 90^o. The latter image was taken to visually control the symmetry of the droplet. Any droplet with no symmetry was disposed and a new droplet was placed. The images were taken immediately after the micro CT-scanner was ready. A total of 840 images were digitally processed to obtain the interface. The results of contact angle calculated are presented in Figure (5.2-1).

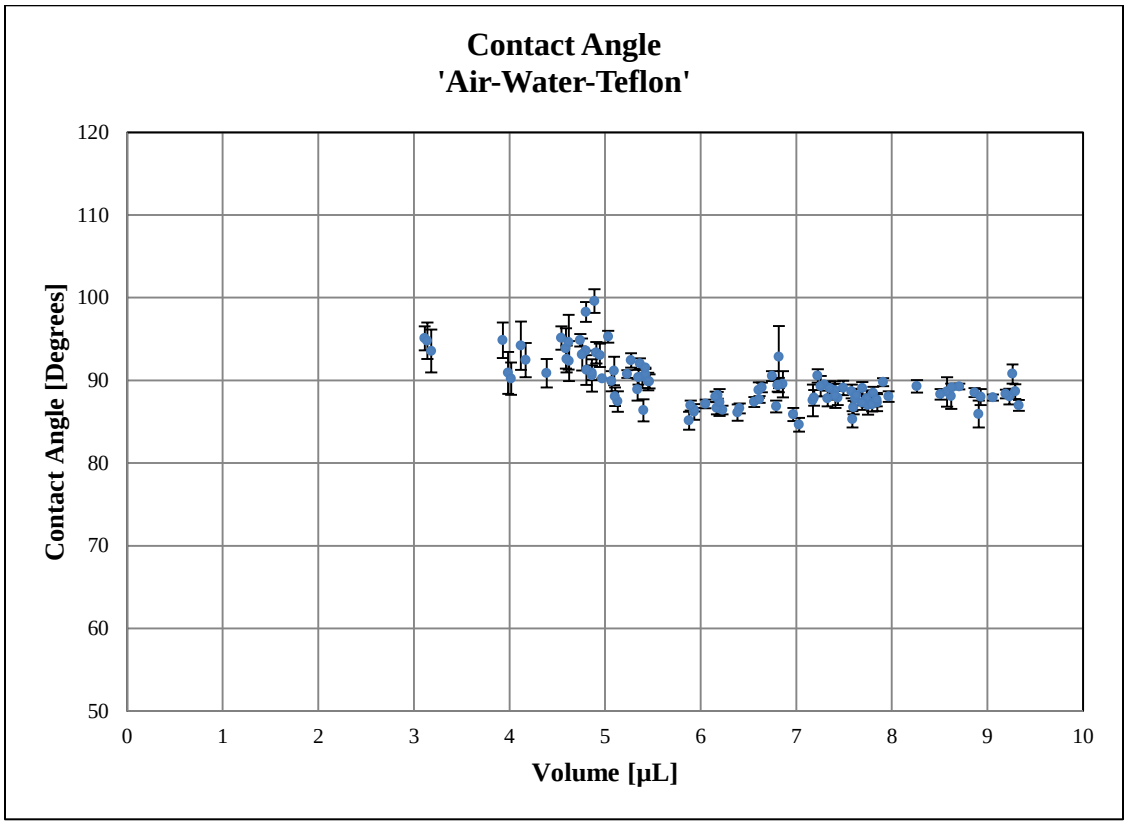

Figure 5.2-1: Air-Water-Teflon Contact Angle

5.2.1.1 Analysis of the results for Contact Angle in Neutral system

Each point in Figure (5.2-1) represents the calculated mean of the contact angle for a droplet of water and its standard deviation. These calculations are from seven images taken of each droplet. The processing of each image was done in the same manner; the definition of the image was enhanced using PhotoScape, after this the image was cropped to minimize the number of possible edges the edge detector could find. The smaller image was then analyzed with a routine developed for Matlab which uses the Canny Edge detector and the profile of the droplet along with others edges were found. A manual deleting of the edges not representing the interface was conducted using Paint and a final image containing only the droplet profile was process in another routine developed for Matlab to obtain the coordinates of all of the points of the whole interface. This procedure could be considered semi-automatic since the process is done with different software; it is the fastest way to process images to obtain the interface. However, the interface detected in some cases is not a continuous curved line as we can see from chapter four, Figure (4.3-3).

From Figure (5.2-1) we can observe a considerable standard deviation for droplets in the region from 3.5µL to 5.5µL; the standard deviation for each droplet decreases when the volume injected to create the droplet increases. We can also observe a bigger fluctuation on the values of the contact angle when the volume of the droplet is less than 5.5µL; the values obtain for this region are over 90 degrees. Over 6µl the contact angle values are less scattered and with the increasing of the volume they tend to be of a constant value. The main possible reasons for this behaviour are roughness of the substrate, dirt on the substrate, effect of tension lines and poor definition of the images.

The effect of the surface roughness on contact angles have been treated theoretically during the past several decades. However, the models proposed to understand how the surface roughness affect the apparent or macroscopic contact angle are based on predetermined patterns of the roughness which does not represent well the complexity of the real surfaces and the geometry of the three-phase contact line. Results from predetermine patterns models show most of the time repeatability in the variation of the contact angle, it is like a constant pulse. This suggests whenever we do not have patterns we should have scattered values of the contact angle. In our results the contact angle has a tendency to a constant value with the increase of the droplet size which implies the variation given specially at low volumes is not the result of the influence of the roughness.

The substrate on this set of experiments was a piece of quartz coated with teflon which has a considerably low surface tension. Low surface tension solids capture less amount of dirt on their surfaces making them easier to keep them cleaned. We can conclude that the influence on the contact angle of the dirt capture on the surface of the substrate for these experiments is negligible.

During the capturing time of the images, we observed in most of the sequences that the images taken at the end were lower in contrast and higher in brightness. We experience this behaviour sometimes since the beginning of the sequence when we have worked for a considerable amount of time. The micro CT-scanner was setup at the same conditions every time we capture images which suggest a malfunction of the equipment. During the processing time of the images,

images with lower quality were enhanced digitally to a good contrast and brightness level. However, the edge detector routine gave a lot of edges and the interface was not a continuous line. The noise detected as edges could also alter the droplet profile causing the method to calculate different contact angles. The same manner, the standard deviation from each droplet is bigger when the images start to get worse on the sequence. This analysis made us conclude that the strongest influence in the variation of the contact angle values is the low quality of the images obtained with the micro CT-scanner.

The results for the neutral system shows a contact angle between 90 and 98 degrees for volumes between 3.5µL to 5.5µL and values around 88 degrees for volumes over 6 µL. We could consider this as the cause of the increasing of the hydrostatic pressure when the volume increases affecting the contact angle. However, to be certain with this consideration, we need to have images with better contrast, especially when the droplets are small.

5.2.1.2 Normality test results for Contact Angle in Neutral system

The normality test was performed using the normal probability plot method and the Anderson-Darling method. Since there are two regions on Figure (5.2-1) the normality test was run considering them. The results are shown in Table (5.2.1-1) for the three experiments and the normal probability plot method for the experiment 1 is shown in Figure (5.2-2) and Figure (5.2-3).

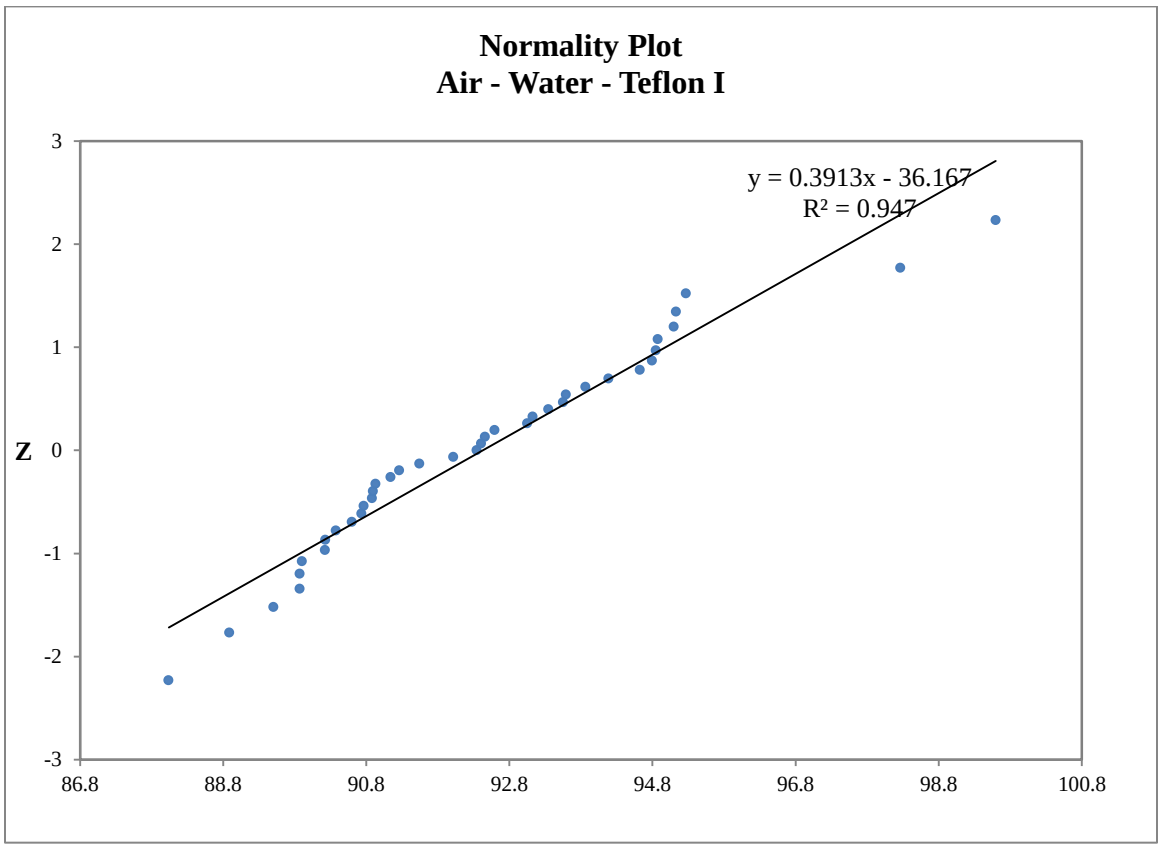

Figure 5.2-2: Contact Angle Air-Water-Teflon Z normality test I

The results from Table (5.2.1-1) for region I show a *p*-value of 0.124 which is bigger than 0.05 and an A-squared value of 0.578 which is smaller than the critical value at 95% which is 0.787 and at 99% which is 1.092. These mean we can be at least 99% confident that the data is normally distributed.

From Figure (5.2-2) we can observe the data is fairly normal distribute around the straight line which confirms what was calculated using the Anderson-Darling method.

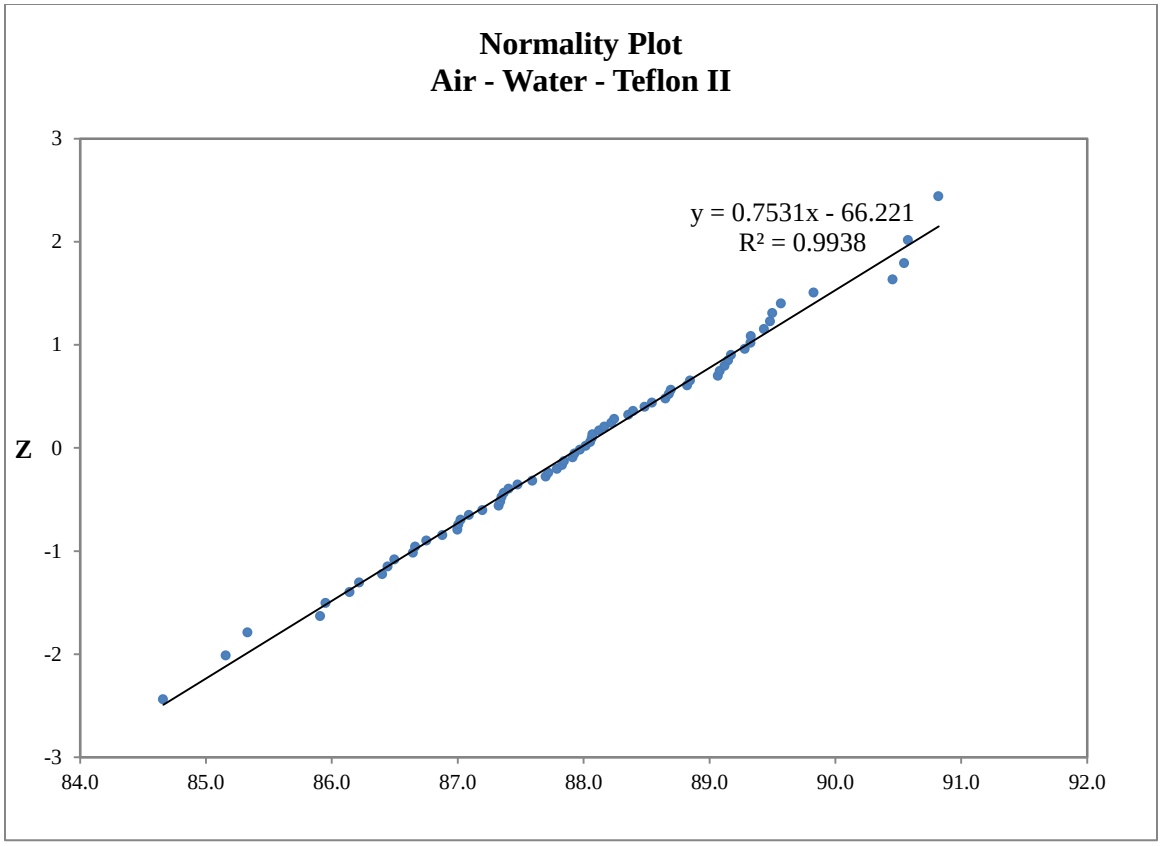

Figure 5.2-3: Contact Angle Air-Water-Teflon Z normality test II

The results from Table (5.2.1-1) for region II show a *p*-value of 0.979 which is bigger than 0.05 and an A-squared value of 0.133 which is smaller than the critical value at 95% which is 0.787 and at 99% which is 1.092. These mean we can be at least 99% confident that the data is normally distributed. Comparing the two regions we could see from the results the data obtained on region II has a better normal distribution than the data obtained for region I.

From Figure (5.2-3) we can observe the data is fairly normal distribute around the straight line which confirms what was calculated using the Anderson-Darling method. From the correlation

obtain from the Z normality test we could also see it has a better normal distribution than region I.

Table 5.2-1: Air-Water-Teflon normality test results equilibrium time

Experiment	**A-Squared**	***p***	**95% Critical Value**	**99% Critical Value**
Neutral System I	0.578	0.124	0.787	1.092
Neutral System II	0.133	0.979	0.787	1.092

5.2.1.3 Analysis of the results for Interfacial Tension in Neutral system

Similarly to the contact angle, we used the ADSAP method to calculate the interfacial tension of water for the system air-water-Teflon.

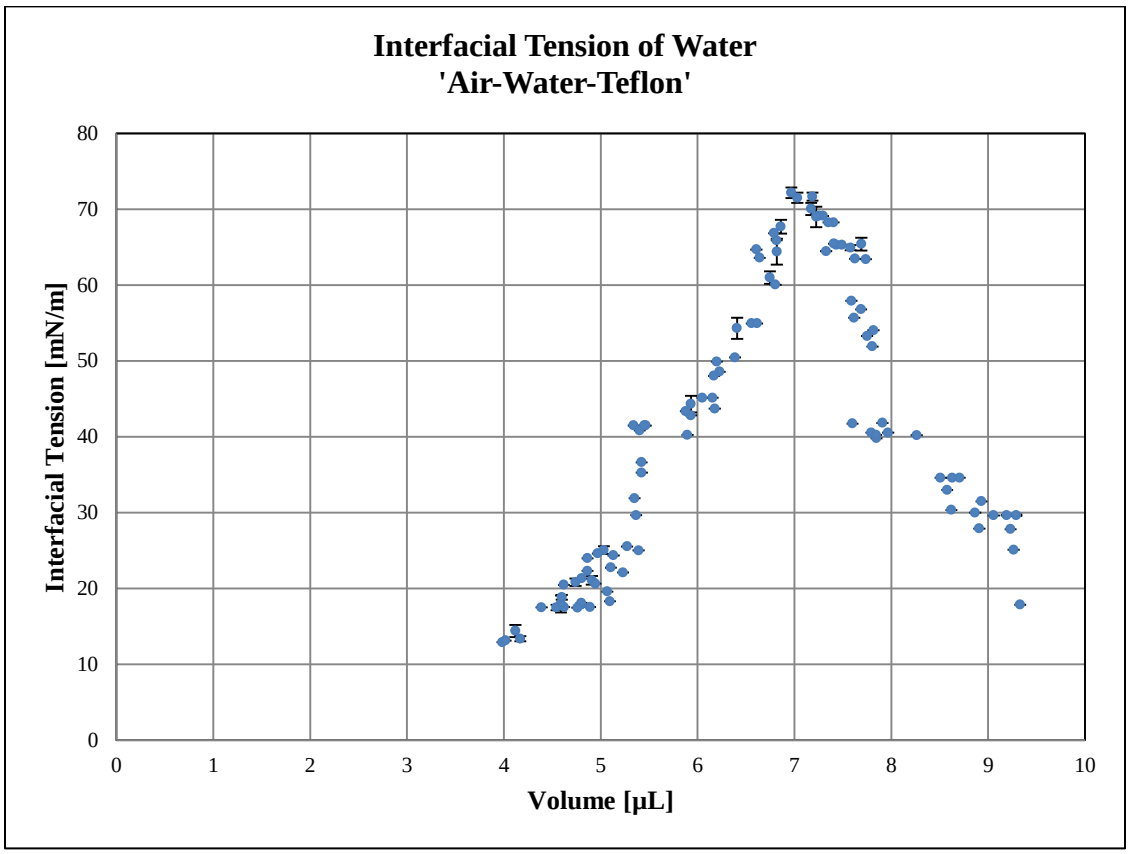

Figure 5.2-4: Air-Water-Teflon Interfacial Tension

Each point in Figure (5.2-4) represents the calculated mean of the interfacial tension for a droplet of water and its standard deviation. These calculations are from seven images taken of each droplet. The analysis procedure to obtain these results is the same as the one explained previously in the contact angle analysis.

From the equilibrium time results which suggested an influence of the droplet size in the IFT, we added to the experimental methodology a syringe pump to control de volume dispensed to create each droplet of water. The rate of injection was kept the same for all the drops. This allows us to create droplets in the range we wanted which was from 3.5µL to 9µL. Initially, the images

were superimposed to determine visually if the volumes were in fact the same. The analysis allowed us to see differences in the sizes of the droplets comparing droplets created using the same volume. The volumes of the droplets were calculated using the experimental profile and are plotted on Figure (5.2-4).

From Figure (5.2-4) we can see a strong dependency of the calculated interfacial tension from the volume of the droplet. Around 5.5µL and 6.7µL we have a considerable change in the IFT value at a very minimum increase of the volume and around 7µL we reached the maximum value of the calculated IFT which is around 72mN/m. This value corresponds to the known value of the IFT of water. In most of the cases, the standard deviation is negligible; this can be explained by taking into account the principles of the ADSA-P method explained in chapter two. The method calculates the interfacial properties minimizing an error function which is the difference between the calculated Laplacian curve and the experimental droplet profile. The fitting of the Laplace curve into the experimental points could smoother the effects of low quality interfaces obtained from some of the images in the sequence taken for each droplet.

The presence of regions where the IFT value changes drastically with the drop size proves the method is not reliable unless a fairly big amount of experiments are run. The ADSA-P method to calculate IFT is mostly use with pendant droplets profiles where the deformation of the droplet is great even in small droplets. The limitations of the micro CT-scanner do not allow us to use pendant drops and instead we use sessile drops. This does not necessary mean that we cannot obtain the interfacial tension from sessile drops but we have to use more volume to create the

droplet. The amount of volume use will depend on the type of substance, some substances will deform faster than others.

The neutral system analyzed has a high contact angle and high IFT which makes harder to create a sessile droplet where we can notice the deformation cause by gravitational forces the way we can see it if we use a pendant drop. This can explain why the IFT changes so drastically with a small change in the volume. The mathematical analysis to determine the reason why the method is extremely sensible when the profiles are close to be of a spherical shape is very complex, so we have to do it experimentally. The results of many research projects prove the instability of the method when the interface is close to be spherical in shape and recommends the use of pendant drops. The sessile drops will work better if the system is more susceptible to the gravitational forces. The complete results for the neutral system are reported from the Table (5.2.1-2) to Table (5.2.1-4).

Table 5.2-2: Experiments results (Air-Water-Teflon)

Volume (µL)	Standard Deviation (µL)	Contact Angle (Degrees)	Standard Deviation (µL)	Interfacial Tension (mN/m)	Standard Deviation (mN/m)
9.23	0.19	88.0	0.9	27.81	0.00
9.26	0.21	90.8	1.2	25.08	0.00
8.62	0.33	88.1	1.5	30.34	0.00
9.06	0.10	87.9	0.4	29.62	0.00
9.19	0.14	88.4	0.5	29.64	0.05
9.29	0.17	88.6	0.9	29.65	0.07
8.91	0.41	85.9	1.6	27.89	0.00
8.87	0.12	88.5	0.5	29.98	0.00
8.58	0.25	88.6	1.8	32.98	0.00
8.93	0.18	88.0	1.0	31.48	0.00
7.91	0.10	89.8	0.5	41.82	0.00
8.51	0.12	88.3	0.6	34.37	0.00
7.44	0.17	87.9	0.9	65.30	0.00
7.60	0.17	86.7	0.8	41.74	0.00
7.85	0.19	87.3	1.0	39.78	0.00
7.49	0.18	89.1	0.9	65.30	0.00
9.33	0.63	87.0	0.7	17.85	0.00
8.26	0.12	89.3	0.8	40.19	0.00
8.71	0.05	89.2	0.4	34.57	0.00
8.63	0.00	89.1	0.00	34.57	0.00
7.74	0.18	87.8	1.0	63.40	0.00
7.82	0.09	87.3	0.4	54.03	0.00
7.75	0.21	87.0	1.1	53.27	0.00
7.81	0.11	88.4	0.8	51.90	0.00
7.59	0.23	85.3	1.0	57.90	0.00
7.97	0.13	88.0	0.6	40.53	0.00
7.62	0.22	87.8	0.8	55.67	0.00
7.79	0.14	87.1	0.8	40.53	0.00
7.84	0.17	87.7	0.8	40.24	0.00
7.69	0.16	87.3	0.9	56.78	0.00
6.80	0.11	89.4	0.8	60.05	0.00
6.79	0.14	86.8	0.7	66.84	0.00
7.69	0.06	89.0	0.8	65.39	0.83
7.58	0.14	88.7	0.8	64.92	0.34
7.26	0.10	89.3	1.2	69.11	0.00
7.33	0.21	87.8	0.9	64.45	0.00
7.40	0.14	88.8	1.1	68.25	0.00
7.41	0.18	88.1	1.5	65.45	0.00
7.35	0.20	89.0	0.8	68.25	0.00
7.29	0.16	89.5	0.3	69.11	0.00

Table 5.2-3: Experiments results (Air-Water-Teflon)

Volume (µL)	Standard Deviation (µL)	Contact Angle (Degrees)	Standard Deviation (Degrees)	Interfacial Tension (mN/m)	Standard Deviation (mN/m)
7.63	0.13	88.2	0.8	63.47	0.00
7.23	0.09	90.5	0.8	68.99	1.36
6.61	0.15	88.8	1.0	64.68	0.00
6.86	0.15	89.5	1.6	67.69	0.91
6.97	0.10	85.9	0.8	72.14	0.70
7.03	0.09	84.6	0.8	71.50	0.66
6.82	0.31	92.8	3.7	64.39	1.71
6.64	0.11	89.1	0.6	63.57	0.00
7.17	0.10	87.6	1.9	70.05	0.80
7.19	0.13	87.9	0.9	71.67	0.53
6.82	0.14	89.4	0.9	65.88	0.00
6.75	0.15	90.5	0.6	60.98	0.84
5.93	0.12	86.2	0.9	42.80	0.00
6.56	0.09	87.4	0.6	54.94	0.00
6.41	0.10	86.6	0.6	54.30	1.40
6.18	0.06	88.2	0.4	43.69	0.00
6.62	0.07	87.7	0.4	54.94	0.00
6.23	0.08	86.4	0.5	48.55	0.00
6.17	0.12	86.6	0.7	48.02	0.00
--	--	--	--	--	--
5.40	0.18	86.4	1.3	40.83	0.00
5.13	0.16	87.4	1.2	24.35	0.00
5.93	0.04	86.5	0.2	44.30	1.09
6.05	0.08	87.2	0.5	45.12	0.00
6.39	0.15	86.1	1.0	50.44	0.00
6.20	0.24	87.3	1.6	49.89	0.00
6.16	0.07	88.0	0.6	45.12	0.00
5.39	0.17	90.4	1.4	24.99	0.00
5.88	0.17	85.1	1.1	43.35	0.00
5.90	0.09	87.0	0.6	40.23	0.00
5.37	0.06	92.0	0.6	29.65	0.00
5.46	0.11	88.9	0.9	41.48	0.00
5.42	0.09	90.7	0.7	35.25	0.00
5.27	0.10	92.4	0.9	25.54	0.00
4.86	0.21	90.6	2.0	22.30	0.00
4.86	0.10	90.9	0.9	23.96	0.00
5.35	0.12	90.4	0.9	31.88	0.00
5.45	0.13	89.9	1.1	41.48	0.00
5.34	0.14	88.9	1.3	41.48	0.00
5.10	0.07	88.0	1.1	22.73	0.00

Table 5.2-4: Experiments results (Air-Water-Teflon)

Volume (µL)	Standard Deviation (µL)	Contact Angle (Degrees)	Standard Deviation (Degrees)	Interfacial Tension (mN/m)	Standard Deviation (mN/m)
5.03	0.18	95.3	0.7	25.05	0.51
5.23	0.07	90.8	0.5	22.09	0.00
5.42	0.03	91.5	0.0	36.62	0.00
4.97	0.01	90.2	0.0	24.60	0.00
4.74	0.14	94.9	0.8	20.82	0.48
4.80	0.03	93.6	0.0	17.88	0.00
--	--	--	--	--	--
--	--	--	--	--	--
--	--	--	--	--	--
--	--	--	--	--	--
5.07	0.13	89.9	1.2	19.59	0.00
3.99	0.37	90.9	2.5	12.89	0.00
5.09	0.16	91.1	1.7	18.30	0.00
4.62	0.21	92.3	2.4	17.53	0.00
--	--	--	--	--	--
4.91	0.12	93.3	1.3	21.07	0.56
4.59	0.22	93.9	2.4	17.93	1.12
4.54	0.05	95.1	1.4	17.47	0.36
4.89	0.13	99.6	1.4	17.53	0.00
4.95	0.12	93.0	1.4	20.61	0.00
4.81	0.13	91.3	1.8	21.30	0.00
3.57	0.24	89.5	4.5	36.50	0.00
4.80	0.11	98.3	1.2	18.08	0.00
4.39	0.20	90.9	1.7	17.50	0.00
4.76	0.17	93.1	1.9	17.45	0.00
4.60	0.06	92.6	1.6	18.83	0.31
4.17	0.16	92.5	2.1	13.36	0.35
4.12	0.03	94.2	2.9	14.39	0.80
4.62	0.29	94.6	3.3	20.46	0.00
4.02	0.14	90.2	2.0	13.12	0.00
--	--	--	--	--	--
3.93	0.04	94.9	2.1	13.97	0.89
3.11	0.12	95.1	1.5	37.10	0.48
3.18	0.13	93.5	2.6	38.52	0.63
3.14	0.10	94.8	2.2	37.57	0.82
--	--	--	--	--	--
--	--	--	--	--	--
--	--	--	--	--	--
--	--	--	--	--	--
--	--	--	--	--	--

5.2.2 Water Wet System

We used air-water-quartz as our water wet system. The big difference on densities between air and water help us to obtain a differentiated interface on the X-ray images. Furthermore, the images have less noise making them easier to process. Quartz plates were cut and left in water for some weeks to try to keep them as clean as possible. Quartz has a considerable high surface tension which makes it easier to capture dirt particles present on the air. The plate chosen for this experiment was carefully analyzed with a magnifying lens.

The experiments were conducted using volumes from 3.5µL to 9µL to create the water droplet. The volume was increased by 0.5µL to work with a total of 12 volumes. To control the injected volume we used a syringe pump. The rate of injection was kept constant for all volumes. For each volume we worked with, 5 droplets of water were analyzed. A total of 60 droplets of water were analyzed. The setup of each droplet of water was the same. The substrate was carefully dry with nitrogen and placed in the cell. The syringe pump dispensed the volume and the droplet created at the tip of the needle was slowly placed on the substrate. Then the cell was closed. Before a droplet was placed, the cell was levelled. This procedure was done every day when we had to re-start the micro CT-scanner. Sometimes it was done more than once a day because after some hours of operation the micro CT-scanner gave bad quality images. To solve this we had to turn off the equipment for two hours or in some cases start fresh the next day.

For each droplet of water 8 images were taken; 7 from 0^o angle and 1 from 90^o. The latter image was taken to visually control the symmetry of the droplet. Any droplet with no symmetry was disposed and a new droplet was placed. The images were taken immediately after the micro CT-

scanner was ready. A total of 420 images were digitally processed to obtain the interface. The results of contact angle calculated are presented in Figure (5.2-5).

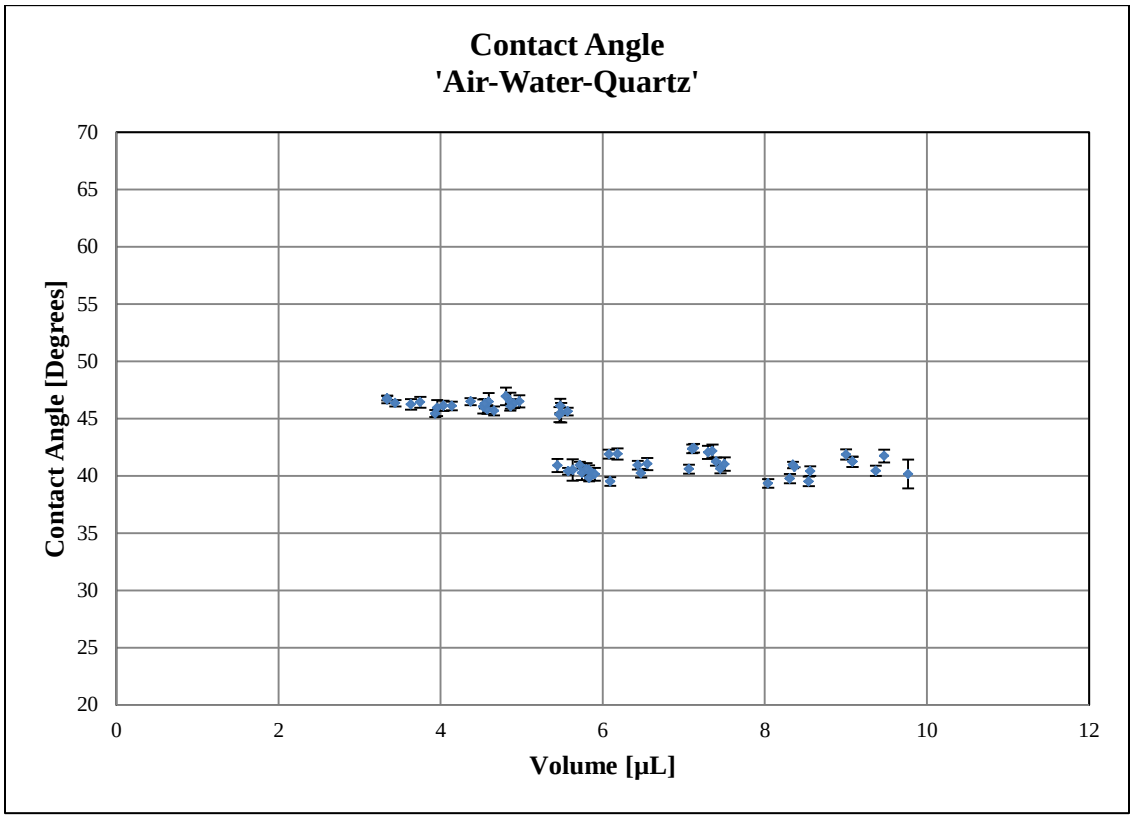

Figure 5.2-5: Air-Water-Quartz Contact Angle

5.2.2.1 Analysis of the results for Contact Angle in Water Wet System

Each point in this figure (5.2-5) represents the calculated mean of the contact angle for a droplet of water and its standard deviation. These calculations are from seven images taken of each droplet. The droplet profile was found after enhancing the definition of the image, using PhotoScape, cropping the image to manually enhance the droplet profile which reduce considerably the edges found by the edge detector; enhancing manually the drop profile allow us to use a higher threshold which eliminates all the edges from noise. This procedure adds

considerable amount of time to the analysis. It is tedious but produces a more defined droplet profile as we could see in Figure (4.3-4) on chapter four. After the image was manually enhanced the analysis procedure is the same as the one explain on the neutral system.

The images we usually had with lower quality at the end of each sequence and sometimes after 4 to 6 hours of work were compensated by manually enhancing the droplet profile. This is the reason why the standard deviation for each droplet is low in most cases. There are two defined regions; one from 3.5µL to 5.5µL and the other from 5.5 µL to 9µL; at smaller volumes the angle tends to be of around 46 degrees while at bigger volumes the tendency is to be of 42 degrees. From figure (5.2-5) we could also notice a small area around 5 to 6 µL where for about the same volume few droplets analyzed gave different values of contact angles which is the results of not being completely leveled when the images were taking and lower definition of the images which added error in the contact angle calculations. The contact angle for the water-wet system is about the half of the one calculated for the neutral system and yet again we have two calculated contact angles. These results eliminate completely the possibility of the influence of gravity forces when the volume of the sessile droplet increases. We have again the same possible factors as the ones analyzed for the neutral system.

The presence of dirt on the substrate is more likely since the surface tension of quartz is quite high and during the setup the system was exposed to the atmospheric conditions. From the Figure (5.2-5) we can see more scattered values of the contact angle when the volume is bigger than 6µl which could be explain by the presence of dirt on the substrate and its roughness.

Conclusive evidence of this influence is hard to find; moreover, the presence of the two regions makes this statement more doubtful.

The drop size dependence of contact angles has also been interpreted in terms of line tensions. This concept was first described by Gibbs and subsequently developed in the generalized theory of capillarity by Boruvka and Neumann (Boruvka *et al.*, 1977). Analogous to surface tension defined for two dimensional surface, line of tension could be define in two ways as: (1) the force operating in the one-dimensional three-phase line which tends to minimize its length, much the same way as the surface tension which tends to minimize the surface area; (2) the free energy per unit length of the three-phase line. For a sessile drop on an ideal and horizontal surface, the three-phase line is a smooth circle. This concept is apply in systems with much smaller volumes than the ones used in these experiments and the contact angle changes exponentially with the volume reaching a constant value at about the smaller volumes we used. This behaviour is very different to the one we have in our range of volumes which made us believe the two regions are the result of other factors.

Similarly to the neutral system, during the capturing time of the images in the water-wet system we observed again diminishing in the contrast of the images taken at the end of each sequence as well as since the very beginning of the sequence after some time of operation of the micro CT-scanner. We also have lower contrast in general in images taken from droplets of small volumes. This behaviour can explain the presence of the two well defined regions of the calculated contact angles. At smaller volumes the images have considerable amount of noise which affects the interface; the manual enhancing improves the definition of the interface but cannot account for

the real location. This explains why we have a considerably improvement in the standard deviation of each sample.

After we have analyzed the neutral and water-wet systems with high IFT and high and moderate contact angle we could conclude that the appropriate volume to determine the contact angle in these systems will be over 6μL to minimize the influence of noise in the interface.

5.2.2.2 Normality test results for Contact Angle in Water Wet System

The normality test was performed using the normal probability plot method and the Anderson-Darling method. Since there are two regions on Figure (5.2-5) the normality test was run considering them. The results are shown in Table (5.2.2-1) for the three experiments and the normal probability plot method for the experiment 1 is shown in Figure (5.2-6) and Figure (5.2-7).

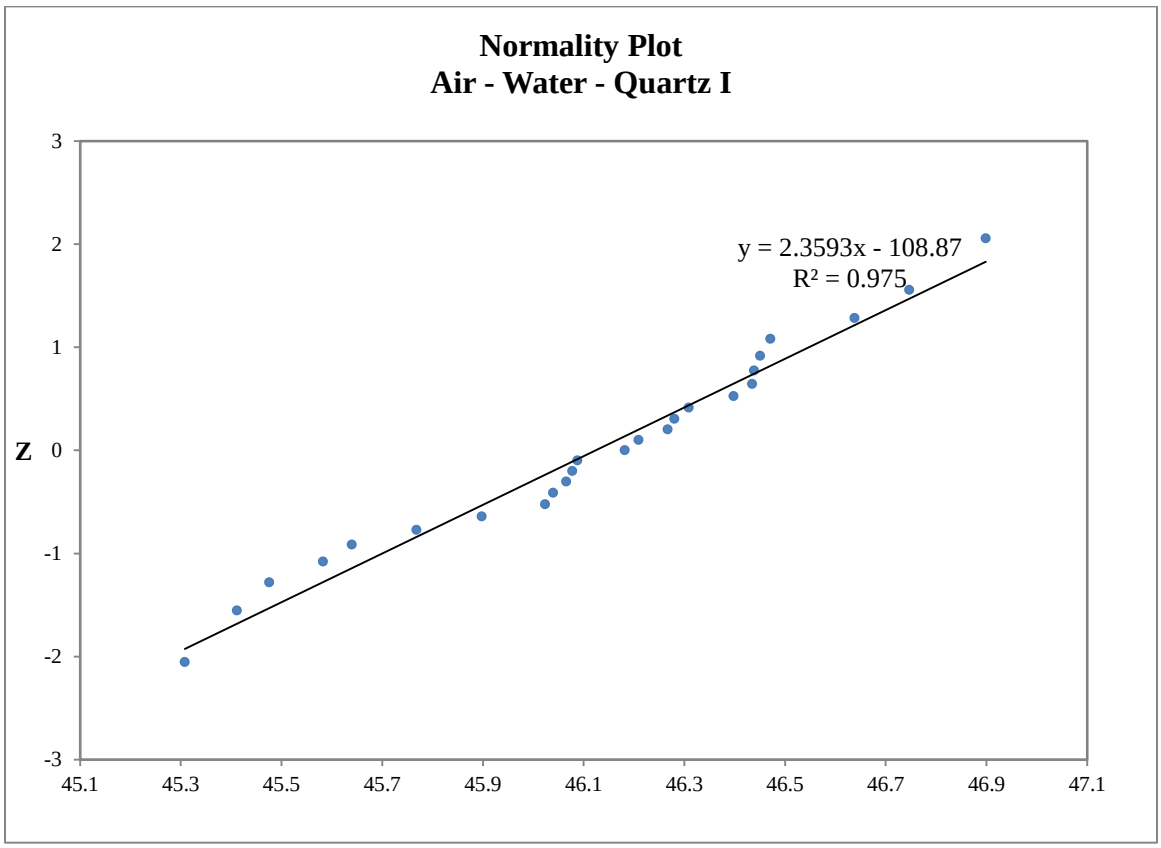

Figure 5.2-6: Contact Angle Air-Water-Quartz Z normality test I

The results from Table (5.2.2-1) for region I show a *p*-value of 0.529 which is bigger than 0.05 and an A-squared value of 0.312 which is smaller than the critical value at 95% which is 0.787 and at 99% which is 1.092. These mean we can be at least 99% confident that the data is normally distributed.

From Figure (5.2-6) we can observe the data is fairly normal distribute around the straight line which confirms what was calculated using the Anderson-Darling method.

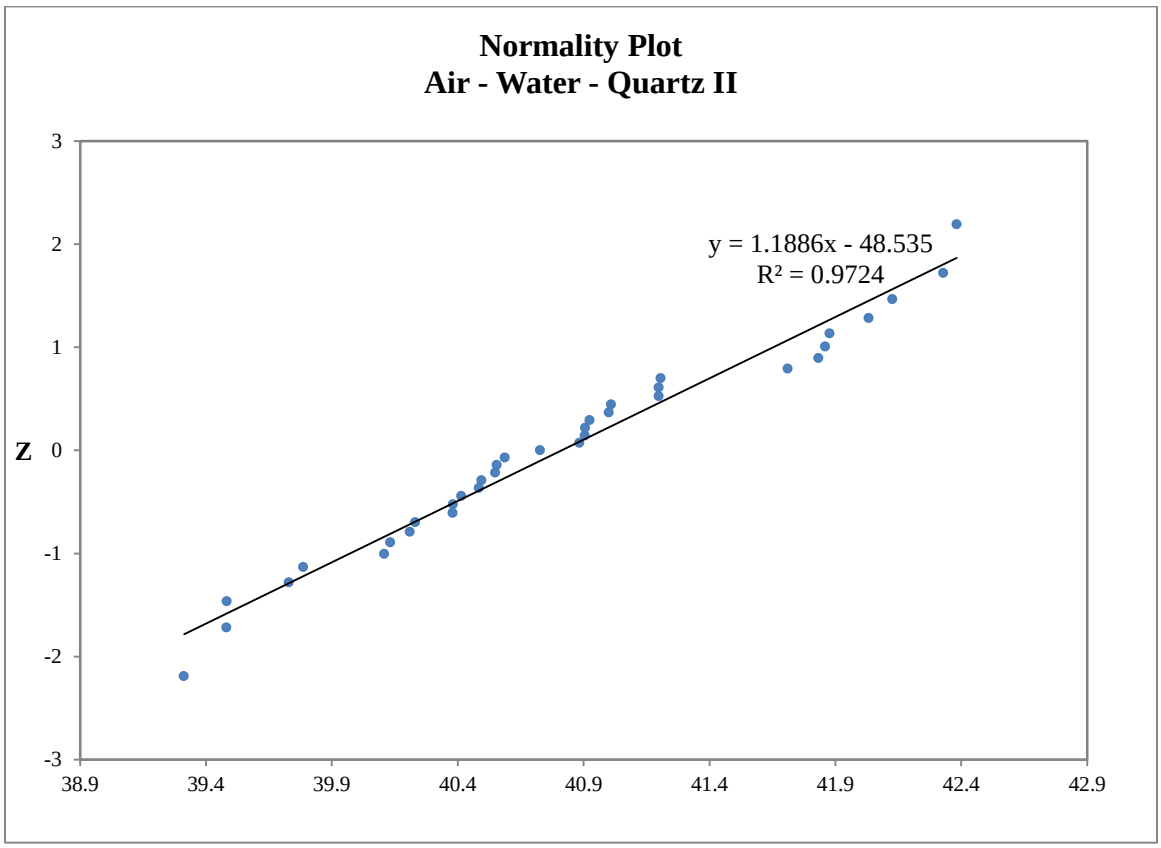

Figure 5.2-7: Contact Angle Air-Water-Quartz Z normality test II

The results from Table (5.2.2-1) for region II show a *p*-value of 0.347 which is bigger than 0.05 and an A-squared value of 0.399 which is smaller than the critical value at 95% which is 0.787 and at 99% which is 1.092. These mean we can be at least 99% confident that the data is normally distributed.

From Figure (5.2-7) we can observe the data is fairly normal distribute around the straight line which confirms what was calculated using the Anderson-Darling method. The correlation obtained from the Z normality test gives a very similar normal distribution between the two regions.

Table 5.2-5: Air-Water-Quartz normality test results equilibrium time

Experiment	A-Squared	*p*	95% Critical Value	99% Critical Value
Water wet system I	0.312	0.529	0.787	1.092
Water wet system II	0.399	0.347	0.787	1.092

5.2.2.3 Analysis of the results for Interfacial Tension in Water-wet system

Similarly to the contact angle, we used the ADSAP method to calculate the interfacial tension of water for the system air-water-quartz.

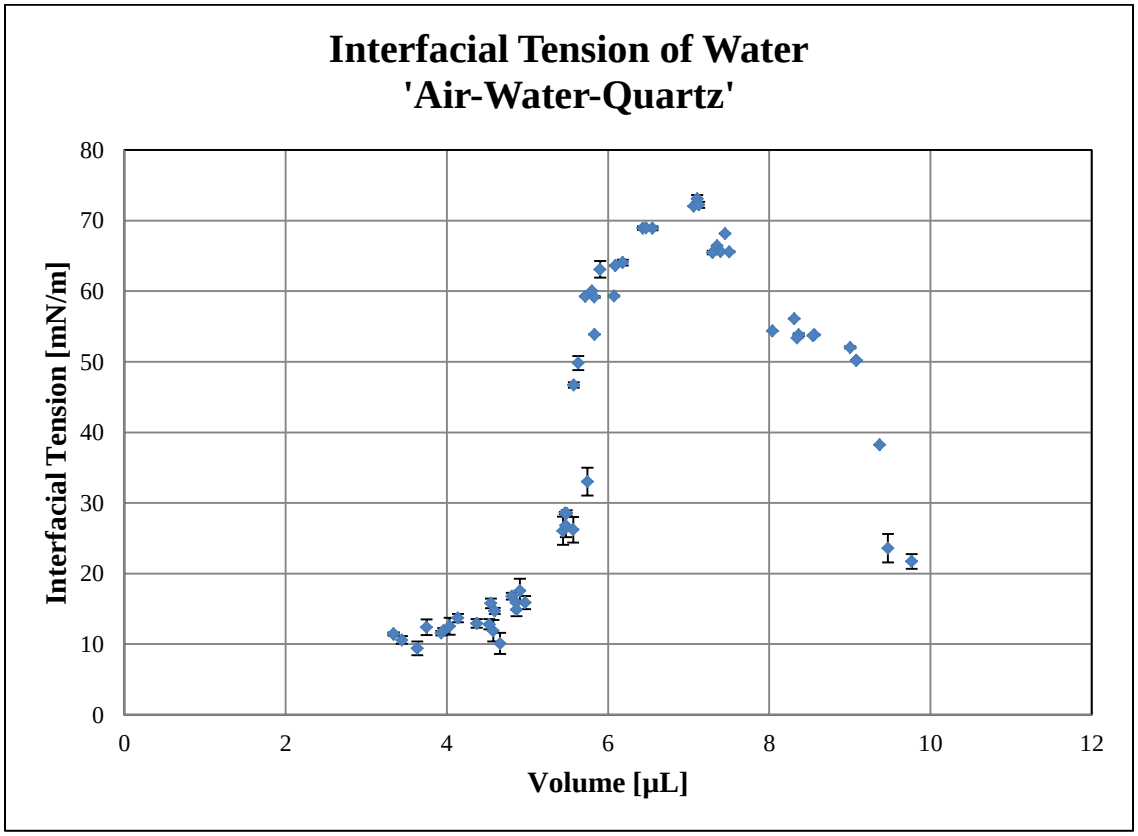

Figure 5.2-8: Air-Water-Quartz Interfacial Tension

Each point in Figure (5.2-8) represents the calculated mean of the interfacial tension for a droplet of water and its standard deviation. These calculations are from seven images taken of each

droplet. The analysis procedure to obtain these results is the same as the one explained previously in the contact angle analysis.

From the equilibrium time results which suggested an influence of the droplet size in the IFT, we added to the experimental methodology a syringe pump to control de volume dispensed to create each droplet of water. The rate of injection was kept the same for all the drops. This allows us to create droplets in the range we wanted which was from 3.5μL to 9μL. Initially, the images were superimposed to determine visually if the volumes were in fact the same. The analysis allowed us to see differences in the sizes of the droplets comparing droplets created using the same volume. The volumes of the droplets were calculated using the experimental profile and are plotted on Figure (5.2-8).

Similarly to the neutral system the water-wet system shows strong influence of the volume on the calculated IFT. We have regions where the value of the IFT changes drastically with a very minimum change in the volume. A maximum value of the IFT was found at around 7μL and it is 72mN/m which is the known value of the IFT of water. We have again determined successfully the IFT of water using a different system and implementing the same technique. However, the strong variability of the IFT with the volume suggests the necessity of great experimental work.

We could notice again from the images the low influence of the gravitational forces on the shape of the interface. As we mentioned in the neutral system analysis, there has been great results using the ADSA-P technique to calculate the IFT but these results have been using pendant drops which are quickly deformed by gravity. In the other hand, when we used sessile drops the

gravitational forces are less notable because the contact area increases when the volume increases which is not the case of a pendant drop where it stays constant. Under this consideration we could start thinking that the ADSA-P technique even though applicable to obtain the IFT should not be recommended to use when we can only work with sessile drops.

As we have mentioned before experimentally the technique has been successful when the deformation of the interface is considerable. The results show that the maximum value calculated represents the real value of the IFT for the system being analyzed. However, we cannot expect to get this value with low variability as we have obtained in the neutral and water-wet systems when we analyze other systems, and in some cases could the variability be as we have in these results for volumes around 5.5µL where the IFT changes between 23 to 50mN/m. Great amount of data was used to create the curve of Figure (5.2-8), this could give us a reliable calculated interfacial tension but at the same time a very extensive work has to be done, a work that is tedious and easy to add error to the calculations due to the manual enhancing of the drop profile. These are main reasons why this methodology implemented to calculate interfacial tension using micro X-rays imaging could be consider not attractive to choose when we want to calculate interfacial properties.

The complete results from the Water-wet system are reported from Table (5.2.2-2) to Table (5.2.2-3)

Table 5.2-6: Experiments results (Air-Water-Quartz)

Volume (µL)	Standard Deviation (µL)	Contact Angle (Degrees)	Standard Deviation (Degrees)	Interfacial Tension (mN/m)	Standard Deviation (mN/m)
9.77	0.28	40.2	1.3	21.73	1.03
9.08	0.23	41.2	0.4	50.18	0.01
9.00	0.28	41.9	0.4	52.63	0.14
9.08	0.23	41.2	0.4	50.18	0.01
9.47	0.25	41.7	0.6	23.62	2.62
8.04	0.34	39.3	0.4	54.37	0.00
8.56	0.32	40.4	0.4	53.82	0.08
8.54	0.25	39.5	0.4	53.70	0.03
9.37	0.33	40.4	0.4	38.23	0.00
8.37	0.24	40.7	0.0	53.82	0.19
6.08	0.25	41.9	0.4	59.32	0.05
8.31	0.28	39.7	0.4	56.11	0.00
7.45	0.31	40.6	0.4	68.17	0.00
5.83	0.24	40.5	0.4	59.18	0.12
5.72	0.21	40.9	0.3	59.28	0.02
7.35	0.23	42.1	0.6	66.42	0.00
8.35	0.26	40.9	0.3	53.36	0.00
7.50	0.29	41.0	0.6	65.59	0.08
7.30	0.27	42.1	0.6	65.50	0.25
7.40	0.22	41.2	0.4	65.62	0.11
5.57	0.26	40.4	0.3	46.69	0.38
5.83	0.24	39.8	0.3	53.90	0.00
7.06	0.18	40.6	0.4	72.04	0.05
7.11	0.18	42.3	0.4	73.11	0.49
7.13	0.13	42.4	0.4	72.23	0.45
6.55	0.25	41.0	0.5	68.90	0.28
5.63	0.33	40.5	0.9	49.83	0.99
6.43	0.21	40.9	0.4	68.91	0.24
6.47	0.17	40.2	0.4	68.97	0.05
5.80	0.28	40.6	0.5	60.03	0.00
6.18	0.23	41.9	0.5	64.06	0.41
5.44	0.07	40.9	0.6	26.06	2.00
5.74	0.17	40.3	0.6	33.02	1.96
5.90	0.17	40.1	0.6	63.09	1.18
6.09	0.15	39.5	0.4	63.62	0.08

Table 5.2-7: Experiments results (Air-Water-Quartz)

Volume (µL)	Standard Deviation (µL)	Contact Angle (Degrees)	Standard Deviation (Degrees)	Interfacial Tension (mN/m)	Standard Deviation (mN/m)
4.58	0.20	45.8	0.4	11.91	1.51
4.66	0.17	45.7	0.4	10.10	1.49
5.49	0.16	45.5	0.8	28.55	0.39
5.57	0.14	45.6	0.3	26.21	1.80
5.47	0.22	45.3	0.7	28.59	0.17
4.86	0.21	46.5	0.8	15.89	0.01
4.81	0.22	46.9	0.8	16.81	0.47
4.97	0.32	46.5	0.5	15.88	0.91
5.48	0.23	46.1	0.6	26.81	1.65
4.03	0.09	46.1	0.5	12.53	1.19
4.53	0.19	46.0	0.6	12.82	0.73
4.37	0.22	46.5	0.3	12.95	0.60
4.91	0.14	46.3	0.4	17.56	1.73
4.59	0.23	46.5	0.8	14.71	0.42
4.86	0.19	46.1	0.2	14.90	0.94
3.93	0.26	45.4	0.3	11.58	0.32
3.75	0.21	46.4	0.5	12.41	1.12
4.55	0.21	46.3	0.4	15.79	0.69
4.14	0.19	46.1	0.4	13.71	0.58
3.96	0.23	45.9	0.7	11.88	0.39
3.34	0.12	46.7	0.3	11.49	0.17
3.34	0.12	46.8	0.2	11.38	0.20
3.63	0.17	46.2	0.5	9.41	0.97
3.44	0.18	46.3	0.3	10.60	0.55
3.63	0.19	46.2	0.6	10.65	0.95

5.2.3 Oil-based Substrate System

We used air-decane-teflon as our oil-based substrate system. The big difference on densities between air and decane will again help us to obtain a differentiated interface on the X-ray images; furthermore, the images will have less noise making them easier to process. The teflon is a piece of quartz coated with a film of teflon of about 2 mm; the coating was done by Topgun a specialized coating company. Teflon is a chemical compound with a very low surface tension which makes it more suitable to measure the interfacial tension of decane. The teflon substrates were kept in water for some weeks. The substrate piece chosen was analyzed carefully with a magnify lens.

The experiments were conducted using volumes from 3.5µL to 9µL to create the water droplet. The volume was increased by 0.5µL to work with a total of 12 volumes. To control the injected volume we used a syringe pump. The rate of injection was kept constant for all volumes. For each volume we worked with, 5 droplets of water were analyzed. A total of 60 droplets of water were analyzed. The setup of each droplet of water was the same. The substrate was carefully dried with nitrogen and placed in the cell. The syringe pump dispensed the volume and the droplet created at the tip of the needle was slowly placed on the substrate. Then the cell was closed. Before a droplet was placed, the cell was levelled. This procedure was done every day when we had to re-start the micro CT-scanner. Sometimes it was done more than once a day because after some hours of operation the micro CT-scanner gave bad quality images. To solve this we had to turn off the equipment for two hours or in some cases start fresh the next day.

For each droplet of water 8 images were taken; 7 from 0^o angle and 1 from 90^o. The latter image was taken to visually control the symmetry of the droplet. Any droplet with no symmetry was

disposed and a new droplet was placed. The images were taken immediately after the micro CT-scanner was ready. A total of 420 images were digitally processed to obtain the interface. The results of contact angle calculated are presented in Figure (5.2-9).

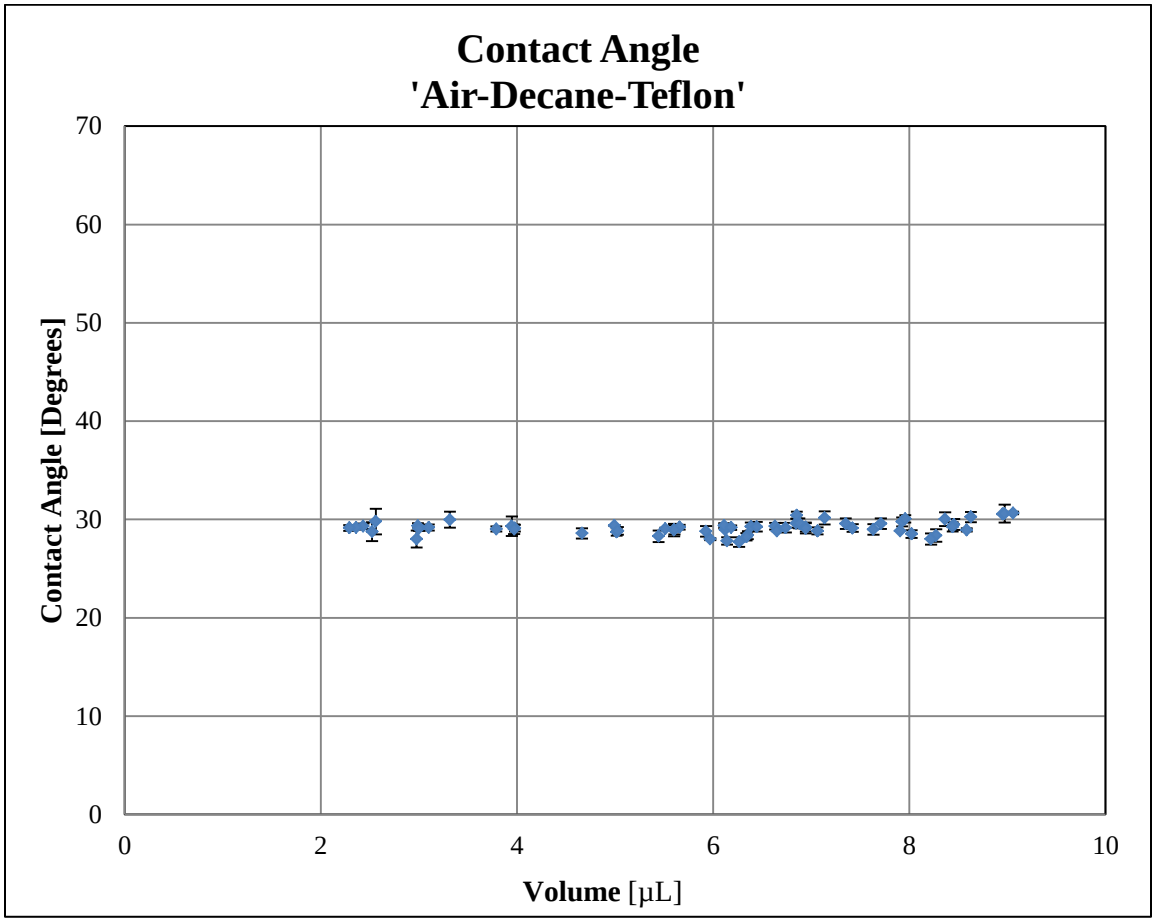

Figure 5.2-9: Air-Decane-Teflon Contact Angle

5.2.3.1 Analysis of the results for Contact Angle in Oil-based substrate System

Each point in Figure (5.2-9) represents the calculated mean of the contact angle for a droplet of decane and its standard deviation. These calculations are from seven images taken of each droplet. The droplet profile was found after enhancing the definition of the image, using

PhotoScape, cropping the image to manually enhance the droplet profile which reduce considerably the edges found by the edge detector; enhancing manually the drop profile allow us to use a higher threshold which eliminates all the edges from noise. This procedure adds considerable amount of time to the analysis; it is tedious but produces a more defined droplet profile as we could see in Figure (4.3-4) on chapter four.

Contrary to the results from the neutral and water-wet systems, the oil-based substrate system results show no dependency of the contact angle from the droplet size. The system has a considerable low contact angle and it is easier to establish the profile of the droplet. Dirt on the surface of the substrate is less likely since the substrate is of low surface tension, and the small variations on the value of the contact angle could be related to the roughness of the surface considering the difficulty of having a surface with a roughness pattern.

The images for the three systems were taken with the same setup of the micro CT-scanner. For smaller volumes the interface close to the substrate had more noise in the neutral and water-wet systems. The smaller contact angle could have helped to be easier to see the interface along with the fact the droplet is of decane. The simple fact that the contact angle is low could make the variation cause by any factor less tangible.

After we have taken and processed such a great amount of images for all of the experiments run we could conclude that the micro CT-scanner has a malfunction problem that are more apparent after it is used for long periods of time. This malfunction causes more noise in the images taken which is more tangible when we analyze systems with small droplets. The equipment gives the

opportunity to magnify the images which is handy when the system is solid. Unstable systems like a sessile drop should not be disturb by any movement; this means we need a cell for each magnification we want to use. Since the contact angle is an intensive property we should use sessile drops with sizes over 6µl to avoid the influence of noise from the images taken.

5.2.3.2 Normality test results for Contact Angle in Oil-based Substrate System

The normality test was performed using the normal probability plot method and the Anderson-Darling method. The results are shown in Table (5.2.3-1) and the normal probability plot method in Figure (5.2-10).

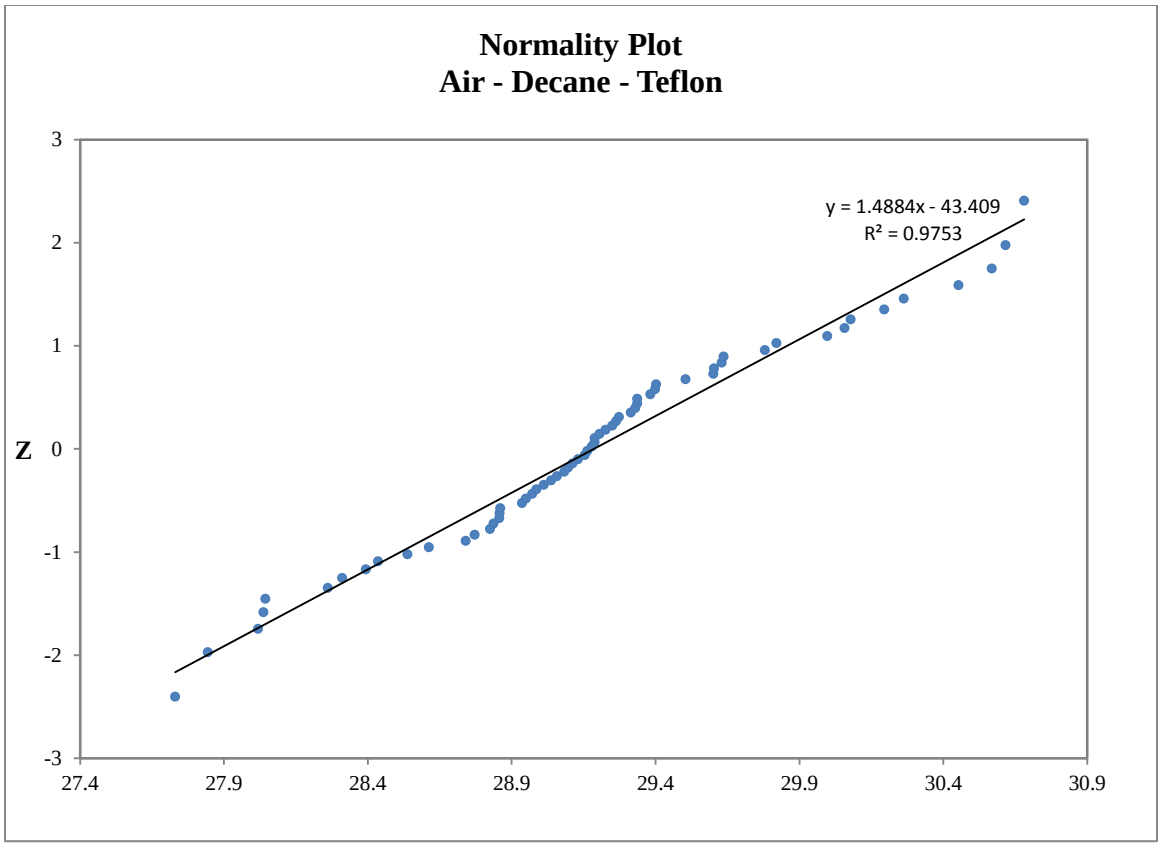

Figure 5.2-10: Contact Angle Air-Decane-Teflon Z normality test

The results from Table (5.2.3-1) show a *p*-value of 0.072 which is bigger than 0.05 and an A-squared value of 0.679 which is smaller than the critical value at 95% which is 0.787 and at 99% which is 1.092. These mean we can be at least 99% confident that the data is normally distributed.

From Figure (5.2-10) we can observe the data is fairly normal distributed around the straight line which confirms what was calculated using the Anderson-Darling method.

Table 5.2-8: Air-Decane-Teflon normality test results

Experiment	**A-Squared**	***p***	**95% Critical Value**	**99% Critical Value**
Oil-based Substrate	0.679	0.072	0.787	1.092

5.2.3.3 Analysis of the results for Interfacial Tension in Oil-based substrate system

Similarly to the contact angle, we used the ADSAP method to calculate the interfacial tension of decane for the system air-decane-teflon.

This system has a low contact angle and the decane has a low surface tension (23mN/m) which makes harder to notice the influence of the gravity on the droplet. To dispense decane trough a small diameter needle is challenging which make it harder to control the amount of decane use to create the droplet; however, we calculated the volume from the profile of the droplet.

Each point in Figure (5.2-11) represents the calculated mean of the interfacial tension for a droplet of decane and its standard deviation. These calculations are from seven images taken of

each droplet. The processing of the images was done is the same manner of the water-wet system.

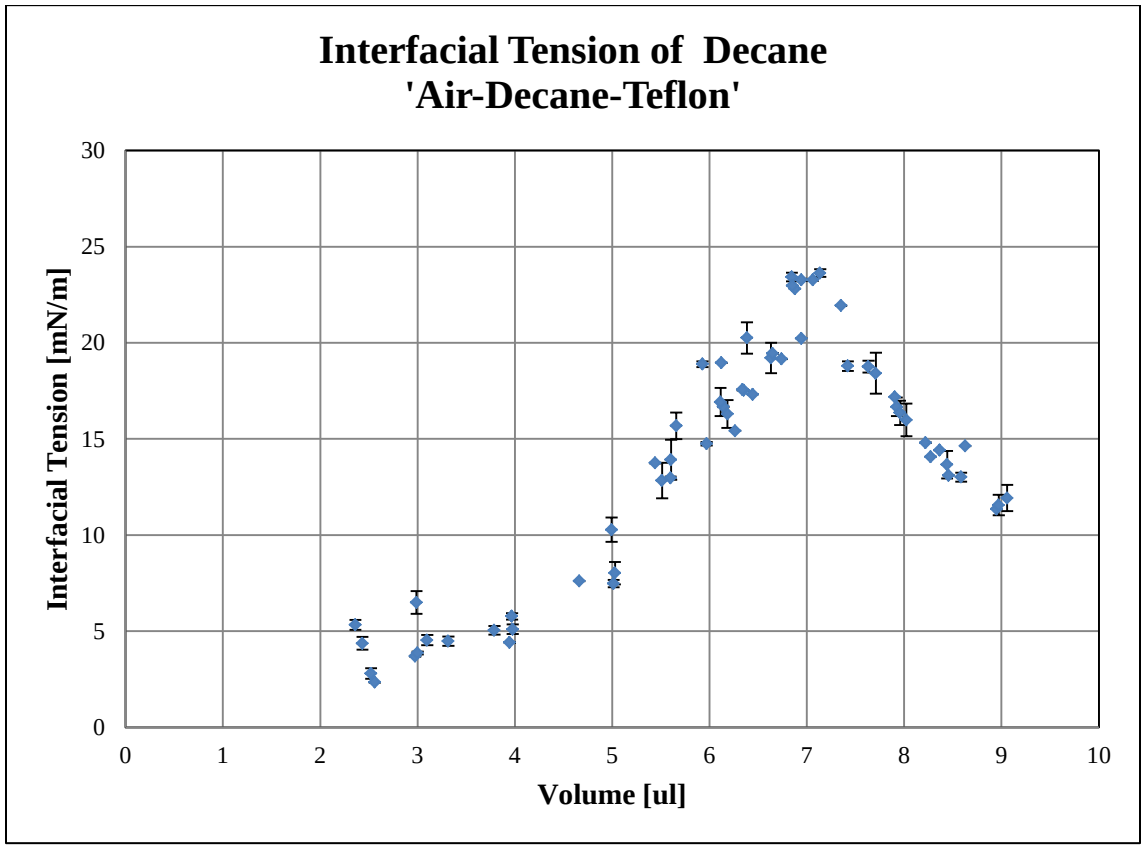

Figure 5.2-11: Air-Decane-Teflon Interfacial Tension

The oil-wet system has a low contact angle and low IFT. The droplet spreads more on the substrate surface creating a more spherical droplet which affects considerable the results of the calculated IFT. A minimum change in the volume affects considerably the IFT which generate a more spread out results. The maximum value is around 23mN/m which is the known value for the IFT of decane.

The contact angle of each system is considerably different. These strongly suggest a sessile drop cannot be deformed sufficiently by the gravitational forces to obtain reliable results of IFT using the ADSA-P technique. In the other hand, this technique could be applied to determine contact angles. Perhaps, the results of three systems are not enough to have a conclusive answer; however, the experience acquired to setup axisymmetric sessile droplets with volumes over 8µL increase the suggestion. When the volume increases it is more difficult to obtain a symmetric droplet, the roughness and dirt on the substrate make the droplet deform quickly.

The complete results for the Oil-based substrate system are reported from Table (5.2.3-2) to Table (5.2.3-3).

Table 5.2-9: Experiments results (Air-Decane-Teflon)

Volume (µL)	Standard Deviation (µL)	Contact Angle (Degrees)	Standard Deviation (Degrees)	Interfacial Tension (mN/m)	Standard Deviation (mN/m)
8.46	0.13	29.5	0.6	13.11	0.00
8.95	0.23	30.5	0.0	11.36	0.01
8.97	0.50	30.6	0.9	11.56	0.53
9.06	0.17	30.7	0.1	11.92	0.68
8.63	0.20	30.2	0.5	14.62	0.00
7.91	0.21	28.8	0.0	17.18	0.00
8.36	0.16	30.0	0.7	14.42	0.01
8.59	0.15	28.9	0.2	13.01	0.23
8.44	0.16	29.2	0.5	13.66	0.71
8.27	0.12	28.4	0.6	14.07	0.00
7.14	0.23	30.2	0.7	23.62	0.20
7.93	0.09	29.8	0.5	16.67	0.48
7.96	0.14	30.1	0.4	16.36	0.63
5.93	0.16	28.8	0.5	18.88	0.14
8.02	0.18	28.5	0.4	15.98	0.85
7.35	0.36	29.6	0.5	21.93	0.01
7.63	0.08	29.0	0.5	18.76	0.31
7.71	0.24	29.6	0.5	18.41	1.07
5.60	0.55	28.9	0.6	12.97	0.07
7.42	0.17	29.1	0.4	18.79	0.25
8.22	0.11	28.0	0.6	14.81	0.02
6.85	0.22	29.6	0.4	23.42	0.22
6.88	0.19	29.6	0.5	22.80	0.00
7.06	0.26	28.8	0.4	23.26	0.03
6.94	0.19	29.2	0.5	23.28	0.06
6.35	0.48	28.4	0.4	17.53	0.01
6.74	0.17	29.2	0.5	19.56	0.01
5.44	0.15	28.3	0.6	13.74	0.01
6.63	0.18	29.3	0.3	19.21	0.79
6.65	0.34	28.8	0.0	19.45	0.02
6.39	0.11	29.3	0.4	20.25	0.81
6.94	0.16	29.1	0.5	20.23	0.00
6.34	0.10	29.2	0.4	17.56	0.03
6.12	0.17	29.0	0.0	18.96	0.01
6.14	0.15	27.8	0.4	16.67	0.01
6.11	0.16	29.4	0.2	16.92	0.73
6.18	0.17	29.2	0.2	16.30	0.73

Table 5.2-10: Experiments results (Air-Decane-Teflon)

Volume (µL)	Standard Deviation (µL)	Contact Angle (Degrees)	Standard Deviation (Degrees)	Interfacial Tension (mN/m)	Standard Deviation (mN/m)
5.66	0.27	29.2	0.2	15.67	0.69
6.26	0.11	27.7	0.5	15.42	0.00
6.85	0.13	30.4	0.4	22.97	0.00
5.60	0.16	29.0	0.5	13.92	1.04
5.51	0.13	29.1	0.1	12.84	0.93
4.99	0.17	29.4	0.1	10.27	0.63
6.45	0.21	29.3	0.5	17.31	0.00
5.97	0.22	28.0	0.1	14.75	0.09
5.02	0.15	28.7	0.4	7.47	0.19
5.03	0.27	28.8	0.4	8.02	0.58
4.66	0.15	28.6	0.5	7.60	0.00
3.98	0.11	29.1	0.3	5.10	0.25
3.95	0.09	29.3	1.0	4.41	0.02
3.79	0.16	29.0	0.3	5.04	0.22
3.97	0.16	29.0	0.5	5.77	0.16
2.99	0.11	29.4	0.3	6.49	0.59
2.98	0.07	28.0	0.9	3.69	0.03
3.00	0.10	29.1	0.2	3.86	0.08
3.10	0.08	29.2	0.3	4.53	0.27
3.32	0.05	30.0	0.8	4.47	0.24
2.43	0.14	29.3	0.3	4.37	0.34
2.52	0.07	28.8	1.0	2.80	0.27
2.56	0.07	29.8	1.3	2.34	0.02
2.36	0.16	29.2	0.2	5.33	0.26
2.29	0.06	29.1	0.3	3.20	0.43

5.3 Analysis of the results for water-wet, neutral and oil-based substrate systems using partial data collected

In order to compare the results between manually enhancing the data and using only the edge detector we decided to take a number of droplets chosen randomly from each volume analyzed on each system. In the case on the neutral system we did a manually enhanced process and for the other two systems we used only the edge detector. The results of the processing are presented and analyzed as follows.

5.3.1 Neutral System

Three droplets from each volume were manually enhanced. The results obtain are shown in Figure (5.3-1)

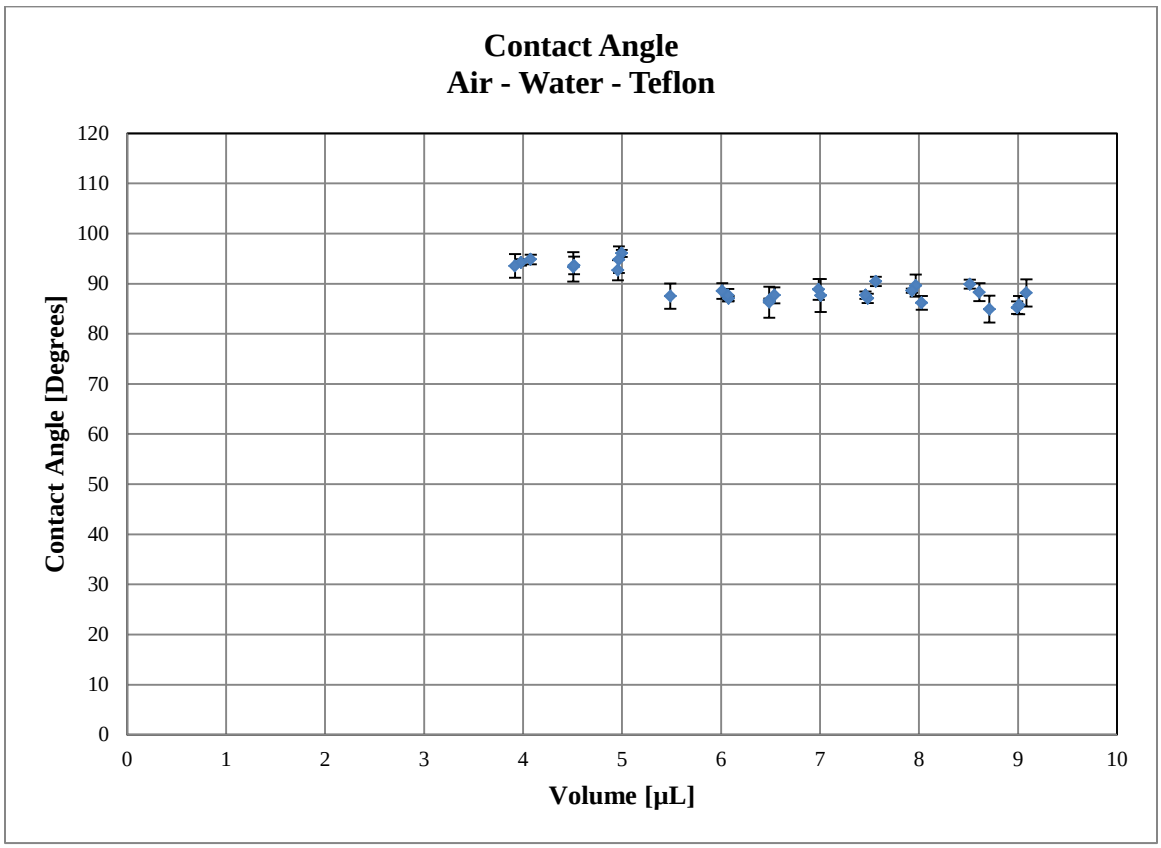

Figure 5.3-1: Air-Water-Teflon Contact Angle

5.3.1.1 Analysis of the results for Contact Angle in Neutral Systems

Comparing these results with the results obtained in Figure (5.2-1) we could see the appearance of the two regions again and even though the deviation for each sample in general terms improved the average value for the contact angle is very much the same as the one obtained when we processed all the data without manually enhancing.

5.3.1.2 Normality test results for Contact Angle in Neutral system

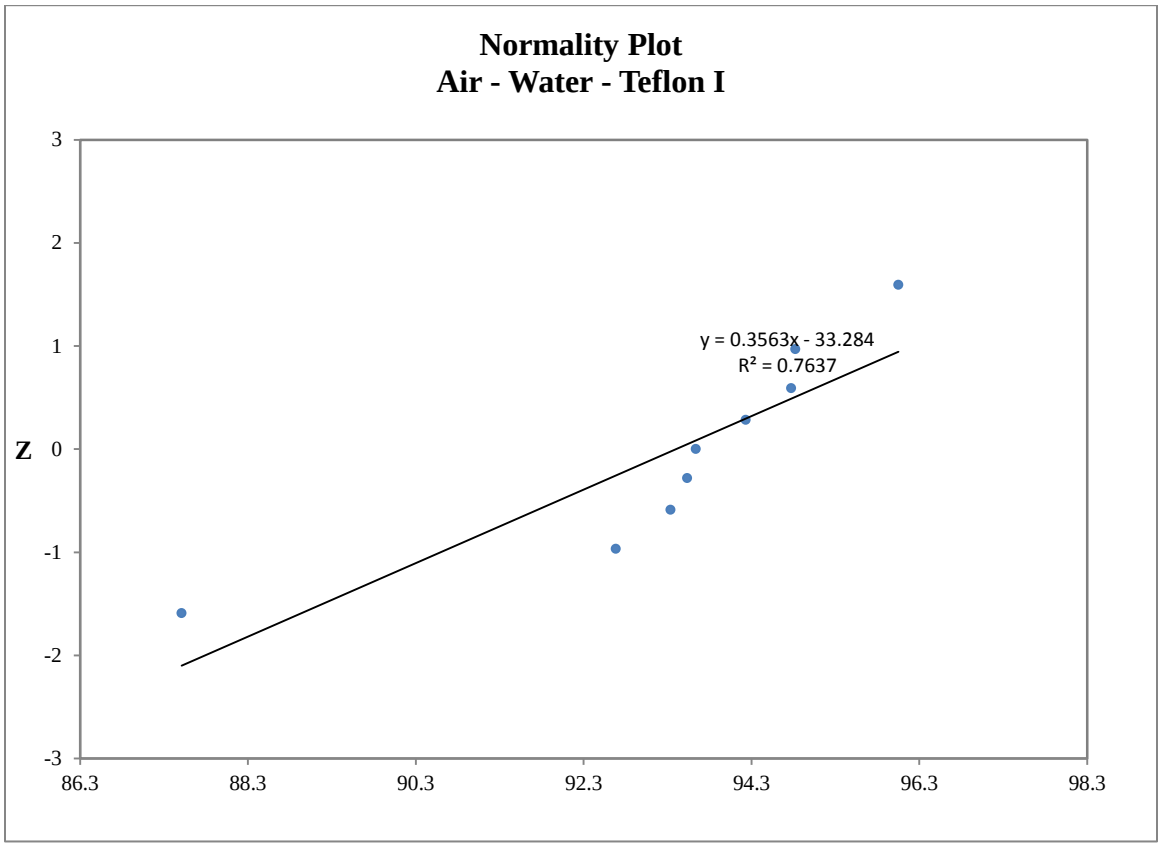

Figure 5.3-2: Contact Angle Air-Water-Teflon Z normality test I

The results from Table (5.3.1-1) for region I show a *p*-value of 0.018 which is smaller than 0.05 and an A-squared value of 0.843 which is bigger than the critical value at 95% which is 0.787 and lower than the critical value at 99% which is 1.092. These mean the data in this region is not normally distributed at alpha of 0.05 but al alpha of 0.01 it is and in this particular case the A-squared method fails to determine the normality of my data. However the Z normality test will help me to determine from Figure (5.3-2) that the data is not normally distributed since the point does not fall into the straight line.

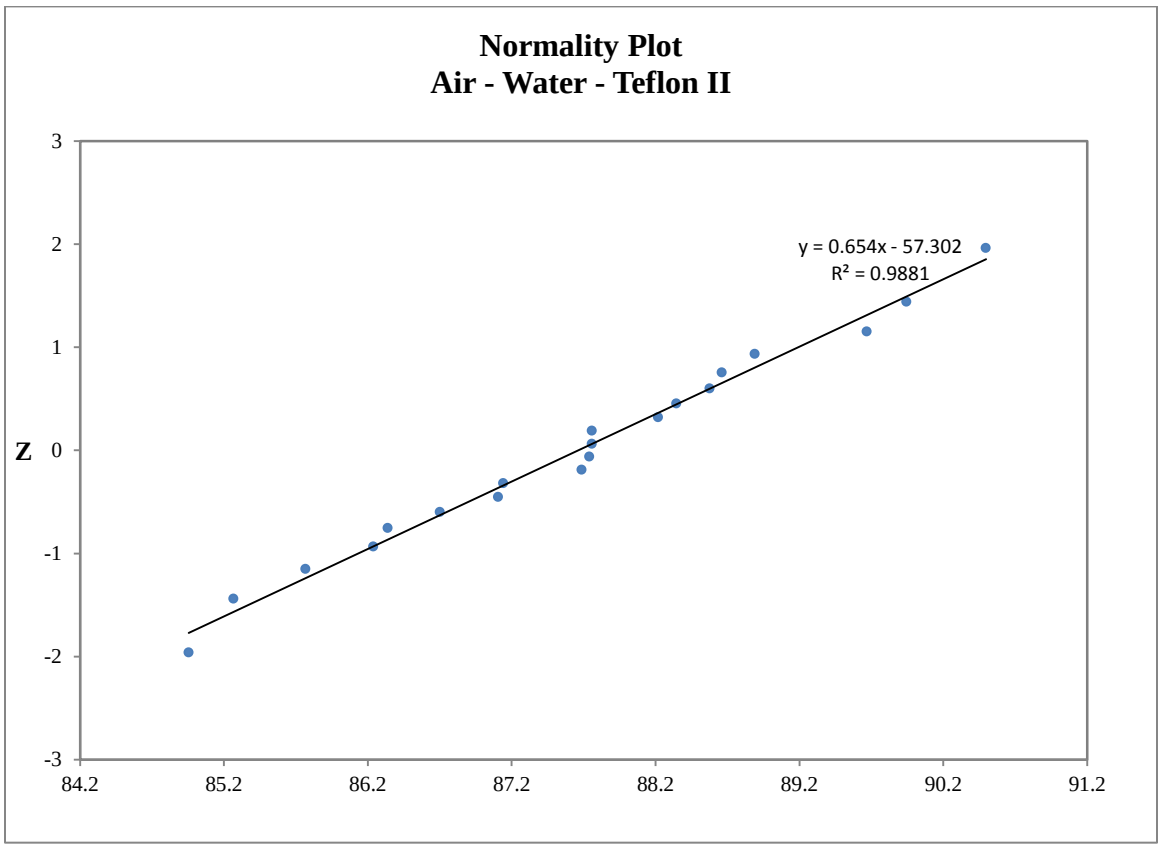

Figure 5.3-3: Contact Angle Air-Water-Teflon Z normality test II

The results from Table (5.3.1-1) for region II show a *p*-value of 0.964 which is bigger than 0.05 and an A-squared value of 0.143 which is smaller than the critical value at 95% which is 0.787 and at 99% which is 1.092. These mean we can be at least 99% confident that the data is normally distributed.

From Figure (5.3-1) we can observe the data is fairly normal distributed around the straight line which confirms what was calculated using the Anderson-Darling method.

Table 5.3-1: Air-Water-Teflon normality test results equilibrium time

Experiment	A-Squared	*p*	95% Critical Value	99% Critical Value
Neutral System I	0.843	0.018	0.787	1.092
Neutral System II	0.143	0.964	0.787	1.092

5.3.1.3 Analysis of the results for Interfacial Tension in Neutral system

From Figure (5.3-4) we can see a very similar result when we manually enhanced the data and when we used only the edge detector as it was in Figure (5.2-2).

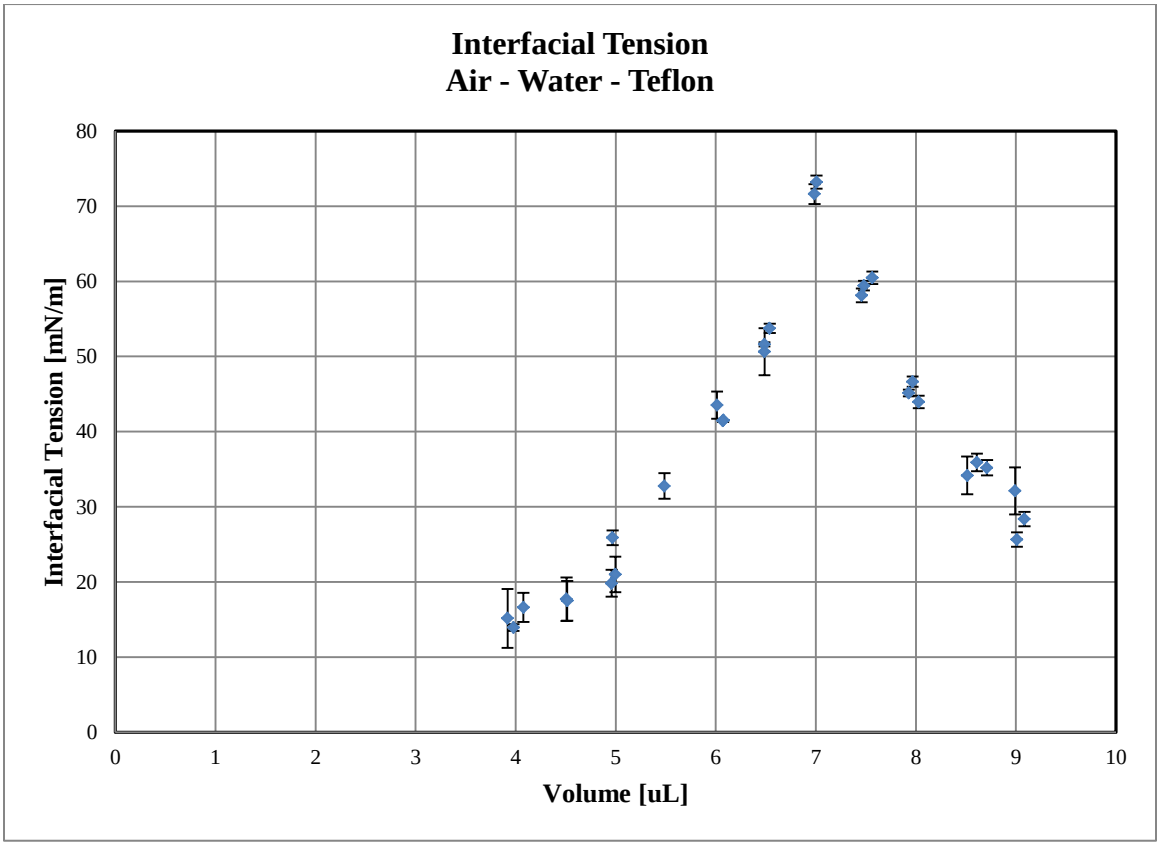

Figure 5.3-4: Air-Water-Teflon Interfacial Tension

The main difference when we used the manual enhancing is a bigger standard deviation from each droplet analyzed which could be explain because we are adding error to the determination of the interface.

Table 5.3-2 Experimental results (Air-Water-Teflon)

Volume (µL)	Standard Deviation (µL)	Contact Angle (Degrees)	Standard Deviation (Degrees)	Interfacial Tension (mN/m)	Standard Deviation (mN/m)
4.0	0.1	94.2	0.7	13.96	0.44
3.9	0.2	93.5	2.4	15.16	3.91
4.1	0.0	94.8	1.0	16.63	1.92
4.5	0.0	93.3	2.9	17.71	2.89
4.5	0.0	93.6	1.8	17.51	2.64
5.0	0.0	96.06	0.7	21.02	2.35
5.0	0.1	94.8	2.7	25.9	0.98
5.0	0.0	92.7	2.0	19.8	1.79
5.49	0.0	87.52	2.5	32.77	1.70
6.08	0.1	87.09	0.5	41.51	0.00
6.07	0.1	87.71	1.2	41.43	0.12
6.01	0.1	88.53	1.6	43.53	1.83
6.54	0.1	87.69	1.6	53.75	0.61
6.49	0.0	86.65	0.4	51.61	0.27
6.49	0.1	86.29	3.1	50.63	3.14
6.99	0.1	88.84	2.1	71.60	1.31
7.01	0.1	87.64	3.3	73.20	0.86
7.48	0.1	87.06	0.9	59.42	0.64
7.46	0.1	87.71	0.7	58.11	0.91
7.56	0.1	90.45	0.9	60.47	0.84
7.97	0.0	89.62	2.2	46.64	0.68
7.93	0.0	88.61	0.4	45.13	0.44
8.03	0.1	86.19	1.4	43.95	0.81
8.61	0.2	88.30	1.8	35.90	1.18
8.71	0.1	84.91	2.7	35.20	1.01
8.51	0.1	89.90	0.9	34.17	2.51
8.99	0.1	85.22	1.3	32.12	3.13
9.01	0.1	85.72	1.8	25.66	0.96
9.08	0.1	88.17	2.7	28.37	0.98

5.3.2 Water Wet System

Initially we had processed the complete data for this system manually enhancing the interface. On this case the random droplets chosen were processed using only the edge detector and the results are shown in Figure (5.3-5).

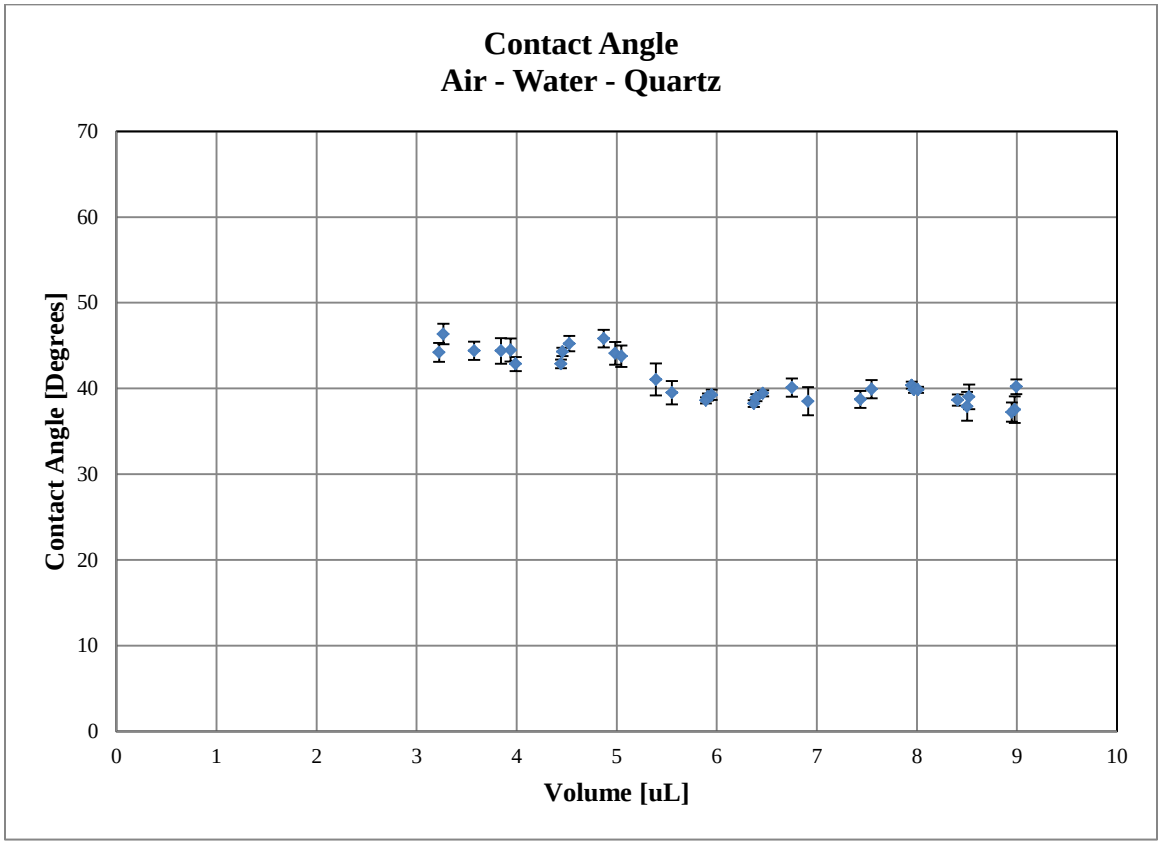

Figure 5.3-5: Air-Water-Quartz Contact Angle

5.3.1.4 Analysis of the results for Contact Angle in Water Wet System

Similarly to the manually enhanced data processing used before for the complete data collected for this system the results show two regions and the values for each region of the average contact angle is very much the same. The first region shows an average contact angle of about 46 degrees while the second region shows an average contact angle of about 42 degrees.

The standard deviation from each sample show very similar behaviour as it was when we manually enhanced the data.

5.3.1.5 Normality test results for Contact Angle in Water Wet System

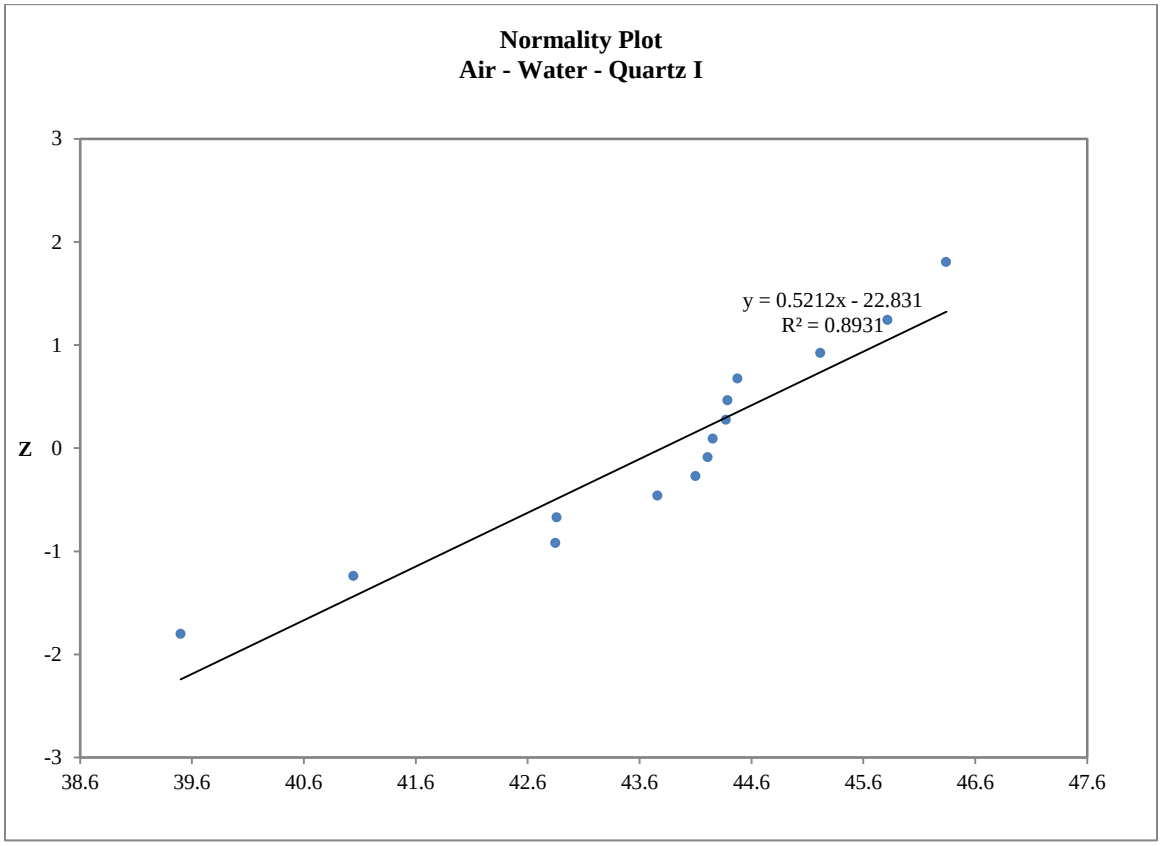

Figure 5.3-6: Contact Angle Air-Water-Quartz Z normality test I

The results from Table (5.3.2-1) for region I show a *p*-value of 0.069 which is bigger than 0.05 and an A-squared value of 0.653 which is smaller than the critical value at 95% which is 0.787 and at 99% which is 1.092. These mean the data in this region is normally distributed. However the Z normality test will help me to determine from Figure (5.3-6) that the data is not normally distributed since the point doesn't fall into the straight line and the correlation is low.

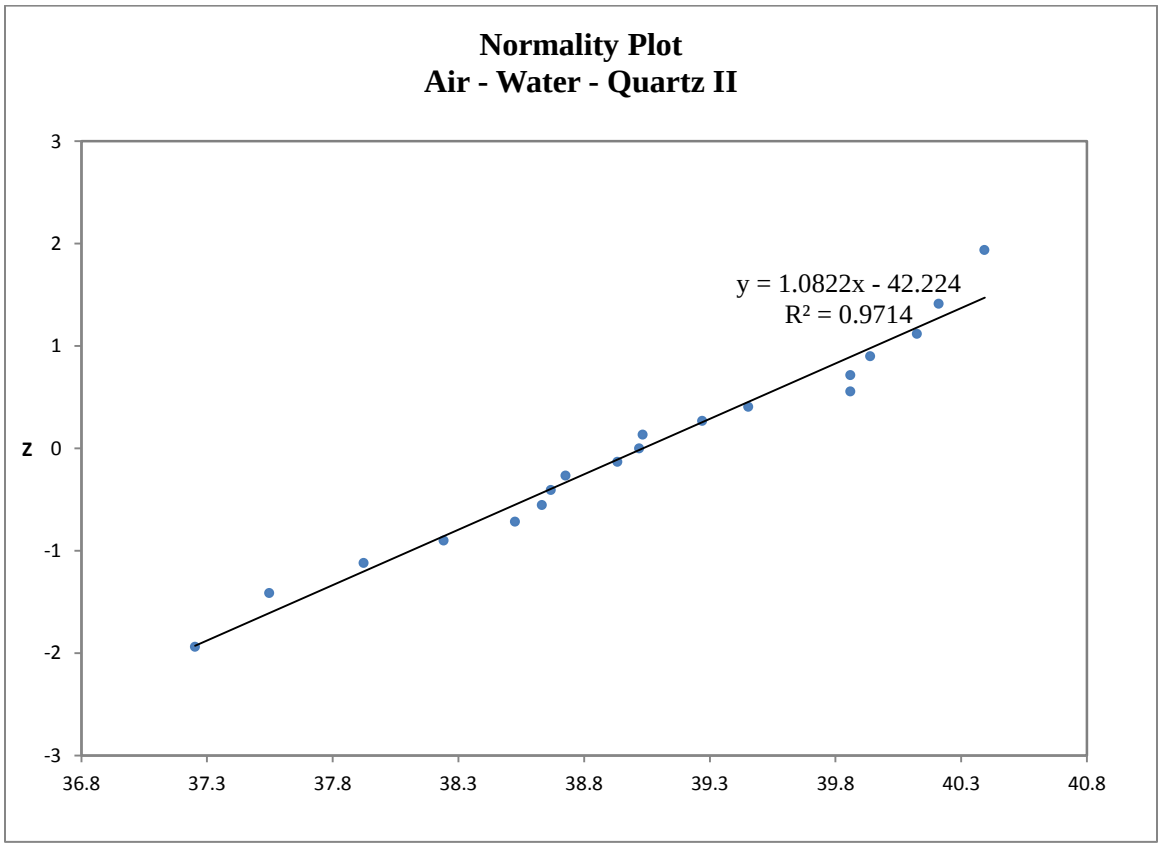

Figure 5.3-7: Contact Angle Air-Water-Quartz Z normality test II

The results from Table (5.3.2-1) for region II show a *p*-value of 0.747 which is bigger than 0.05 and an A-squared value of 0.238 which is smaller than the critical value at 95% which is 0.787 and at 99% which is 1.092. These mean we can be at least 99% confident that the data is normally distributed.

From Figure (5.3-7) we can observe the data is fairly normal distributed around the straight line which confirms what was calculated using the Anderson-Darling method.

Table 5.3-3: Air-Water-Quartz normality test results equilibrium time

Experiment	A-Squared	*p*	95% Critical Value	99% Critical Value
Water wet system I	0.653	0.069	0.787	1.092
Water wet system II	0.238	0.747	0.787	1.092

5.3.1.6 Analysis of the results for Interfacial Tension in water wet system

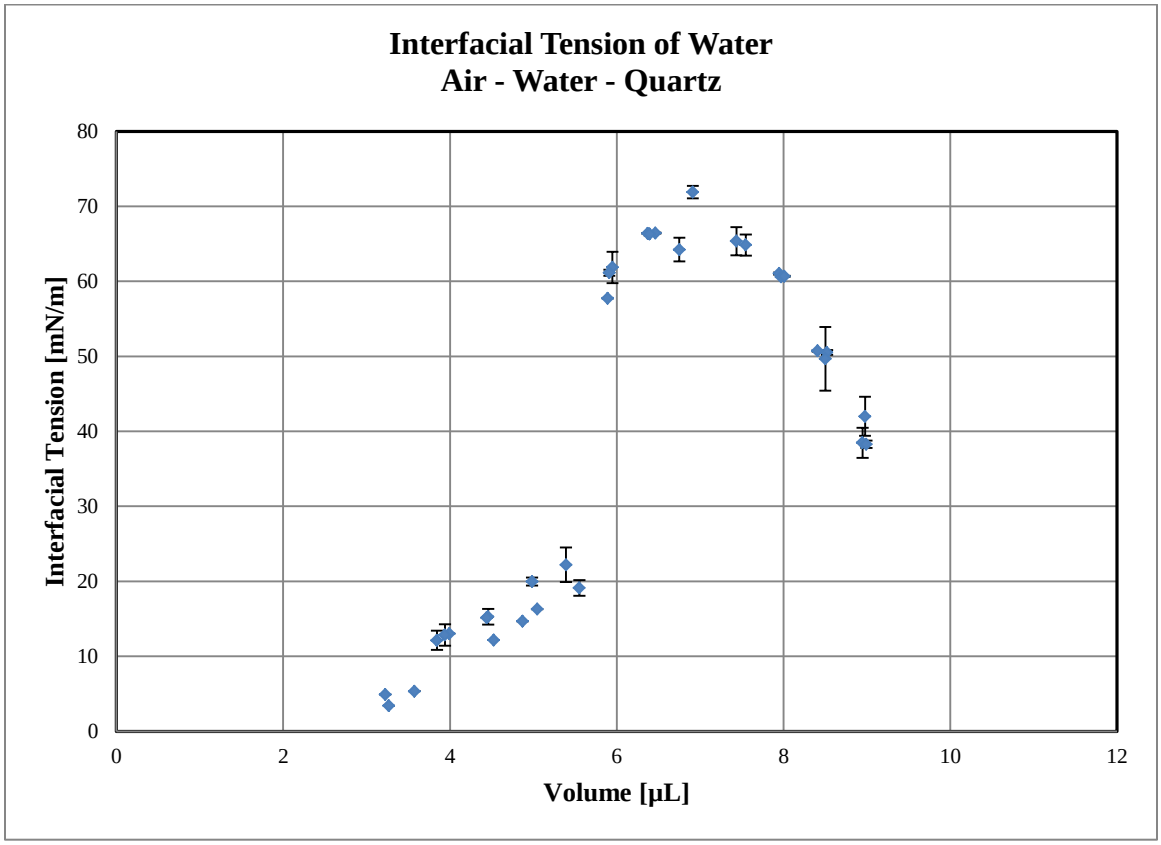

Figure 5.3-8: Air-Water-Quartz Interfacial Tension

The results from Figure (5.3-8) show a similar behaviour than the ones in Figure (5.2-4) where we manually enhanced the data before we used the edge detector. Overall the standard deviation of the data for each droplet increase showing the influence of the quality of the images taken.

Table 5.3-4 Experimental results "Air-Water-Quartz"

Volume (µL)	Standard Deviation (µL)	Contact Angle (Degrees)	Standard Deviation (Degrees)	Interfacial Tension (mN/m)	Standard Deviation (mN/m)
3.3	0.1	46.3	1.2	3.41	0.01
3.6	0.1	44.4	1.1	5.35	0.00
3.2	0.1	44.2	1.1	4.93	0.00
3.8	0.1	44.4	1.5	12.14	1.27
4.0	0.0	42.9	0.8	13.02	0.00
3.9	0.1	44.48	1.3	12.86	1.44
4.5	0.0	44.3	0.5	15.3	1.04
4.5	0.1	45.2	0.9	12.2	0.00
4.44	0.1	42.87	0.5	15.13	0.01
4.87	0.0	45.82	1.0	14.66	0.02
4.98	0.0	44.11	1.3	19.98	0.54
5.05	0.0	43.77	1.2	16.29	0.01
5.39	0.0	41.05	1.9	22.20	2.29
5.55	0.0	39.51	1.4	19.12	1.06
5.95	0.0	39.26	0.6	61.86	2.08
5.91	0.1	39.01	0.4	61.16	0.40
5.89	0.1	38.62	0.4	57.75	0.05
6.37	0.1	38.23	0.4	66.39	0.04
6.46	0.1	39.44	0.3	66.44	0.05
6.39	0.1	38.92	0.4	66.30	0.20
6.91	0.1	38.51	1.6	71.88	0.83
7.43	0.1	38.71	1.0	65.37	1.88
6.75	1.7	40.11	1.1	64.24	1.60
7.55	0.0	39.92	1.1	64.84	1.41
7.95	0.1	40.38	0.4	61.05	0.14
7.97	0.1	39.85	0.4	60.61	0.02
8.01	0.1	39.85	0.4	60.68	0.06
8.52	0.1	39.02	1.4	50.53	0.31
8.41	0.0	38.65	0.6	50.74	0.10
8.50	0.1	37.91	1.7	49.67	4.25
8.98	0.0	37.53	1.5	42.00	2.60
8.95	0.0	37.24	1.1	38.47	2.01
8.99	0.1	40.20	0.9	38.27	0.50

5.3.2 Oil-based Substrate System

Similarly to the water wet system, the oil-based substrate system was processed using only the edge detector. The results are shown in Figure (5.3-9).

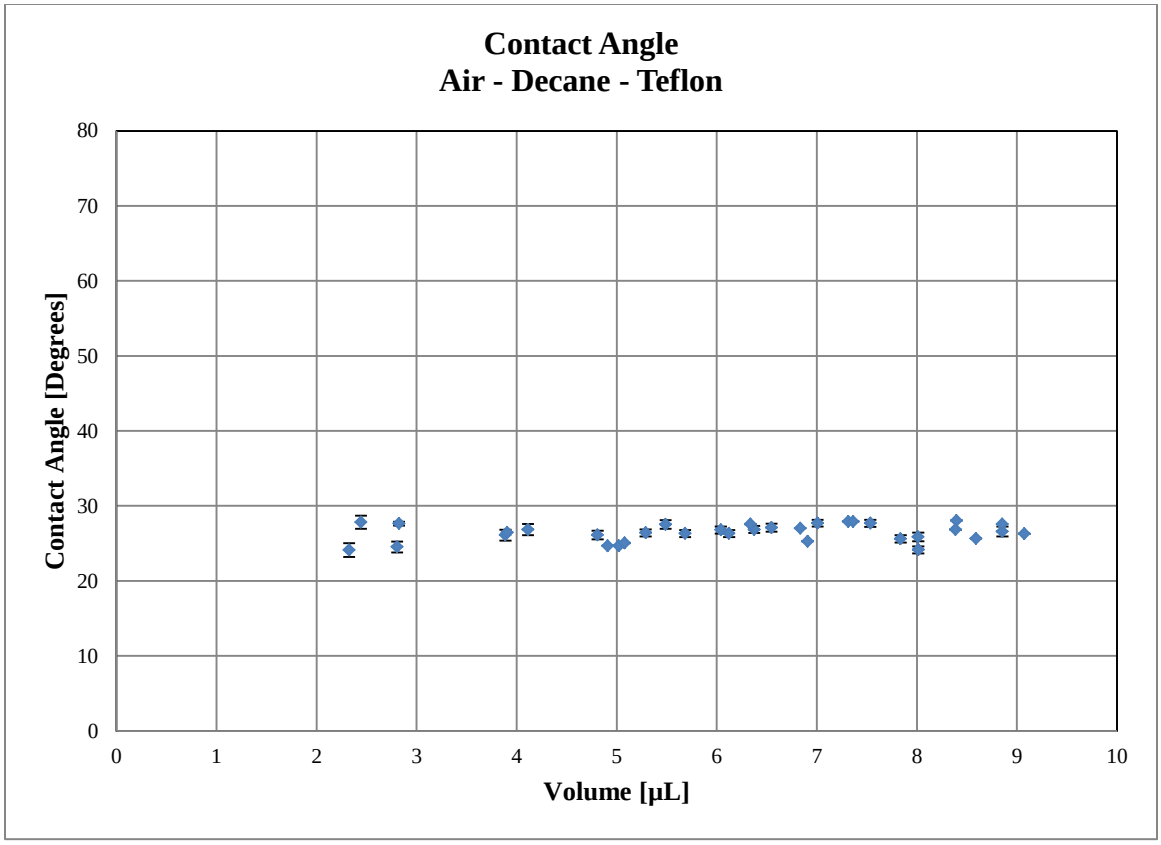

Figure 5.3-9: Air-Decane-Teflon Contact Angle

5.3.2.1 Analysis of the results for Contact Angle in Oil-based substrate System

The results from Figure (5.3-9) obtained when we used only the edge detector show a similar trend of the ones obtained when we manually enhanced the interface which we can see in Figure (5.2-5). However, in this case there is a small difference in the average contact angle calculated. For the manually enhanced the contact angles is an average of 29 degrees while in this case we

can see an average of about 27 degrees. This could have been caused by a low quality of the images.

The two ways to process the images yield very similar average values of the contact angle. These results are consistent in the three systems which tell us that we do not need to manually enhance the interface. This conclusion is very important because it minimizes the amount of work when we processed the results.

5.3.2.2 Normality test results for Contact Angle in Oil-based Substrate System

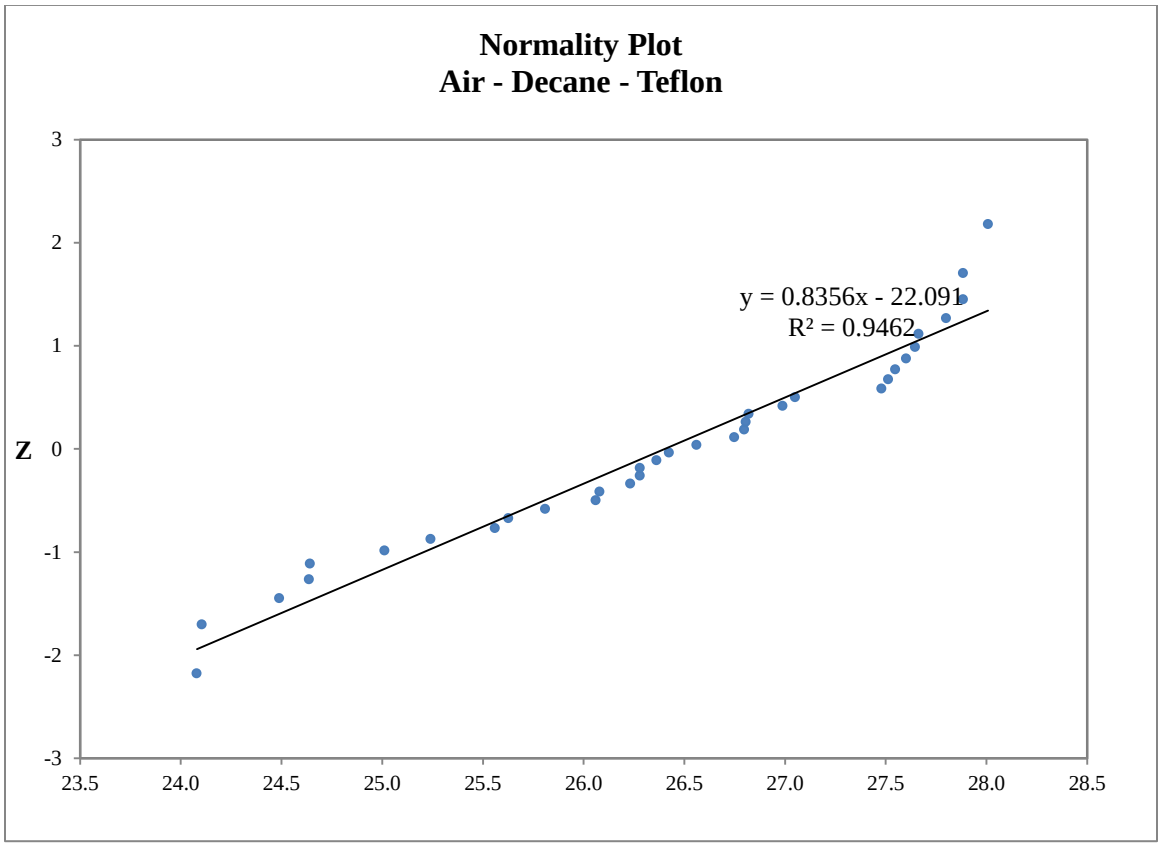

Figure 5.3-10: Contact Angle Air-Decane-Teflon Z normality test

The results from Table (5.3.3-1) show a *p*-value of 0.113 which is bigger than 0.05 and an A-squared value of 0.596 which is smaller than the critical value at 95% which is 0.787 and at 99% which is 1.092. These mean we can be at least 99% confident that the data is normally distributed.

From Figure (5.3-10) we can observe the data is fairly normal distributed around the straight line which confirms what was calculated using the Anderson-Darling method.

Table 5.3-5: Air-Decane-Teflon normality test results

Experiment	**A-Squared**	***p***	**95% Critical Value**	**99% Critical Value**
Oil-based Substrate	0.596	0.113	0.787	1.092

5.3.2.3 Analysis of the results for Interfacial Tension in Oil-based substrate system

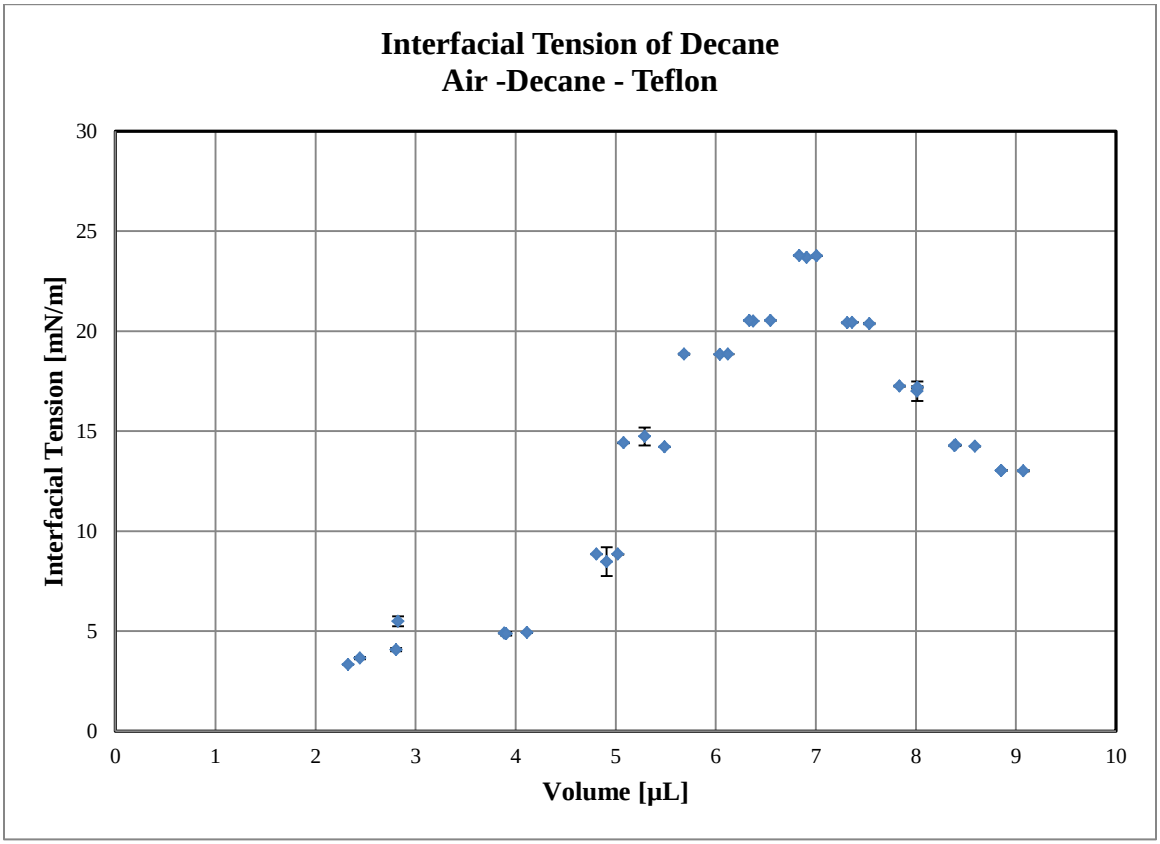

Figure 5.3-11: Air-Decane-Teflon Interfacial Tension

Similarly to the interfacial tension results from the previous systems the oil-based substrate system in Figure (5.3-11) shows a very similar behavior to the one with the manually enhanced processing showed in Figure (5.2-6).

From the interfacial tension determination we can also conclude that the manually enhancing of the interface does not change the values of the interfacial tension and therefore it is an extra work we can cut off to speed up the calculation of the interfacial properties.

Table 5.3-6 Experimental results "Air-Decane-Teflon"

Volume (µL)	Standard Deviation (µL)	Contact Angle (Degrees)	Standard Deviation (Degrees)	Interfacial Tension (mN/m)	Standard Deviation (mN/m)
2.4	0.0	27.8	0.9	3.65	0.05
2.3	0.1	24.1	0.9	3.33	0.02
2.8	0.1	27.6	0.3	5.49	0.24
2.8	0.1	24.5	0.7	4.07	0.08
3.9	0.0	26.1	0.7	4.9	0.02
3.9	0.0	26.5	0.0	4.9	0.09
4.11	0.1	26.84	0.8	4.93	0.02
4.81	0.1	26.11	0.6	8.85	0.01
4.91	0.0	24.68	0.0	8.47	0.72
5.02	0.1	24.67	0.0	8.84	0.02
5.49	0.1	27.51	0.6	14.21	0.01
5.29	0.1	26.40	0.5	14.73	0.45
5.08	0.0	25.05	0.0	14.41	0.02
6.04	0.0	26.78	0.5	18.84	0.01
5.68	0.1	26.32	0.5	18.85	0.02
6.12	0.1	26.32	0.5	18.85	0.01
6.38	0.0	26.85	0.5	20.50	0.00
6.34	0.1	27.55	0.0	20.53	0.02
6.55	0.0	27.09	0.5	20.53	0.02
7.01	0.0	27.70	0.4	23.76	0.01
6.91	0.1	25.28	0.0	23.68	0.01
6.83	0.0	27.02	0.0	23.78	0.02
8.01	0.0	25.84	0.6	16.99	0.49
7.84	0.0	25.59	0.5	17.25	0.02
8.01	0.0	24.14	0.5	17.19	0.06
7.53	0.1	27.68	0.5	20.37	0.03
7.31	0.0	27.92	0.0	20.42	0.03
7.36	0.1	27.92	0.0	20.44	0.01
8.40	0.0	28.04	0.0	14.30	0.01
8.59	0.0	25.66	0.0	14.24	0.01
8.39	0.0	26.83	0.0	14.27	0.02
9.07	0.0	26.27	0.0	13.01	0.03
8.85	0.0	26.60	0.7	13.03	0.01
8.85	0.0	27.58	0.0	13.03	0.01

Chapter Six: Conclusions

6.1 Conclusions from preliminary testing

- The symmetry of the droplet depends strongly on the way the droplet is placed on the substrate. Some of the factors that can significantly affect the symmetry are the distance of the injection needle from the surface, the size of the falling drop and the pressure applied to inject the drop. Therefore, some preliminary tests have been run to investigate these changes and avoid them. Yet, some of the unusual changes in the contact angle of the systems can be a consequence of the asymmetry of some drop cause by the method of drop injection.

- The contact angle is affected significantly by the movement needed to place the cell levelled and at the correct height to take the images. A new cell was designed based on these observations. The setup of the new cell became easier and faster.

- The biggest limitation given by the micro CT-scanner is the setup of the system. The system has to be setup exposed to the atmosphere. The substrate is kept in water and rinsed every other day to keep it as clean as possible. However, substrates expose to the atmosphere are quickly contaminated even if they have low surface tension.

- In a sequence of images taken at the same conditions we observed diminishing of the quality of the image with the sequence. Sometimes after some hours of operation the micro CT-scanner gave us low quality images since the beginning of the sequence being taken. This behaviour of the equipment can contribute to error in the determination of the contact angle.

6.2 Conclusions from the equilibrium time

- It is extremely important to keep the system completely level as well as the droplet shape as symmetric as possible in order to obtain consistent values of contact angles. This was observed in the experiment 2 where we obtained a value of contact angle 7 degrees bigger that the values obtain in experiment 1 and 3. For each experiment we used the same system except for the volume of the droplet of water. Other factors that could have influence the contact angle in experiment 2 are the presence of dirt and possible hydrophilic patches on the substrate. In microscopic scale the quartz surface is not very smooth and that affects the contact angle.

- The standard deviation from each sequence of images is in most cases negligible. The cases where we have standard deviations around three degrees are where the sequence got lower quality images. Most of the low quality images started to appear after the fourth image taken and in some cases since the beginning. Since the micro CT-scanner was operated under the same conditions; this behaviour can only be a malfunction of the equipment.

- The mean value of the contact angle determine for each sequence has a minimum variation with time for each experiment. This indicates the system reach the equilibrium once it is placed on the substrate. In preliminary experiments we were obtaining a constant change in the contact angle every time we took images. This could be explain by the constant movement the system had to go through to get it levelled which could have affected the symmetry of the drop. With the new designed cell we avoided these problems.

6.3 Conclusions from the Neutral, Water Wet and Oil-based Substrate Systems

6.3.1 Contact angle

- The digital processing of the images without manual enhancing gives in some cases a considerable standard deviation; this is a consequence of the lower definition of some images in the sequence of some samples. Most often, this occurred between the 4 and 7 images taken in the sequence and some times since the beginning of it. However, after processing the images from each system using manually enhancing and without it we could observe the average values of the contact angle does not change significantly. This can make the method faster without losing accuracy in the determination of the contact angle

- The two regions we can observe on the results show no dependency of the contact angle with the volume of the droplet which was observed in the experiments to establish the equilibrium time. The contact angle tends to be of a constant value when the volume of the droplet increases. Taking into account that we used in the neutral system a low surface tension substrate and in the water wet system a high surface tension substrate we can conclude that the appearance of the two regions in this two systems are not caused by contamination on the surface of the substrate. This is the consequence of the setup we used to run the micro CT. Under the setup used for magnification of the image a pixel is the representation of 11µm which could be enhanced to 5µm. When we use a magnification that represents 11µm per pixel for droplets of volume less than 6µl the equipment fail to detect properly the interface at the contact point.

6.3.2 Interfacial Tension

- The interfacial tension is less influenced by the quality of the images processed. The standard deviation in most of the samples is minimal. This is the result of the fitting of all the points of the interface into a Laplacian curve which minimizes the influence of the poor location of the points located close to the substrate.

- The interfacial tension has a strong influence from the volume of the droplet. The values of the interfacial tension change sharply with a small change on the volume which makes it harder to determine when we use volumes between 3.5µl and 9µl; it would be necessary to obtain many points to populate the graphic and consider the results reliable. This translates into a greater amount of work.

- From the three systems we were able to calculate the interfacial tension using the ADSA-P method. Even though there is a sharp change in the values of the IFT with the volume we could observe that the known value of the IFT for the three systems was obtained at around 7µL. This could tell us what volumes of droplets we should use to determine the IFT when we use sessile droplets. However, we need to consider the influence on the difference in the densities of the phases present. Since the interfacial properties are determined by a balance of forces between the phases; the determination of the IFT in systems where the difference in densities are smaller may affect the volume of the droplet we need to use to determine the IFT.

Chapter Seven: Recommendations

- The methodology used in this project proved to be reliable to calculate interfacial properties using micro CT imaging. The practicality of the method could be improved by trying different X-ray equipment that could have an easier setup of the system.

- The use of this methodology in reservoir engineering systems and conditions could have a problem due to the sensitivity of micro X-ray imaging to the density of the components of the system. This could be improved by adding doping substances that could enhance the contrast at the interface.

- The new designed cell improved significantly the setup of the system for the micro CT used in this project. Improvements to the cell should be studied specifically in how to create the axisymmetric droplet. A different way of injection is advisable.

- The methodology proved to be effective in the determination of the interfacial properties at standard conditions. Studies of systems at high temperature and high pressure should be the next step since micro X-ray imaging can be implemented under any conditions of temperature and pressure as long as the system is safe.

References

Adamson, A. W. and A. P. Gast (1997). Physical Chemistry of Surfaces Sixth, John Wiley & Sons, Inc.

Alvarez, J. M., A. Amirfazli and A. W. Neuman (1999). "Automation of the axisymetric drop shape analysis-diameter for contact angle measurements." Colloids and Surfaces A: Physicochemical and Engineering Aspects **156**(1-3): 163-176.

Amirfazli, A., J. Graham-Eagle, S. Pennell and A. W. Neuman (2000). "Implementation and examination of a new drop shape analysis algorithm to measure contact angle and surface tension from the diameters of two sessile drops." Colloids and Surfaces A: Physicochemical and Engineering Aspects **161**(1):63-74.

Anderson, W. G. (1986a). "Wettability Literature Survey- Part 1: Rock/Oil/Brine interactions and the Effects of Core Handling on Wettability." Journal of Petroleum Technology **38**(11): 1125-1144.

Anderson, W. G. (1986b). "Wettability Literature Survey- Part 2: Wettability Measurement." Journal of Petroleum Technology **38**(12): 1246-1262.

Bashford, F. and J. C. Adams (1892). An Attempt to Test the theory of Capillary Action, Cambridge, Cambridge University Press and Deighton Bell.

Batteni, A., S. S. Susnar, A. Amirfazli and A. W. Neuman (2003). "A high-accuracy polynomial fitting approach to determine contact angles." Colloids and Surfaces A: Physicochemical and Engineering Aspects **219**(1-3):215-231.

Boruvka L. and A. W. Neumann (1977). "Generalization of the classical theory of capillarity." Journal of Chemical Physics **66**(12): 5464-5476.

Butt, H. J., K. Graf and M. Kappl (2006). Physics and Chemistry of Interfaces Second, Wiley-VCH.

Cabezas, M.G., A. Bateni, J. M. Montanero and A. W. Neuman (2004). " A new drop-shape methodology for surface tension measurement." Applied Surface Science **238**(1-4): 480-484.

Cabezas, M.G., A. Bateni, J. M. Montanero and A. W. Neuman (2005). " A new method of image processing in the analysis of axisymetric drop shapes." Colloids and Surfaces A: Physicochemical and Engineering Aspects **255**(1-3):193-200.

Cheng. P., D. Li, L. Boruvka, Y. Rotenberg and A. W. Neuman (1990). "Automation of axisymetric drop shape analysis for measurements of interfacial tensions and contact angles." Colloids and Surfaces **43**(2):151-167.

Dandekar, A. Y. (2006). Petroleum Reservoir Rock and Fluid Properties, CRC Press.

del Rio, O. I., D. Y. Kwok, R. Wu, J. M. Alvarez and A. W. Neuman (1998). "Contact angle measurements by axisymetric drop shape analysis and an automated polynomial fit program." Colloids and Surfaces A: Physicochemical and Engineering Aspects **143**(2-3):197-210.

Dingle, N. M. (2005). A finite element based algorithm for determining interfacial tension and contact angle from pendant and sessile drop profiles. United States – Indiana, Perdue University.

Dobrzynski, L. (1978). Handbook of Surfaces and Interfaces. 1, Garland STPM Press.

Erbil, H. Y. (2006). Surface Chemistry of Solid and Liquid Interfaces, Wiley-Blackwell.

Fordham, S. (1948). "On the Calculation of Surface Tension from Measurements of Pendant Drops." Processing of Royal Society London A **194**.

Gu, Y. (2001). "Drop size dependence of contact angles of oil drops on a solid surface in water". Colloids and Surfaces A: Physicochemical and Engineering Aspects **181**(1-3): 215-224.

Hartland, S. and R. W. Hartley (1976). Axisymmetric Fluid-Liquid Interfaces, Amesterdanm, Elsevier.

Holgado-Terriza, J. A., J. F. Gomez-Lopera, P. L. Luque-Escamilla, C. Atae-Allah and M. A. Cabrerizo-Vilchez (1999). « Measurement of ultralow interfacial tension with ADSA using an entropic edge-detector." Colloids and Surfaces A: Physicochemical and Engineering Aspects **156**(1-3):579-586.

Hoorfar, M. and A. W. Neumann (2006). "Recent progress in Axisymetric Drop Shape Analysis (ADSA)". Advances in Colloid and Interface Science **121**(1-3):25-49.

Iliev, S. and N. Pesheva (2006). "Nonaxisymetric drop shape analysis and its application for determination of the local contact angles." Journal of Colloid and Interface Science **301**(2): 677-684.

Israelachvilli, J. N. (1985) Intermolecular and Surface Forces: with Applications to Colloidal and Biological Systems, Academic Press.

Jaycock, M. J. and G. D. Parfitt (1981). Chemistry of Interfaces, Prentice Hall Europe.

Kantzas, A. (1990). "Investigation of Physical Properties of Porous Rocks and Fluid Flow Phenomena in Porous Media Using Computer Assisted Tomography" In Situ**14**91):56.

Lam, C. N. C., N. Kim, D. Hui, D. Y. Kwok, M. L. Hair and A. W. Neumann (2001a). "The effect of liquid properties to contact angle hysteresis." Colloids and Surfaces A: Physicochemical and Engineering Aspects **189**(1-3):265-278.

Lam, C. N. C., R. H. Y. Ko, L. M. Y. Yu, A. Ng, D. Li, M. L. Hair and A. W. Neumann (2001b). "Dynamic cycling Contact Angle Measurements: Study of Advancing and Receding Contact Angles." Journal of Colloids and Interface Science **243**(1):208-218.

Li, D., P. Cheng and A. W. Neumann (1992). "Contact angle measurement by axisymmetric drop shape analysis (ADSA)." Advances in Colloid and Interface Science **39**:347-382.

Li, D., A. W. Neumann (1990). "Determination of line tension from the drop size dependence of contact angles." Colloids and Surfaces **43**(2): 195-206.

Malcolm, J. D. And H. M. Paynter (1981). "Simultaneous determination of contact angle and interfacial tension from sessile drop measurements." Journal of Colloids and Interface Science **82**(2).

Matijevic, E., Ed. (1969a). Surface and Colloid Science. Vol. 2, Willey-Interscience.

Matijevic, E., Ed. (1969b). Surface and Colloid Science. Vol. 1, Willey-Interscience.

Maze, C. And G. Burnet (1969). "A non-linear regression method for calculating surface tension and contact angle from the shape of a sessile drop." Surface Science**13**(2).

Maze, C. And G. Burnet (1971). "Modifications of a non-linear regression technique used to calculate surface tension from sessile drops" Surface Science**24**(1).

Mees, F., R. Swennen, M. V. Geet and P. Jacobs (2003). "Application of X-ray Computed Tomography in the Geoscience." Geological Society**215**:6.

Moy, E., P. Cheng, Z. Policova, S. Treppo, D. Kwok, D. P. Mack, P. M. Sherman and A. W. Neumann (1991). "Measurement of contact angles from the maximum diameter of non-wetting drops by means of a modified axisymmetric drop shape analysis." Colloids and Surfaces **58**(3):215-227.

Padday, J. F., Ed. (1969). Surface and Colloid Science. Vol. 1. New York, John Willey and Sons.

Padday, J. F. and A. Pitt (1972). "AXISYMETRIC MENISCUS PROFILES". Journal of Colloid And Interface Science **38**(2):323-&.

Peacock, G. and J. Murray, Eds. (1855). Miscellaneous Works of Thomas Young. Vol. 1. London.

Princen, H. M., I. Y. Z. Zia and S. G. Mason (1967b). "Measurement of Interfacial Tension from the Shape of a Rotating Drop." Journal of Colloid and Interface Science **23**: 99-107.

Rajayi. M (2010). Interfacial Phenomena of Bitumen and Water at Elevated Temperatures and Pressures. Canada -- Alberta, Calgary University.

Rio, O. I. d. And A. W. Neumann (1997). "Axisymmetric Drop Shape Analysis: Computational Methods for the Measurement of Interfacial Properties from the Shape and Dimensions of Pendant and Sessile Drops." Journal of Colloid and Interface Science **196**(2): 136-147.

Rotenberg, Y., L. Boruvka and A. W. Neumann (1982). "Determination of Surface Tension and Contact Angle from the Shapes of Axisymmetric Fluid Interfaces." Journal of Colloid and Interface Science **93**(1): 15.

Schembre, J. M. (2004). Temperature, surface forces, wettability and their relationship to relative permeability of porous media. United States – California, Stanford University.

Skinner, F. K., Y. Rotenberg and A. W. Neumann (1989). "Contact angle measurements from the contact diameter of sessile drops by means of a notified axisymmetric drop shape analysis." Journal of Colloid and Interface Science **130**(1):25-34.

Spelt, J. K., Y. Rotenberg, D. R. Absolom and A. W. Neumann (1987). "Sessile-drop contact angle measurements using axisymmetric drop shape analysis." Colloids and Surfaces **24**(2-3):127-137.

Susnar, S. S., P. Chen, O. I. del Rio and A. W. Neumann (1996). "Surface tension response to area changes using axisymmetric drop shape analysis." Colloids and Surfaces A: Physicochemical and Engineering Aspects **116**(1-2):181-194.

Wellington, S. L. and H. J. Vinegar (1987). "X-Ray Computerized Tomography." Journal of Petroleum Technology: 14.

Wulf, M., S. Michel, K. Grundke, O. I. del Rio, D. Y. Kwow and A. W. Neumann (1999). "Simultaneous Determination of Surface Tension and Density of Polymer Melts Using Axisymmetric Drop Shape analysis." Journal of Colloid and Interface Science **210**(1): 172-181.

Zuo, Y. Y., M. Ding, A. Bateni, M. Hoorfar and A. W. Neumann (2004a). "Improvement of interfacial tension measurement using a captive bubble in conjunction with axisymmetric drop shape analysis (ADSA)." Colloids and Surfaces A: Phycochemical and Engineering Aspects **250**(1-3):223-246.

APPENDIX A: COMPUTER ROUTINES

A.1. Edge detection

```
I = imread('name of the file.bmp');
I = I(:,:,1);
imshow(I)
threshhold = 0.2;  %Adjust the threshold to minimize edges
BW2 = edge(I,'canny',threshhold);
figure, imshow(BW2)
```

A.2. Coordinates of the interface

```
I = imread('name of the file.bmp');
dim = size(I);
n = 0;
for j = 1 : dim(1,2)
   for i = 1 :dim(1,1)
      if BW3(i,j)> 0
         n = n+1;
         xy(n,1)=j;
         xy(n,2)= dim(1,1) - i + 1;
      end;
   end;
end;
dim=size(xy);
a=dim;
z=dim(1,1);
n=1;
for i = 1 : (z-1)
   if xy(i,1) == xy(i+1,1)
      if n<z
         a(n,1)= xy(n,1);
         a(n,2)=xy(n,2);
         a(n+1,1)=xy(n+1,1);
         a(n+1,2)=xy(n+1,2);
         n=n+1;
      end;
      n=n+1;
    end;
```

```
 end;
dim=size(a);
j=0;
n=0;
counter=0;
for i=1:(dim(1,1)-1)
   if a(i,1) == a(i+1,1)
      n=n+1;
      counter=counter+a(i,2);
   else
      counter=counter+a(i,2);
      n=n+1;
      j=j+1;
      b(j,1)=a(i,1);
      b(j,2)=counter/n;
      n=0;
      counter=0;
   end;
   if i==(dim(1,1)-1)
      counter=counter+a(i+1,2);
      j=j+1;
      b(j,1)=a(i,1);
      b(j,2)=counter/(n+1);
   end;
end;
```

A.3. ADSA-P Routine

```
'*************************************************************************
Option Explicit     '...Force the declaration of all variables
Option Base 1       '...All arrays and vectors start at index = 1
'*************************************************************************
'Declaration of Global Variables that can be used in any part of the code
Public q1 As Double         '...X0 - x coordinate of the origin
Public q2 As Double         '...Z0 - z coordinate of the origin
Public q3 As Double         '...R0 - Radius of curvature at the origin
Public q4 As Double         '...(Drho*g*R0^2)/gamma) - Shape parameter

Global Const PI As Double = 3.141592654     '...A value for PI
Global Const NoEQ As Double = 3             '...Number of ODEs in the system
Global Const NoSteps As Integer = 50        '...Number of Intervals for the ODE Integration
```

```
'...Defines a structure for the settings and parameters needed to use the integrator functions
Type ODESettings

   SolveMethod As String      '...Numerical method to solve the ODE system
   Init As Double             '...Initial value for the ODE
   Final As Double            '...End value for the ODE
   StepSize As Double         '...Size of the integration step for the ODE
End Type

'*************************************************************************
Sub Solve_ODESystem(ByRef x_dimless() As Double, ByRef z_dimless() As Double, ByRef
                                AllResults() As Double, ByRef FirstCell As Range)

'Routine to drive the program to solve the ODE system that represents the drop in the ADSAP
methodology

'...Declaration of variables
   Dim ODE_Settings As ODESettings        '...Integration settings
   Dim y(1 To NoEQ) As Double             '...y() at each step
   Dim dy(1 To NoEQ) As Double            '...Change in y() for each step
   Dim y0(1 To NoEQ) As Double            '...Initial y()
   Dim X As Double                    '...Arch length
   Dim NoPoints As Long                 '...Number of points coordinates
   Dim X_Coord() As Double              '...X coordinates
   Dim Z_Coord() As Double              '...Z coordinates
   Dim x_shifted() As Double            '...x coordinates shifted to X0 =0
   Dim z_shifted() As Double            '...z coordinates shifted to Z0 = 0
   Dim col As Long, row As Long         '...Address for the first data point
   Dim check As Boolean                 '...Boolean
   Dim i As Integer, j As Integer       '...Counters

   '...Initializations of all parameters
   '...Initialize the ODE Dettings for the Integration
   ODE_Settings.StepSize = 0.01
   ODE_Settings.Init = 0#
   ODE_Settings.Final = PI

   '...Load the coordinate Vectors
   Call Load_DropCoordinates(X_Coord, Z_Coord, FirstCell)

   '...Shift the coordinates
   NoPoints = UBound(X_Coord)
   ReDim x_shifted(NoPoints)
   ReDim z_shifted(NoPoints)
```

```
    ReDim x_dimless(NoPoints)
    ReDim z_dimless(NoPoints)
    For i = 1 To NoPoints
        x_shifted(i) = Abs(X_Coord(i) - q1)
        z_shifted(i) = Abs(Z_Coord(i) - q2)
        '... Now make them dimensionless
        x_dimless(i) = x_shifted(i) / q3
        z_dimless(i) = z_shifted(i) / q3
    Next

    '...Actual Calcualtions begin
        '...Initialize the ODEs
    y(1) = 0.00001          '...x coordinate
    y(2) = 0#               '...z coordinate
    y(3) = 0#               '...phi turning angle
    j = 1   '...row


    '...Record the initial conditions
    ReDim AllResults(NoEQ + 1, j)
    AllResults(1, j) = X        '...curvature lenght
    AllResults(2, j) = y(1)     '...x coordinate
    AllResults(3, j) = y(2)     '...z coordinate
    AllResults(4, j) = y(3)     '...phi turning angle

    '...Calculations for the rest of the integrations steps are made in a loop

    Do While X < ODE_Settings.Final
        '...INcrease the conunter for the output
        j = j + 1

        '...Calculate the next step
        check = RK4order(X, y(), ODE_Settings)

        '...Record the results from the current step
        ReDim Preserve AllResults(NoEQ + 1, j)
        AllResults(1, j) = X        '...curvature lenght
        AllResults(2, j) = y(1)     '...x coordinate
        AllResults(3, j) = y(2)     '...z coordinate
        AllResults(4, j) = y(3)     '...phi turning angle
    Loop

End Sub
```

```
'*************************************************************************
Public Sub ShowExcelSolver()

'...Loads default problem settings and runs the Excel Solver
'...The routine must be called when the first X point cell is selected

   Dim FirstCell As Range          '...Top Left Data Point
   Dim strObjective As String      '...String defining the Objective Function cell
   Dim strParams As String         '...String define the parameters the solver can change
   Dim lngRow As Long              '...Cell's Row
   Dim lngCol As Long              '...Cell's column

   '...Get the Cell's information

   Set FirstCell = ActiveCell

   '...Determine the cells address using the pre-defined layout

   With FirstCell
      lngRow = .row
      lngCol = .Column
   End With

   With ActiveSheet
      strObjective = .Cells(lngRow + 5, lngCol + 7).Address
      strParams = .Cells(lngRow - 1, lngCol + 7).Address & ":" & .Cells(lngRow + 2, lngCol +
                  7).Address
   End With

   SolverReset       '...Clear all Solver settings

   '...Set the target functions, the Manipulated variables and show the solver

   SolverOkDialog SetCell:=strObjective, MaxMinVal:=2, ValueOf:=0, Bychange:=strParams

End Sub

'*************************************************************************
Option Explicit            'force the declaration of all variables
Option Base 1              'all arrays and vectors start at index =1
'*************************************************************************
Public Function GetContactAngle(ByVal par1 As Double, ByVal par2 As Double, ByVal par3
                                As Double, ByVal par4 As Double, ByVal FirstCell As
                                Range, ByVal ContactPoint As Range) As Double
```

```
'this function calculates the contact angle by solving the ODE system with the optimized
parameters q1, q2, q3 and q4
'...par1 : q1
'...par2 : q2
'...par3 : q3
'...par4 : q4
'...FirstCell : Top left cell of the measured coordinates
'...ContactPoint : cell of the x coordinates for the measured contact point

    Dim TheResults() As Double          '...Matrix that holds the calculated curve
    Dim x_dimless() As Double           '...x coordinates dimensionless (X/R0)
    Dim z_dimless() As Double           '...z coordinates dimensionless (Z/R0)
    Dim NoPoints As Long            '...Number of point coordinates
    Dim lngCol As Long, lngRow As Long      '...address for the first data point
    Dim idxMinDist As Long
    Dim MinDist As Double
    Dim j As Integer, k As Integer

    '...Load the function arguments to the global variables

    q1 = par1
    q2 = par2
    q3 = par3
    q4 = par4

    '...solve the ODE systen to obtain the curve

    Call Solve_ODESystem(x_dimless, z_dimless, TheResults, FirstCell)

    '...Get the address for the contact data point
    lngCol = ContactPoint.Column
    lngRow = ContactPoint.row

    '...find the curvature distance to each of the points
    If Not (lngRow = FirstCell.row) Then
        NoPoints = lngRow - FirstCell.row + 1               '...only the contact point
    Else
        NoPoints = 1            '..The contact point is the first cell
    End If

    '...Initialize conters
    j = UBound(TheResults, 2)
    ReDim Distance(1, j) As Double
    idxMinDist = 0 '...initialize values
    MinDist = 1E+30         '...initialize values
```

```
    For k = 1 To j
        '...probably don't need this anymore as we are using absolute values
        '...in the coordinates
        If x_dimless(NoPoints) < 0 Then
            Distance(1, k) = 0.5 * ((TheResults(2, k) + (x_dimless(NoPoints))) ^ 2 + (TheResults(3,
                                    k) - (z_dimless(NoPoints))) ^ 2)
        Else
            Distance(1, k) = 0.5 * ((TheResults(2, k) - (x_dimless(NoPoints))) ^ 2 + (TheResults(3,
                                    k) - (z_dimless(NoPoints))) ^ 2)

        End If
    Next

        '... Find the minimum distances and get the summation for all points

    Dim DistError As Double
    DistError = 0#
    For k = 1 To j
        '...take into account only the first twirl
        If (MinDist > Distance(1, k)) And (TheResults(4, k) <= PI) Then
            MinDist = Distance(1, k)
            idxMinDist = k
        End If
    Next
    DistError = DistError + MinDist

    '...Return the value
    GetContactAngle = TheResults(4, idxMinDist)         '...Radians
    '...Correct phase taken into account
    GetContactAngle = GetContactAngle * (180 / PI)  '...Degrees


End Function
'*************************************************************************
Public Function GetSumOfErrors(ByVal par1 As Double, ByVal par2 As Double, ByVal par3
                                    As Double, ByVal par4 As Double, ByVal FirstCell As
                                    Range) As Double

'This function calculates the sum of errors between each measured point and the closest point in
a curve calculated with q1,q2,q3,q4.

'...par1 : q1
'...par2 : q2
'...par3 : q3
```

```
'...par4 : q4
'...FirstCell : Top left of the measured coordinates

    Dim TheResults() As Double          '...Matrix that holds the calculated curve
    Dim x_dimless() As Double           '...x coordinates dimensionless (X/R0)
    Dim z_dimless() As Double           '...z coordinates dimensionless (Z/R0)
    Dim NoPoints As Long            '...Number of point coordinates
    Dim j As Integer, k As Integer, i As Integer

    '...load the function arguments to the global variables
    q1 = par1
    q2 = par2
    q3 = par3
    q4 = par4

    '...solve the ODE system to obtain a curve
    Call Solve_ODESystem(x_dimless, z_dimless, TheResults, FirstCell)

    '...Find the curvature distance to each oif the points
    NoPoints = UBound(x_dimless)
    j = UBound(TheResults, 2)       '..number of rows

    ReDim Distance(NoPoints, j) As Double, MinDist(NoPoints) As Double
    ReDim idxMinDist(NoPoints) As Integer

    For i = 1 To NoPoints
       idxMinDist(i) = 0          '...Initialize values
       MinDist(i) = 1E+30          '...Initialize values
       For k = 1 To j
          If x_dimless(i) < 0 Then
           Distance(i, k) = 0.5 * ((TheResults(2, k) + (x_dimless(i))) ^ 2 + (TheResults(3, k) –
                                   (z_dimless(i))) ^ 2)
          Else
           Distance(i, k) = 0.5 * ((TheResults(2, k) - (x_dimless(i))) ^ 2 + (TheResults(3, k) –
                                   (z_dimless(i))) ^ 2)
          End If
       Next
    Next

    '...Find the minimum distances and get the summation for all points
    Dim DistError As Double
    DistError = 0#
    For i = 1 To NoPoints
       For k = 1 To j
          '...take into account only the first twirl
```

```
            If (MinDist(i) > Distance(i, k)) And (TheResults(4, k) <= PI) Then
               MinDist(i) = Distance(i, k)
               idxMinDist(i) = k
            End If
         Next
         DistError = DistError + MinDist(i)
      Next
         '...Return the value
      GetSumOfErrors = DistError

End Function
'*************************************************************************
Public Function GetGamma(ByVal pQ3 As Double, ByVal pQ4 As Double, ByVal DeltaRho As
                         Double, ByVal aG As Double, ByVal Pixels As Double, ByVal
                         Length As Double) As Double

'function to calculate the interfacial tension (Gamma)

'...pQ3:       optimized Q3 parameter (Radius of curvature at the origin)
'...pQ4:       optimized Q4 parameter (shape factor)
'...DeltaRho:   density difference between the fluids in [kg/m^3]
'...aG:        Acceleration of gravity in [m/s^2]
'...Pixels:    Number of pixels in the selected length
'...Length:    Length equivalent to the number of pixels in [mm]

   Dim num As Double, scaledR0 As Double

   '...scale the radius of curvature
   scaledR0 = pQ3 * Length / Pixels       '...in [mm]
   scaledR0 = scaledR0 / 1000#            '...in [m]

   '...Calculate the numerator
   num = DeltaRho * aG * (scaledR0 ^ 2)

   '...Return the function value
   GetGamma = num / pQ4

End Function
'*************************************************************************
Public Function GetXApexGuess(ByVal FirstCell As Range) As Double

'functions to guess the X coordinate for the appex from the measured values

'...first cell :top left cell of the measured coordinates
```

```
    Dim X_Coord() As Double             '...X coordinates
    Dim Z_Coord() As Double             '...Z Coordinates
    Dim i As Long

    Call Load_DropCoordinates(X_Coord, Z_Coord, FirstCell)

    '...Do a rudimentary search
    i = GetMinMaxIndex(Z_Coord, "Max")        '...look for the highest Y

    GetXApexGuess = X_Coord(i)              '...Return the X coordinate

End Function

'*************************************************************************
Public Function GetYApexGuess(ByVal FirstCell As Range) As Double

'functions to guess the Y coordinate for the apex from the measured values

'...firstcell ; top left cell of the measured coordinates

    Dim X_Coord() As Double             '...X coordinates
    Dim Z_Coord() As Double             '...Z Coordinates
    Dim i As Long

    Call Load_DropCoordinates(X_Coord, Z_Coord, FirstCell)

    '...Do a rudimentary search
    i = GetMinMaxIndex(Z_Coord, "Max")        '...look for the highest Y

    GetYApexGuess = X_Coord(i)              '...Return the Y coordinate

End Function
'*************************************************************************
Public Function GetContactCellGuess(ByVal FirstCell As Range) As Range

'function to guess the cell where the X coordinate for the contact point is
'...firstcell : Top left cell of the measured coordinates


    Dim X_Coord() As Double             '...X coordinates
    Dim Z_Coord() As Double             '...Z Coordinates
    Dim i As Long

    Call Load_DropCoordinates(X_Coord, Z_Coord, FirstCell)
```

```
    '...Do a rudimentary search
    i = GetMinMaxIndex(Z_Coord, "Min")          '...look for the smallest Y

    '...Return the cell
    Set GetContactCellGuess = ActiveSheet.Cells(FirstCell.row + i - 1, FirstCell.Column)

End Function
'*************************************************************************
Public Function GetContactCellGuessAddress(ByVal FirstCell As Range) As String

'function to guess the cell where the X coordinate for the contact point is

'...firstcell : Top left cell of the measured coordinates

    Dim X_Coord() As Double              '...X coordinates
    Dim Z_Coord() As Double              '...Z Coordinates
    Dim i As Long

    Call Load_DropCoordinates(X_Coord, Z_Coord, FirstCell)
       '...Do a rudimentary search
    i = GetMinMaxIndex(Z_Coord, "Min")          '...look for the smallest Y
       '...Return the cell
    GetContactCellGuessAddress = ActiveSheet.Cells(FirstCell.row + i - 1,
FirstCell.Column).Address
End Function
'*************************************************************************
Public Function CalcDerivatives(X As Double, y() As Double, dy() As Double) As Boolean

'function that contains the dimensionless ODE system
'...The equations are defined in the paper:
'...Determination of surface tension and contact angle from the shapes of
'...axisymetric fluid interfaces; roterberg, T., L. Boruvka, & A.W. Newmann
'...JOurnal of colloid and interface science, v. 93, n. 1, pp 169-183, 1983

'...dy(1) : dx/ds = cos(phi)  Eq. 12a
'...dy(2) : dx/ds = sin(phi)   Eq. 12d
'...dy(3) : dphi/ds = 2+((Drho*g*RO^2)/gamma)*z-sin(phi)/x  Eq. 12c

    '...calculate the ODE system
    dy(1) = Cos(y(3))
    dy(2) = Sin(y(3))
    dy(3) = 2# + q4 * y(2) - Sin(y(3)) / y(1)

    CalcDerivatives = True
End Function
```

```
'*************************************************************************
Public Function CountNumericRowsDown(ByRef TopLeftCell As Range) As Long

'this function counts the number of consecutive rows that contain numeric
'values starting on the cell provided and going down

    Dim lngCol As Long, lngRow As Long      '...address for the first cell
    Dim count As Integer

    '...get the address to start
    lngCol = TopLeftCell.Column
    lngRow = TopLeftCell.row

    count = 0
    '...conut the rows
    With Worksheets(TopLeftCell.Worksheet.Name)
      Do While .Cells(lngRow + count, lngCol) <> "" And IsNumeric(.Cells(lngRow + count,
lngCol))
        '...Update the counter
        count = count + 1
      Loop
  End With

  CountNumericRowsDown = count

End Function
'*************************************************************************
Private Function GetMinMaxIndex(ByRef vector() As Double, ByVal strMinMax As String) As
Long

'generic function to return the vector index of a minimum or maximum

'...vector():   The vector in which the search wi8ll happen
'...strMinMax:  type of search

  Dim i As Long, idx As Long
  Dim dTiny As Double
  Dim dHuge As Double

  dTiny = 1E+300         '...initial value
  dHuge = -1E+300        '...initial value

  Select Case strMinMax
    Case "Min"
      For i = 1 To UBound(vector)
```

```
            If vector(i) < dTiny Then
               idx = i
               dTiny = vector(i)
            End If
         Next
      Case "Max"
         For i = 1 To UBound(vector)
            If vector(i) > dHuge Then
               idx = i
               dHuge = vector(i)
            End If
         Next
   End Select

   GetMinMaxIndex = idx

End Function
'*************************************************************************
Public Sub gErrorMessage(Location As String, errNumb As Long, errDesc As String)

'renders an error message and presents it to the user in a message box

'...Location - function or routine calling this routine
'...errNumb - error number
'...errDesc - error description

   MsgBox ("an error ocurred in " & Location & vbCrLf & "ErrNum:" & CStr(errNumb) &
vbCrLf & "ErrDesc:" & errDesc)

End Sub
'*************************************************************************
Sub Load_DropCoordinates(ByRef X() As Double, ByRef Z() As Double, ByRef FirstCell As
                                 Range)

'this subroutine loads the coordinates for the current drop
   Dim lngCol As Long, lngRow As Long          '...Address for the first data point
   Dim count As Integer

   '...Get the address fro the first data point
   lngCol = FirstCell.Column
   lngRow = FirstCell.row

   count = 1
   '...Load the data from the spreadsheet
   With Worksheets(FirstCell.Worksheet.Name)
```

```
    Do While .Cells(lngRow + count - 1, lngCol) <> "" And IsNumeric(.Cells(lngRow + count
                        - 1, lngCol))
      '...Redefine the vector/arrays
      ReDim Preserve X(count)
      ReDim Preserve Z(count)
      '...Append the values to the vector/arrays
      X(count) = .Cells(lngRow + count - 1, lngCol).Value
      Z(count) = .Cells(lngRow + count - 1, lngCol + 1).Value
      '...Update the counter
      count = count + 1
    Loop
  End With

End Sub

'*************************************************************************
Option Explicit          '...Force the declaration of all variables
Option Base 1            '...all arrays and vectors start at index=1
'*************************************************************************
Public Function RK4order(X As Double, y() As Double, Settings As ODESettings) As Boolean

'this function implements the fourth order runge-kutta method to solve
'ordinary diferential equations.  References are chapter 16 of the numerical
'recipies in C; cambridge university press; electronic version and chapter
'25 of the numerical methods for engineers; chapra, steven; 3rd ed. McGrawHill

  Dim h As Double
  Dim k1(1 To NoEQ) As Double, k2(1 To NoEQ) As Double
  Dim k3(1 To NoEQ) As Double, k4(1 To NoEQ) As Double
  Dim i As Integer
  Dim yk1(1 To NoEQ) As Double, yk2(1 To NoEQ) As Double
  Dim yk3(1 To NoEQ) As Double, yk4(1 To NoEQ) As Double
  Dim dy(1 To NoEQ) As Double
  Dim check As Boolean

    '...load the step size for the ODE system solving
  h = Settings.StepSize

  '...Implement the fourth order runge-kutta numerical method
  '...CalcDerivatives is the function containing the ODE System
  check = yk(y(), k1(), 0, yk1())
  check = CalcDerivatives(X, yk1(), dy())
  For i = 1 To NoEQ
    k1(i) = h * dy(i)
  Next i
```

```
    check = yk(y(), k1(), 0.5, yk2())
    check = CalcDerivatives(X + h * 0.5, yk2(), dy())

    For i = 1 To NoEQ
       k2(i) = h * dy(i)
    Next i

    check = yk(y(), k2(), 0.5, yk3())
    check = CalcDerivatives(X + h * 0.5, yk3(), dy())
    For i = 1 To NoEQ
       k3(i) = h * dy(i)
    Next i

    check = yk(y(), k3(), 1, yk4())
    check = CalcDerivatives(X + h, yk4(), dy())

    For i = 1 To NoEQ
       k4(i) = h * dy(i)
    Next i

    '...update the values of y
    For i = 1 To NoEQ
       y(i) = y(i) + k1(i) / 6# + (k2(i) + k3(i)) / 3# + k4(i) / 6#
    Next i

    '...update the values of x
    X = X + h

    RK4order = True

End Function
'*************************************************************************
Public Function yk(y() As Double, k() As Double, weight As Double, newy() As Double) As
Boolean

'this function updates the value of the vector y() to be used in the RK routine

    Dim j As Integer

    For j = 1 To NoEQ
       newy(j) = y(j) + k(j) * weight
    Next j

    yk = True
```

```
End Function
'*************************************************************************
```

APPENDIX B: OBSERVATIONS

I would like to add an appendix of observations from my experiences which I believe it could be very helpful to whoever wants to keep on developing this new methodology to determine interfacial properties.

The equipment implemented has a strong limitation in terms of the space and easiness to set up any system. It was designed to work with solid systems. However, it is possible to overcome these difficulties by designing a cell that could be easily level which I accomplished in this project and an injection system that allow the creation of axisymmetric droplets in an easier manner.

The results show that for bigger values of contact angles (neutral of oil wet systems) micro X-ray imaging produces two zones of values of contact angles. At the same time, the known values of IFT for the systems analyzed were determined at 7µl which is at the second zone on the contact angles results. These two zones are the result of how micro X-ray imaging recreates images of the systems exposed to X-rays. To avoid this I recommend using volumes from 7µl and to increase the height of the cell to increase the magnification of the image. Another way to avoid this is to increase the magnification. I used 11µm per pixel and the equipment can go to 5µm per pixel. To change the magnification the height of the cell has to be modified accordingly.

The calibration of the micro CT scanner to determine the real value of the length that a pixel represents in very important to determine the values of the IFT. The contrast and brightness chosen must be the same to all the images otherwise you can obtain bigger or smaller droplet profiles from the same droplet. I advise to have a thorough review of this calibration.